

FLUORESCENT REAGENTS TO IMPROVE THE ANALYTICAL
INFRASTRUCTURE OF CAPILLARY ELECTROPHORETIC SEPARATIONS

A Dissertation

by

MING-CHIEN LI

Submitted to the Office of Graduate Studies of
Texas A&M University
in partial fulfillment of the requirements for the degree of

DOCTOR OF PHILOSOPHY

May 2012

Major Subject: Chemistry

FLUORESCENT REAGENTS TO IMPROVE THE ANALYTICAL
INFRASTRUCTURE OF CAPILLARY ELECTROPHORETIC SEPARATIONS

A Dissertation

by

MING-CHIEN LI

Submitted to the Office of Graduate Studies of
Texas A&M University
in partial fulfillment of the requirements for the degree of

DOCTOR OF PHILOSOPHY

Approved by:

Chair of Committee,	Gyula Vigh
Committee Members,	Coran Watanabe
	Daniel Romo
	Victor Ugaz
Head of Department,	David H. Russell

May 2012

Major Subject: Chemistry

ABSTRACT

Fluorescent Reagents to Improve the Analytical Infrastructure of Capillary
Electrophoretic Separations.

(May 2012)

Ming-Chien Li, B.S., Tankang University;

M.S., National Tsing Hua University

Chair of Advisory Committee: Dr. Gyula Vigh

Two types of fluorescent molecules had been designed and synthesized to improve the analytical infrastructure of capillary electrophoretic separations. First, a hydrophilic version of the permanently cationic acridine-based fluorophore, HEG₂Me₂-DAA was synthesized. HEG₂Me₂-DAA has a $\lambda^{\text{ex}}_{\text{max}}$ of 490 nm which matches the 488 nm line of the commonly used argon ion laser. The emission spectra of HEG₂Me₂-DAA are pH-independent. HEG₂Me₂-DAA was used in capillary electrophoresis with an aqueous background electrolyte and was found to be free of the detrimental peak tailing of the acridine orange-based fluorophore that was caused by adsorption on the inner wall of the fused silica capillary. Bovine serum albumin was labeled with excess of the designed amine reactive reagent and the lowest concentration at which the tagged bovine serum albumin was tested was 15 nM. Chicken ovalbumin was also labeled with FL-CA-PFP and analyzed by capillary isoelectric focusing (cIEF) with LIF detection. The *pI* values of the tagged proteins shifted in the alkaline direction by about 0.02 compared to the *pI*

values of the non-tagged proteins. A tri-functional probe intended to enable selective enrichment and selective detection of a variety of molecules (*e.g.*, natural products, pharmaceuticals, inhibitors, *etc.*) was also designed and synthesized by combining FL-CA with biotin and an azide group in a “proof-of-principle” level experiment.

In cIEF, the profile of the pH gradient can only be determined with the help of *pI* markers. A large set of pyrene-based fluorescent *pI* markers was rationally designed to cover the *pI* range 3 to 10. To prove the feasibility of the proposed synthetic approach, the subgroup of the *pI* markers having the greatest structural complexity was synthesized and characterized. The classical zone electrophoretic *pI* determination methods failed due to severe chromatographic retention of the APTS based *pI* markers on the capillary wall. Exploratory work was done to design a new *pI* value determination method that combines the advantages of the immobilized pH gradient technology of the OFFGEL instrument and the carrier-ampholyte-based IEF technology. The method aspects of cIEF have also been improved in this work. The new segmented loading method yielded a more linear pH gradient than the previously known cIEF methods. To exploit a unique property of the newly developed fluorescent *pI* markers, we used them as pyrene-based ampholytic carbohydrate derivatizing reagents. The *pI*4 carbohydrate derivatization reagent proved advantageous over 8-aminopyrene-1,3,6-trisulfonic acid (APTS): the *pI*4 conjugates have higher molar absorbance at 488 nm than the APTS conjugates and become detectable in positive ion mode of MS affording better detection sensitivity.

ACKNOWLEDGEMENTS

I would like to express my sincere gratitude to all my committee members for their help.

I am heartily thankful for the generous support and resources provided by Dr. Daniel Romo and his group which enabled the completion of this work.

I want to thank Dr. Roy Estrada who has been a great mentor to me.

Lastly, I want to thank my advisor, Dr. Gyula Vigh. Without his guidance, I could not have achieved my dream.

“A teacher affects eternity; he can never tell where his influence stops.”

– HENRY ADAMS

TABLE OF CONTENTS

	Page
ABSTRACT	iii
ACKNOWLEDGEMENTS	v
TABLE OF CONTENTS	vi
LIST OF FIGURES	x
LIST OF TABLES	xviii
1. INTRODUCTION.....	1
1.1 Fluorescent Labeling Reagents in Capillary Electrophoresis (CE).....	1
1.1.1 Capillary Electrophoresis for Bioanalysis.....	1
1.1.2 Fluorescence Detection in CE	1
1.1.3 Examples of Fluorescent Labels Used in CE	2
1.1.3.1 Fluorescein	2
1.1.3.2 NBD Dyes	3
1.1.3.3 FQ and CBQCA	4
1.2 Requirements and Limitations of Existing Fluorescent Labeling Reagents	4
1.2.1 Good Water Solubility	4
1.2.2 pH-Dependent Fluorescence	5
1.2.3 Changes in Analyte Properties after Labeling.....	6
1.3 Capillary Isoelectric Focusing (cIEF)	6
1.3.1 Principle of cIEF	6
1.3.2 cIEF Technologies.....	7
1.3.2.1 Mobilization Mode and Detection.....	7
1.3.2.2 Capillary	8
1.3.2.3 Additives	9
1.3.2.4 Carrier Ampholytes	10
1.4 pI Markers	13
2. DEVELOPMENT OF A HYDROPHILIC ACRIDINE-BASED AMINE- REACTIVE FLUORESCENT LABELING REAGENT THAT HAS pH- INDEPENDENT SPECTRAL PROPERTIES.....	15

2.1	Design and Synthesis	15
2.1.1	Background and Objective	15
2.1.2	Materials and Method.....	19
2.1.2.1	Chemicals and Equipment.....	19
2.1.2.2	Synthesis of Mono-Tosylated Tetra(Ethylene Glycol) (mTs-TEG)	20
2.1.2.3	Synthesis of Mono-Tosylated Tetra(Ethylene Glycol) –Aldehyde	25
2.1.2.4	Synthesis of DAAPS (4)	27
2.1.2.5	Synthesis of TsTEG2-DAAPS (5)	32
2.1.2.6	Synthesis of HEG2-DAAPS (6).....	34
2.1.2.7	Synthesis of Me ₂ HEG2-DAAPS (FL) (7)	35
2.1.2.8	Synthesis of FL-CA (9).....	37
2.1.2.9	Synthesis of FL-CA-PFP (10).....	40
2.2	Spectral Properties.....	41
2.2.1	Background and Objective	41
2.2.2	Materials and Method.....	42
2.2.3	Results and Discussion.....	42
2.3	Chromatographic Properties.....	45
2.3.1	Background and Objective	45
2.3.2	Materials and Method.....	45
2.3.3	Results and Discussion.....	46
2.4	Labeling Reactions Using FL-CA-PFP	46
2.4.1	Background and Objective	46
2.4.2	Materials and Method.....	47
2.4.2.1	Labeling of Amino Acids and Their Analysis by CE-LIF and RP-HPLC.....	47
2.4.2.2	Labeling of Bovine Serum Albumin (BSA) and Its Analysis by SDS-CGE-LIF	47
2.4.2.3	Labeling of Chicken Ovalbumin (Ov) and Its Analysis by cIEF	48
2.4.3	Results and Discussion.....	49
2.4.3.1	Labeling of Amino Acids and Their Analysis by CE-LIF	49
2.4.3.2	Labeling of Bovine Serum Albumin (BSA) and Its Analysis by SDS-CGE-LIF	52
2.4.3.3	Labeling of Chicken Ovalbumin (Ov) and Its Analysis by cIEF	53
2.5	Design and Synthesis of a FL-CA-Based Trifunctional Probe	55
2.5.1	Background and Objective	55
2.5.2	Materials and Method.....	57
2.5.2.1	Synthesis of Biotin-Azide Compound 6.....	57
2.5.2.2	Synthesis of the Desired Trifunctional Probe	59
2.6	Concluding Remarks	61

3. DESIGN AND SYNTHESIS OF A FAMILY OF PYRENE-BASED FLUORESCENT pI MARKERS	64
3.1 Design and Synthesis	64
3.1.1 Background and Objective	64
3.1.2 Materials and Method	85
3.1.2.1 Chemicals and Equipment	85
3.1.2.2 Synthesis of Compound 2	85
3.1.2.3 Synthesis of Compound 3	87
3.1.2.4 Synthesis of Compound 4	90
3.1.2.5 Synthesis of Compounds 5 and 6	93
3.1.2.6 Sulfation of the TEG Derivatives of Compound 6	97
3.1.2.7 LC-MS Analysis of APTS-based pI Makers after Purification	98
3.2 pI Value Determination	102
3.2.1 Background and Objective	102
3.2.2 Materials and Method	103
3.2.2.1 Pressure-Mediated Capillary Electrophoresis (PreMCE)	104
3.2.2.2 Effective Mobility of a Polyprotic Electrolyte as a Function of pH	107
3.2.2.3 Capillary Isoelectric Focusing (cIEF)	109
3.2.3 Results and Discussion	110
3.2.3.1 pI Value Determinations by PreMCE	110
3.2.3.2 pI Values Measured by Capillary Isoelectric Focusing (cIEF)	126
3.3 Ampholytic APTS-based Carbohydrate Tagging Reagent	133
3.3.1 Background and Objective	133
3.3.2 Carbohydrate Derivatization	134
3.3.2.1 Chemicals and Equipment	134
3.3.2.2 Derivatization of D-glucose with the pI4 Reagent	135
3.4 Concluding Remarks	140
4. CONCLUSIONS	144
4.1 Amine-Reactive Fluorescent Labeling Reagent	144
4.2 Pyrene-based Fluorescent pI Markers	145
REFERENCES	149
APPENDIX A	156

VITA 167

LIST OF FIGURES

FIGURE	Page
1.1 Structures of fluorescein-based amine-reactive labeling reagents	2
1.2 Reaction scheme for labeling an amine with NBD-F	3
1.3 Structures of FQ and CBQCA.....	4
1.4 Structures of fluorescein and rosamine	5
1.5 The relationship of buffering power (β) and the pK_a values which determine the pI of lysine and bicine	11
1.6 Reaction scheme of making CAs according to Vesterberg.....	12
2.1 (a) Acridine orange-based and (b) Me_2HEG_2 -DAA-based amine-reactive fluorescent labeling reagent.....	15
2.2 Calculated $\log P$ of $[(EtO)_n]_2$ -DAA as a function of the mer-number of the ethoxy groups	16
2.3 Synthetic scheme for making HEG_2Me_2 -DAAPS	18
2.4 Synthetic scheme for elongation of the tether and activation of the HEG_2Me_2 -DAA-based amine-reactive fluorescent labeling reagent	18
2.5 Reaction scheme for making mono-tosylated tetra(ethylene glycol).....	20
2.6 RP-HPLC of (a) mono-tosylated TEG reaction mixture, (b) aqueous phase obtained after work-up, (c) oil phase obtained after workup	23
2.7 1H NMR spectrum of mono-tosylated tetra(ethylene glycol) in $CDCl_3$	23
2.8 ESI mass spectrum of mono-tosylated tetra(ethylene glycol).....	24
2.9 Reaction scheme for making mono-tosylated TEG-aldehyde.....	25
2.10 RP-HPLC analysis of the mono-tosylated tetra(ethylene glycol)-aldehyde reaction mixture. (Insert: 1H -NMR spectrum of mono-tosylated tetra(ethylene glycol)-aldehyde)	27
2.11 Reaction scheme for making $(AcO)_2$ -DAAPS	27

2.12	LC-MS analysis of the AcO ₂ -DAA and 1,3-propane sultone reaction mixture after 7 minutes of heating in a microwave oven. (a) TIC, (b) UV absorbance trace at 250 nm	28
2.13	RP-HPLC of the reaction mixture of AcO ₂ -DAA with CaO and without base	29
2.14	RP-HPLC of (a) AcO ₂ -DAA, (b) quaternarization reaction mixture of AcO ₂ -DAA, (c) product after workup	30
2.15	ESI mass spectrum of AcO ₂ -DAAPS	31
2.16	Reaction scheme for making DAAPS	31
2.17	RP-HPLC of AcO ₂ -DAAPS and of the reaction mixture during hydrolysis of AcO ₂ -DAAPS	32
2.18	Reaction scheme for making TsTEG ₂ -DAAPS	32
2.19	RP-HPLC of DAAPS and of the reaction mixture that contains TsTEG ₂ -DAAPS	33
2.20	Reaction scheme for making HEG ₂ -DAAPS	34
2.21	RP-HPLC monitoring of the progress of the reaction during making HEG ₂ -DAAPS.	35
2.22	Reaction scheme for making Me ₂ HEG ₂ -DAAPS (FL)	35
2.23	RP-HPLC analysis of HEG ₂ -DAAPS and the reaction mixture of Me ₂ HEG ₂ -DAAPS. (Insert: UV absorbance spectra of HEG ₂ -DAAPS and Me ₂ HEG ₂ -DAAPS)	36
2.24	ESI mass spectrum of Me ₂ HEG ₂ -DAAPS (FL)	37
2.25	Reaction scheme for making FL-Me-CA	37
2.26	CE-LIF analysis of the extension of the tether of FL to FL-Me-CA	38
2.27	Reaction scheme for making FL-CA	38
2.28	RP-HPLC analysis of the hydrolysis of FL-Me-CA to FL-CA	39
2.29	ESI mass spectrum of FL-CA	39

2.30	Reaction scheme for making FL-CA-PFP.	40
2.31	RP-HPLC analyses of FL-CA and its activated form, FL-CA-PFP.....	40
2.32	ESI mass spectrum of FL-CA-PFP	41
2.33	Comparisons of $\lambda_{\text{ex max}}$ for proflavine, acridine orange and HEG2Me2-DAA	41
2.34	UV absorbance spectra of differently alkylated 3,6-diaminoacridines	42
2.35	Comparison of the fluorescence excitation (A) and emission (B) spectra of acridine orange (dashed line) and HEG2Me2-DAA (solid line).....	43
2.36	Fluorescence emission spectra of HEG2Me2-DAA in H3PO4/ NaOH aqueous buffers from pH 2.4 to 11 with 10 mM ionic strength	44
2.37	CE analysis of acridine orange propane sulfonate and Me2HEG2-DAAPS....	46
2.38	CE analyses of FL-CA-PFP tagged amino acids. (a) tagged arginine, (b) tagged histidine, (c) tagged glutamic acid and (d) tagged glycine.	50
2.39	RP-HPLC analyses of FL-CA-PFP tagged amino acids. (a) tagged arginine, (b) tagged histidine, (c) tagged glutamic acid and (d) tagged glycine.	51
2.40	ESI mass spectra of FL-CA-PFP tagged amino acids. (a) tagged arginine, (b) tagged histidine, (c) tagged glutamic acid and (d) tagged glycine.	51
2.41	SDS-CGE analysis of labeled bovine serum albumin using LIF detection	53
2.42	Mobilization traces obtained in the cIEF analysis of chicken ovalbumin with UV absorbance detection and labeled chicken ovalbumin with LIF detection.	54
2.43	Combined reproducibility of the labeling reaction and the cIEF analysis of the same chicken ovalbumin sample.....	55
2.44	Synthetic scheme for making compound 6	56
2.45	Synthetic scheme for making the desired trifunctional probe.....	57
2.46	LC-MS analysis of compound 6	58

2.47	LC-MS analysis of the reaction mixture obtained during the final assembly of the trifunctional probe. (Insert: UV absorbance spectrum of the trifunctional probe.).....	59
2.48	Reaction scheme of coupling a cyclopropanated derivative of parthenin with the trifunctional probe.	60
2.49	LC-MS analysis of the reaction mixture of the trifunctional probe coupled with a cyclopropanated derivative of parthenin: (a) total ion chromatogram in positive ion mode; (b) Extracted ion chromatogram at the target m/z of 2074; (c) Extracted ion chromatogram of the trifunctional probe at m/z = 1675 and (d) calculated average mass spectrum for the 23.3 to 24.6 min retention time range.	61
3.1	Peptide sequences and characteristic properties of the synthetic pI marker	65
3.2	List of the structures of the 19 UV absorbing pI markers designed by Slais <i>et al</i>	67
3.3	Characteristic properties of the synthetic UV absorbing pI markers	68
3.4	Peptide sequences and characteristic properties of the tetramethylrhodamine - tagged peptide pI markers	70
3.5	Synthetic scheme (left) and the summarized properties (right) of fluorescein -based pI markers	71
3.6	One of the possible generic structures of the pyrene-based pI markers.....	72
3.7	An effective charge versus pH curve generated by SPARC for a pI marker utilizing β -alanine as the source of the buffering groups and N,N-dimethylamino bromoethane as the source of the titrating group.	73
3.8	Synthetic scheme of making the pyrene-based fluorescent pI markers.	83
3.9	Structures of the pyrene-based pI markers synthesized and their calculated pI values	84
3.10	Reaction scheme for making compound <u>2</u>	85
3.11	RP-HPLC analysis of compound <u>2</u> . (Insert: overlay of the UV absorbance spectra of APTS and compound <u>2</u>)	87

3.12	Reaction scheme for making compound 3	87
3.13	(a) ESI mass spectrum (negative ion mode) of compound 3 and (b) RP-HPLC analysis of the reaction mixture and compound 3	89
3.14	Reaction scheme for making compound 4	90
3.15	RP-HPLC analysis of compound 3 and its alkoxy derivatives. (Insert: UV/VIS absorbance spectra of compounds 3 , 4a and 4b).....	91
3.16	ESI mass spectra of compounds 4a and 4b	92
3.17	Reaction scheme for making compound 4c	92
3.18	LC-MS analysis of the reaction mixture of compound 4c	93
3.19	Reaction scheme for making compounds 5 and 6	93
3.20	Overlaid chromatograms of compounds 4 and 5	94
3.21	RP-HPLC analysis of the reaction mixtures obtained during reductive amination to make the respective compound 6 derivatives. (a) general structure of compound 6 , (b) to (f) chromatograms.....	96
3.22	Sulfation of the TEG derivative of compound 6	97
3.23	LC-MS analysis of the sulfation reaction mixture of the histidine derivative of compound 6	98
3.24	ESI mass spectrum of the APTS-based pI marker having a calculated pI value of 3.07 (Insert: chromatogram of the purified compound).....	99
3.25	ESI mass spectrum of the APTS-based pI marker having a calculated pI value of 4.16 (Insert: chromatogram of the purified compound).....	99
3.26	ESI mass spectrum of the APTS-based pI marker having a calculated pI value of 5.73 (Insert: chromatogram of the purified compound).....	100
3.27	ESI mass spectrum of the APTS-based pI marker having a calculated pI value of 7.45 (Insert: chromatogram of the purified compound).....	100
3.28	ESI mass spectrum of the APTS-based pI marker having a calculated pI value of 8.34 (Insert: chromatogram of the purified compound).....	101

3.29	ESI mass spectrum of the APTS-based <i>pI</i> marker having a calculated <i>pI</i> value of 9.42 (Insert: chromatogram of the purified compound).....	101
3.30	ESI mass spectrum of the APTS-based <i>pI</i> marker having a calculated <i>pI</i> value of 10.5 (Insert: chromatogram of the purified compound).....	102
3.31	Detector trace obtained in a PrEMCE experiment.....	106
3.32	The LIF detector trace recorded in a PrMCE experiment with the <i>pI</i> marker having a calculated <i>pI</i> value of 9.42 and loaded as the first band in a background electrolyte of pH 9.6, in a Polybrene-coated capillary.	111
3.33	The LIF detector trace recorded in a PrMCE experiment with the <i>pI</i> marker having a calculated <i>pI</i> value of 4.16 and loaded as the first band at a background electrolyte of pH 3.6, in a Polybrene-coated capillary.	113
3.34	The LIF detector trace recorded in a PrMCE experiment with the <i>pI</i> marker having a calculated <i>pI</i> value of 4.16 and loaded as the first band at a background electrolyte of pH 3.6, in a poly (vinylsulfonate)-coated capillary.....	113
3.35	The LIF detector trace recorded in a PrMCE experiment with the <i>pI</i> marker having a calculated <i>pI</i> value of 4.16 and loaded as the first band at a background electrolyte of pH 3.6, in a cross-linked polyacrylamide coated capillary.....	114
3.36	The LIF detector trace recorded in a PrMCE experiment with the <i>pI</i> marker having a calculated <i>pI</i> value of 4.16 and loaded as the first band at a background electrolyte of pH 3.6, in a Guarant TM capillary (ALCOR Biosystems).	114
3.37	The LIF detector trace recorded in a PrMCE experiment with the <i>pI</i> marker having a calculated <i>pI</i> value of 7.45 and loaded as the first band at a background electrolyte of pH 9.0, in a poly (vinylsulfonate)-coated capillary.....	115
3.38	The LIF detector trace recorded in a PrMCE experiment with the <i>pI</i> marker having a calculated <i>pI</i> value of 7.45 and loaded as the first band at a background electrolyte of pH 9.0, in a Polybrene-coated capillary.....	115
3.39	The LIF detector trace recorded in a PrMCE experiment with the <i>pI</i> marker having a calculated <i>pI</i> value of 7.45 and loaded as the first band at a background electrolyte of pH 9.0, in a cross-linked polyacrylamide coated capillary.....	116

3.40	The LIF detector trace recorded in a PrMCE experiment with the <i>pI</i> marker having a calculated <i>pI</i> value of 7.45 and loaded as the first band at a background electrolyte of pH 9.0, in a Guarant™ capillary (ALCOR Biosystems)	116
3.41	Schematic diagram of the OFFGEL electrophoretic process	117
3.42	The OFFGEL experiment with the <i>pI</i> marker having a calculated <i>pI</i> value of 7.45 (a) loaded into the well numbered 18 and (b) focused into the well numbered 17	119
3.43	Photographs of the fractions collected from the OFFGEL experiment with the <i>pI</i> marker having a calculated <i>pI</i> value of 7.45. The vials were illuminated by the 280 nm beam of a UV light: (a) blank of the focused carrier ampholyte fractions in the absence of a <i>pI</i> marker (background fluorescence, blue); (b) <i>pI</i> marker sample loaded into the well numbered 18 (sample fluorescence green); (c) the collected fractions after 6.2kV hours of focusing and (d) the collected fractions after 17.5 kV hours of focusing....	119
3.44	The pH gradient profile obtained in the OFFGEL experiment after 17.5 kV hours of focusing.	120
3.45	The relationship between the pH gradient profile and focusing volt hours obtained in the OFFGEL experiments with a 4% w/w solution of a 3 < <i>pI</i> < 10 CA mixture (Agilent).	122
3.46	Photographs of the fractions collected from the OFFGEL experiment with the <i>pI</i> marker having a calculated <i>pI</i> value of 4.16. The vials were illuminated by the 280 nm beam of a UV light: (a) <i>pI</i> marker sample loaded into the well numbered 2; (c) the collected fractions after 44.8kVh of focusing..	123
3.47	Photographs of the fractions collected from the OFFGEL experiment with the <i>pI</i> marker having a calculated <i>pI</i> value of 5.73. The vials were illuminated by the 280 nm beam of a UV light: (a) <i>pI</i> marker sample loaded into the well numbered 7; (c) the collected fractions after 24.3kVh of focusing..	124
3.48	Photographs of the fractions collected from the OFFGEL experiment with the <i>pI</i> marker having a calculated <i>pI</i> value of 7.45. The vials were illuminated by the 280 nm beam of a UV light: (a) <i>pI</i> marker sample loaded into the well numbered 19; (c) the collected fractions after 11.9kVh of focusing.	124

3.49 (a) cIEF separation of 7 pyrene-based <i>pI</i> markers, the mobilization trace was obtained by simultaneously applying both pressure (0.5 psi) and potential (21 kV). The gray trace shown is the corresponding current. (b) The relationship between the calculated <i>pI</i> values of the markers and the mobilization times in the run shown in (a).	126
3.50 (a) cIEF separation of 7 pyrene-based <i>pI</i> markers, the trace was obtained using pressure-only mobilization (1 psi). The gray trace is the corresponding current. (b) The relationship between the calculated <i>pI</i> values of the markers and their mobilization time in the run shown in (a).	130
3.51 (a) In this cIEF test, the anodic blocker, analytes dissolved in the CAs and the cathodic blocker were loaded into the capillary as separate segments. (b) cIEF separation of 4 fluorescent <i>pI</i> markers. The gray trace is the corresponding current. (c) The relationship between the <i>pI</i> values of the markers and their mobilization time in the run shown in (b).	132
3.52 Structures of pyrene-based carbohydrate tagging reagents	133
3.53 Reaction scheme of derivatizing D-glucose with the <i>pI4</i> reagent.....	135
3.54 RP-HPLC analysis of samples of (a) D-glucose and (b) maltodextrin ladder derivatized with the <i>pI4</i> reagent.	136
3.55 Overlaid UV absorbance spectra of the <i>pI4</i> derivatizing agent and the derivatized D-glucose.....	137
3.56 ESI mass spectra of D-glucose tagged with the <i>pI4</i> derivatizing agent in positive ion mode (top) and negative ion mode (bottom).	138
3.57 CE analyses of the <i>pI4</i> derivatizing agent and its (a) D-glucose and (b) maltodextrin ladder derivatives	139
3.58 cIEF analyses of the <i>pI4</i> derivatizing agent and its D-glucose derivative	140

LIST OF TABLES

TABLE	Page
2.1 Comparison of the mono-tosylated tetra(ethylene glycol) synthesis and purification methods.....	25
3.1 A list of the possible pyrene-based fluorescent <i>pI</i> markers ($3 < pI < 4$).....	74
3.2 A list of the possible pyrene-based fluorescent <i>pI</i> markers ($4 < pI < 5$).....	76
3.3 A list of the possible pyrene-based fluorescent <i>pI</i> markers ($5 < pI < 7$).....	77
3.4 A list of the possible pyrene-based fluorescent <i>pI</i> markers ($7 < pI < 9$).....	79
3.5 A list of the possible pyrene-based fluorescent <i>pI</i> markers ($9 < pI < 10$).....	80
3.6 Seven synthesized pyrene-based <i>pI</i> markers.....	82
3.7 Background electrolytes used in the PreMCE experiments.....	105
3.8 Comparison of calculated and measured <i>pI</i> values of the pyrene-based <i>pI</i> markers.....	125
4.1 Calculated <i>pI</i> values of the eighteen selected pyrene-based <i>pI</i> markers having a ΔpI of 0.5 and a pyrene-based neutral marker.....	148

1. INTRODUCTION

1.1 Fluorescent Labeling Reagents in Capillary Electrophoresis (CE)

1.1.1 Capillary Electrophoresis for Bioanalysis

In 1981, Jorgenson and Lukacs [1] performed the first high performance zone electrophoretic experiment in an open-tubular capillary of 75 μm i.d. with a separation potential of 30 kV. They successfully separated fluorescent derivatives of standard amino acids, dipeptides and amines, as well as components of a human urine sample, and detected them with a homemade on-column fluorescence detector. They demonstrated a separation efficiency of over 400,000 theoretical plates. CE is known as a rapid and high-resolution separation technique that can handle limited sample amounts such as those encountered in proteomic analysis, especially when coupled with on-line capillary separation-MS detection, allowing high-sensitivity detection, wide dynamic range and high throughput [2].

1.1.2 Fluorescence Detection in CE

Sensitivity is an important issue in bioanalysis where nanomolar or lower sample concentrations are common. The sensitivity of UV absorbance detection in CE suffers from the short light path length across the capillary: detection sensitivity is in the micromolar range. Laser-induced fluorescence (LIF) is one of the alternatives for

This dissertation follows the style and format of *Electrophoresis*.

superior detection sensitivity compared to UV absorbance detection [3]. In 1995, Yeung's group [4] was able to monitor the reaction of a single molecule with LIF detection in a capillary.

1.1.3 Examples of Fluorescent Labels Used in CE

Compared to lasers that operate in the ultraviolet region, lasers that operate in the visible region are usually less expensive and more reliable. The argon-ion laser emitting at 488 nm is the most commonly used laser source with the commercially available CE instruments. A considerable variety of fluorescent dyes had been designed and synthesized [5-9]. One of the most common ways of labeling biomolecules with fluorescent dyes is by reacting them with the amino groups of the lysine residues since lysine is a relatively prevalent amino acid and is most often located at the surface of the protein. Here are some examples of amine-reactive fluorescent labels which can be excited with the argon ion laser [10].

1.1.3.1 Fluorescein [11]

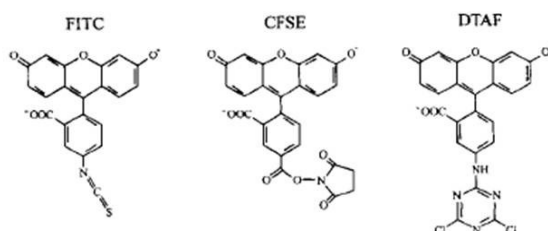


Figure 1.1 Structures of fluorescein-based amine-reactive labeling reagents [11].

Fluorescein possesses high absorptivity and quantum yield which are ideal for highly sensitive detection. Fluorescein-based amine-reactive labeling reagents, structures shown in Figure 1.1, include fluorescein isothiocyanate (FITC), carboxyfluorescein succinimidyl ester (CFSE) and 5-(4,6-dichlorotriazinyl) aminofluorescein (DTAF): they have different labeling reactivities and efficiencies.

1.1.3.2 NBD Dyes [12]

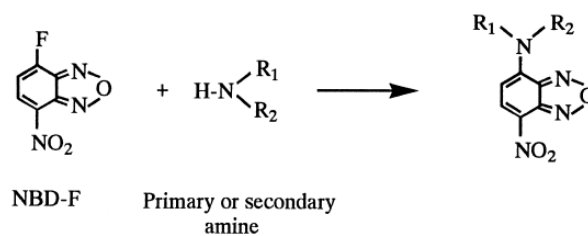


Figure 1.2 Reaction scheme for labeling an amine with NBD-F [12].

The structure of 4-fluoro-7-nitro-2,1,3-benzoxadiazole (NBD-F) is shown in Figure 1.2. It has been reported that the fluorescence of NBD derivatives is independent of pH in the 2 to 9 range. However, the fluorescence intensity is sensitive to solvent polarity.

1.1.3.3 FQ and CBQCA [13, 14]

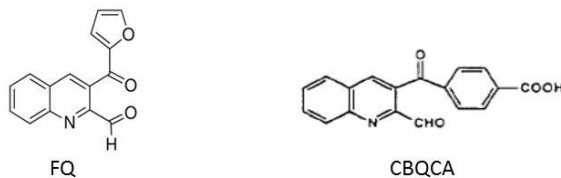


Figure 1.3 Structures of FQ [13] and CBQCA [15].

3-(2-Furoyl)quinoline-2-carboxyaldehyde (FQ) and 3-(4-carboxybenzoyl)-2-quinolinecarboxaldehyde (CBQCA) showed in Figure 1.3 are both quinolone based fluorogenic labels that react with amines forming fluorescent isoindoles.

1.2 Requirements and Limitations of Existing Fluorescent Labeling Reagents

High fluorescence intensity and good quantum yield basically define a good fluorophore, however, it's not enough for fluorescent labeling reagents used in CE. The required properties and limitations of the current fluorescent labeling reagents for CE are discussed as follows.

1.2.1 Good Water Solubility

Labeling reagents with good water solubility are crucial in CE since most of the CE experiments are carried out in aqueous background electrolytes (BGEs). Water miscible organic solvents and detergents can be used to improve the solubility of the fluorophore but it doesn't work for tests in which ionic strength and pH are critical. Moreover, if not

used in a hydrophilic coated capillary, there is hydrophobic interaction between the hydrophobic fluorophore core and the wall of the fused silica capillary that results in adsorption and seriously tailed peaks. It's been reported that the solubilities of proteins were altered by labeling due to the hydrophobicity of Cy-dyes [16]. One way of making a more water soluble dye is by modifying the fluorophore with strong electrolyte functional groups. For example, introduction of sulfonate groups on cyanine dyes had been reported [17, 18].

1.2.2 pH-Dependent Fluorescence

pH is an important parameter in CE; some measurements will be hindered or limited if the fluorescent spectral properties of a fluorophore vary with pH of the BGEs. This property is especially critical in capillary isoelectric focusing (cIEF) analysis where the pH changes in the capillary, *e.g.*, from 3 to 10. Fluorophores that have weak acid or weak base functional groups conjugated to an aromatic ring structure often display pH-dependent fluorescence. For instance, the fluorescence of rosamine showed in Figure 1.4 is less pH sensitive than that of fluorescein in acidic solutions due to the removal of the carboxylate group from the conjugation [19].

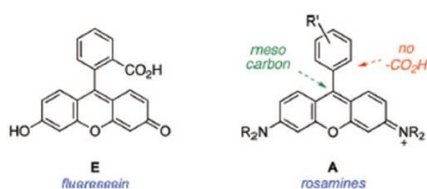


Figure 1.4 Structures of fluorescein and rosamine [19].

1.2.3 Changes in Analyte Properties After Labeling

Often, the properties of the analytes change after labeling. For example, the size, overall charge, hydrophobicity, *etc.* can change. A change in the charge-to size ratio influences the electrophoretic mobility. If the degree of modification is relatively high and derivatization is random, a mixture of labeled products can be obtained leading to a group of distributed peaks in CE analysis. A more selective and specific labeling mechanism is the solution to the problem. In amine-reactive labeling, an amino group is replaced with a label and the overall charge of the analyte can be altered accordingly. Exchanging a basic amino group by an acidic moiety on a protein may lead to a noticeable change in the pI value which alters the results in cIEF analysis. In this case, a better approach would be a basic label which minimizes the change in the pI value of the analyte [20].

1.3 Capillary Isoelectric Focusing (cIEF)

1.3.1 Principle of cIEF

Isoelectric focusing (IEF) is a separation technique which separates ampholytic components based on differences in their isoelectric points. IEF is frequently used for the separation of peptides and proteins. Isoelectric point is defined as the pH at which the ampholyte is immobile in an electric field [21]. In IEF, since the surface charge of an ampholyte depends on the pH, the ampholyte moves with its corresponding mobility along the pH gradient until it reaches a position where its net mobility decreases to zero: the pH at this position indicates the pI value of the ampholyte. Capillary IEF (cIEF) is

an IEF process taking place in a capillary. A pH gradient can be created in a capillary by using a mixture of carrier ampholytes (CAs), *i.e.*, a mixture of polyamino polycarboxylic acids. Before applying voltage, the pH is uniform in the capillary and it is set by the mixture of CAs. Once the voltage is switched on, electrophoretic transport causes the CAs to migrate based on their transient mobility determined by the environment. For example, take a CA with a pI value of 3 in a CA mixture of pI 3 to 10: it remains anionic through out most of the capillary and tends to move toward the anode. It becomes neutral and stops moving until it gets protonated by a more acidic molecule. A higher degree of protonation is also possible: it converts the pI 3 CA into a cationic specie and makes it to move toward the cathode. This pendulum-like motion keeps the pI 3 CA in a confined band and if the concentration of the CA is high enough, sets the local pH equal to the pI of the CA. The same behavior applies to the rest of the CAs: the CAs get focused and stacked according to their pI values forming a pH gradient [22].

1.3.2 cIEF Technologies

1.3.2.1 Mobilization Mode and Detection

When a cIEF separation is monitored with a fixed, single-point detector, the focused, isoelectric, non-moving components need to be moved past the detector to obtain the cIEF trace. There are two types of mobilization techniques: “hydrodynamic” and “electrophoretic”. Hydrodynamic mobilization can be generated by either pressure [23, 24] or gravity [25]. An electric field is sometimes maintained during hydrodynamic mobilization to minimize the band broadening caused by the laminar flow [25-27].

Electrophoretic mobilization is also called chemical or salt mobilization: it can be done by exchanging the analyte with the catholyte or *vice versa* [28]. For instance, by replacing the hydroxide ion in the catholyte by another anion, (e.g., acetate), the pH will decrease in the cathodic end of the capillary, the high *pI* components become protonated and move past the detection window toward cathode. It is a cationic isotachophoretic (ITP) process with hydronium acting as the leading electrolyte [29]. In these “two-step” cIEF experiments, mobilization is initiated after focusing is finished. A moderately strong EOF had also been utilized in cIEF for mobilization. In this manner, focusing and mobilization occur simultaneously yielding what is considered a “one-step” cIEF process. One of the challenges in this case is to balance electrophoretic transport (focusing) and electroosmotic displacement to avoid incomplete focusing before the components are pumped out of the capillary [30, 31].

1.3.2.2 Capillary

Coated capillaries are used in most of the cIEF experiments for two main reasons, to minimize the adsorption of analytes on the capillary wall, and to control the EOF. Proteins and peptides are polyvalent ampholytes and their surface charges change depending on the pH: the resulting electrostatic interaction can cause adsorption on the bare fused silica wall. Depending on the structure of proteins, hydrophobic interactions are also possible with the wall of the fused silica capillary. A coating with neutral and hydrophilic surface properties is the most suitable choice for cIEF use. A linear polyacrylamide (LPA) coating was developed by Hjerten [32] which includes the

coupling of 3-methacryloxypropyltrimethoxysilane to the silanol groups of the capillary wall, and is followed by copolymerization with acrylamide. LPA-coated capillaries have been widely used in cIEF [33-35]. Gao and Liu [36] later improved the stability of the LPA coating by incorporating a cross-linking reagent to make crosslinked polyacrylamide (CPA). This coating covers the capillary wall more completely, leads to better suppression of the EOF and is more resistant to hydrolytic degradation.

Hydrophilic polymers are also used to dynamically coat bare fused silica capillaries, alone or in combination with covalently coated capillaries [37]. For example, soluble cellulose derivatives [38, 39], poly(vinyl alcohol) (PVA), linear PAA [40] and poly(ethylene glycol) [31, 41] were used as dynamic coating agents in cIEF.

1.3.2.3 Additives

In cIEF, the analyte is concentrated during focusing. In addition, its solubility decreases when it reaches its *pI*. Sample precipitation after focusing is more pronounced for proteins. The additives used in the cIEF mixture to improve the solubility of proteins and avoid their precipitation are called solubilizers. The solubilizers have to be neutral or zwitterionic components: for example, urea [42, 43], glycerol [33, 44], ethylene glycol, propylene glycol [45], *etc.* Another type of additive used in cIEF is called a blocker or a sacrificial agent [46, 47]. Bidirectional isotachopheresis (ITP) in cIEF can cause the loss of CAs at both the acidic and basic edges of the pH gradient. To overcome this problem, one can add ampholytic components that have higher and lower *pI* values than the *pI* values of the CAs in the pH gradient. In this case, instead of losing

the CAs which participate in building the pH gradient, the blocker moves out of the capillary first by ITP leaving behind the CAs of interest in the capillary.

1.3.2.4 Carrier Ampholytes

“Two ampholytes, *e.g.* proteins can only be separated by stationary electrophoresis if there is a third ampholyte with an intermediate isoelectric point,” stated Vesterberg [48], based on Svensson’s work in 1962 [21]. Ampholytes are characterized by the number of protolytic groups and their corresponding pK_a values. For most of the low-molecular ampholytes, the pI value can be calculated from the two pK_a values that exert the greatest influence on the ionization of the molecule around the pI value according to the following equation (1.1) [21]:

$$pI = \frac{1}{2} (pK_{a1} + pK_{a2}) \quad (1.1)$$

where $pK_{a1} < pI < pK_{a2}$.

For an ampholyte focused at its own pI , if its pK_{a1} and pK_{a2} values are close enough to each other, the focused band will contain - along with the zwitterions - an appreciable amount of cations and anions. These contribute to conductance over the pH gradient. Also, the buffering capacity of an ampholyte is proportional to the slope of the titration curve. In this case, the closer the two pK_a values, the more their dissociation steps overlap, which results in a steeper slope in the titration curve [49].

A good carrier ampholyte should have ΔpK_a ($pI - pK_a$) values as low as possible and no greater than 2 pH units. Righetti [50] called it the iron law of Svensson-Rible and this law can be understood by considering Figure 1.5 in which the buffering power (β) of both lysine and bicine are plotted against pH. Lysine has a pI of 9.8 and exhibits a high buffering power at its pI . On the other hand, bicine which is one of Good's buffers has a pI of about 5.1 where the buffering capacity is close to zero because, as can be seen in the graph, the two pK_a values of bicine are at least 6 pH units apart.

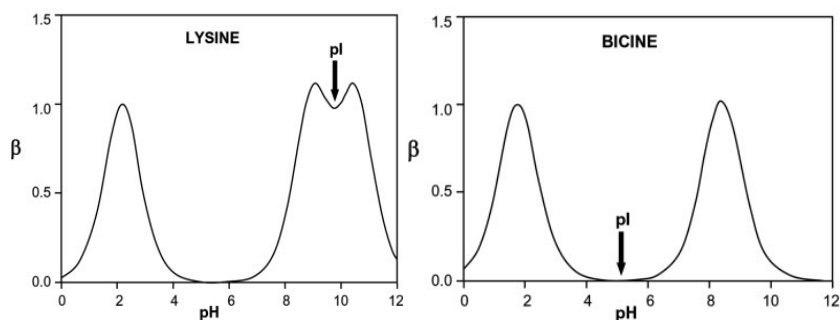


Figure 1.5 The relationship of buffering power (β) and the pK_a values which determine the pI of lysine and bicine [50].

Vesterberg [48] summarized the desired properties of carrier ampholytes as follows: (1) The carrier ampholytes should have a buffering capacity of at least 0.3 $\mu\text{equiv}/\text{mg pH}$. (2) The adjacent carrier ampholytes should have pI value differences of less than 0.1 to permit a reasonable resolution. (3) The pI values of carrier ampholytes should cover the 2.5-11 range allowing the separation of most proteins. (4) Carrier ampholytes must have good water solubility to avoid their precipitation after focusing. (5) The carrier

as the third dimension. Based on the analysis, the molecular weights of CAs were found to be between 200 and 1,200. For a given molecular weight, the CAs in the acidic range had higher numbers of isoforms than in the basic range. The focusing behavior of CAs was correlated by the number of Rotofor fractions in which they were found: a decrease in focusing efficiency was seen from the acid (pH 2-4) to the basic (pH > 8) end of CAs.

1.4 pI Markers

A pI marker is an ampholytic compound with a known pI value and is used to profile the pH gradient. The theoretical background for the selection and design of pI markers is discussed in [21, 27, 53, 54]. The focusing ability of an ampholytic component in IEF depends on its $-d\mu/d(\text{pH})$ value at its pI, *i.e.* $[-d\mu/d(\text{pH})]_{\text{pI}}$, where μ denotes the effective electrophoretic mobility of the ampholyte. Since μ is roughly proportional to the charge, $[-d\mu/d(\text{pH})]_{\text{pI}}$ is approximately proportional to $[-dz/d(\text{pH})]_{\text{pI}}$, where z is the net charge of an ampholyte at a given pH. The relation of $[-dz/d(\text{pH})]_{\text{pI}}$ to the $\text{p}K_{\text{a}}$ values of the ampholyte can be described by Equation (1.2) [27]:

$$[-dz/d(\text{pH})]_{\text{pI}} = 2.303 \sum_i \frac{K_{a_i} 10^{-\text{pI}}}{(K_{a_i} + 10^{-\text{pI}})^2} \quad (1.2)$$

The length of the focused ampholytes zones, expressed as the zone variance, σ^2 , can be calculated as [54]:

$$\sigma^2 = RT / \{FE[-dz/d(pH)]_{pI} d(pH)/dx\} \quad (1.3)$$

where R is the universal gas constant, F is the Faraday constant, E is the electric field strength and $d(pH)/dx$ is the steepness of the pH gradient at the pI value. Based on the above equations, the value of $[-dz/d(pH)]_{pI}$ becomes large when the pK_a value is close to the pI of the ampholyte. Since it is inversely proportional to σ^2 , the greater the value of $[-dz/d(pH)]_{pI}$ the narrower the focused ampholyte band. It has been reported that an ampholyte should have a $[-dz/d(pH)]_{pI}$ value larger than 0.045 to focus into a band. The types of pI markers are discussed in 3.1.1.

2. DEVELOPMENT OF A HYDROPHILIC ACRIDINE-BASED AMINE-REACTIVE FLUORESCENT LABELING REAGENT THAT HAS pH-INDEPENDENT SPECTRAL PROPERTIES

2.1 Design and Synthesis

2.1.1 Background and Objective

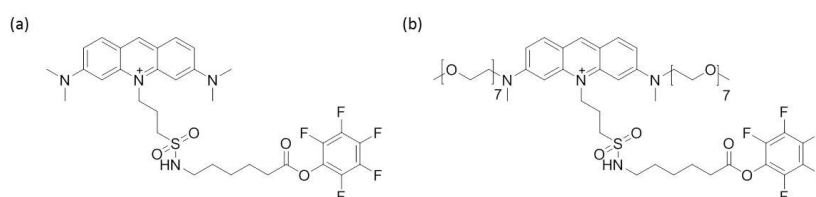


Figure 2.1 (a) Acridine orange-based and (b) Me₂HEG₂-DAA-based amine-reactive fluorescent labeling reagent.

An ideal fluorescent labeling reagent for capillary electrophoresis should exhibit the following properties [55]: (1) high purity; (2) high solubility in water; (3) high stability of the conjugate; and (4) strong and pH-independent fluorescence emission of the conjugates. Acridine orange can be obtained in high purity and it has a visible-range $\lambda^{\text{ex}}_{\text{max}}$ around 490 nm making it compatible with the 488 nm line of the argon ion laser. In addition, it possesses pH-independent fluorescent properties. An acridine orange-based amine-reactive monocationic fluorescent labeling reagent [56], shown in Figure 2.1 (a), synthesized in our laboratory, has most of the desired properties mentioned above, except for good aqueous solubility. Acridine orange is not appreciably soluble in water.

When an acridine orange-based fluorescent label was used in capillary electrophoresis with an aqueous background electrolyte, serious peak tailing was observed due to hydrophobic adsorption of the acridine orange core on the silica wall of the capillary. At least 20% of a water-miscible organic solvent, such as acetonitrile, dimethylformamide or dimethylsulfoxide had to be added to the background electrolyte for the acridine orange-based fluorophore to have a reasonably shaped peak. To improve the aqueous solubility of the core fluorophore while maintaining the desired spectral properties of the acridine-based fluorescent reagent, we designed a hydrophilic version of the acridine-based fluorophore by connecting oligo(ethylene glycol) groups to the acridine core structure (Figure 2.1 (b)).

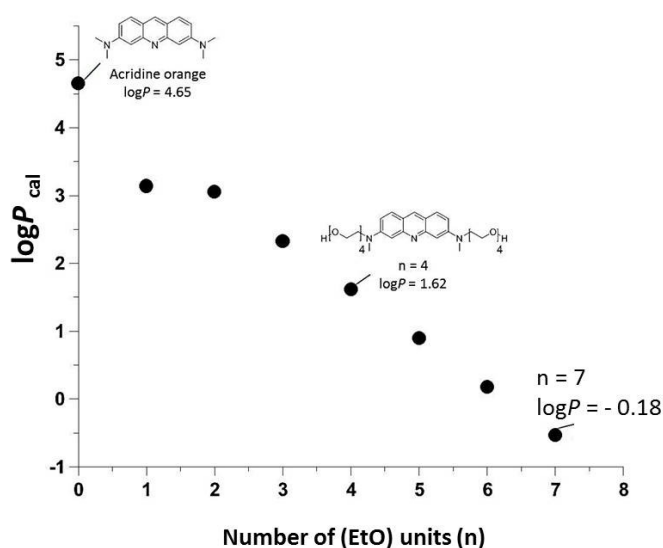


Figure 2.2 Calculated $\log P$ of $[(\text{EtO})_n]_2\text{-DAA}$ as a function of the mer-number of the ethoxy groups.

$\log P$ serves as an indication of the hydrophobicity of a component as shown in Equation 2.1:

$$\log P_{\frac{octanol}{water}} = \log \frac{[solute]_{octanol}}{[solute]_{water}} \quad (2.1)$$

where P is the partition coefficient, a ratio of the concentrations of a component partitioned between n-octanol and water. The calculated $\log P$ values are plotted in Figure 2.2 as a function of the mer-number of the ethoxy groups on DAA. Acridine orange has a calculated $\log P$ value of about 4.65. By replacing a methyl group on both amino groups with a tetra(ethylene glycol) ($n = 4$) group, calculated $\log P$ drops to 2.33, representing a solubility in water that is about 200 times higher. To improve the solubility of the fluorescent label in aqueous solutions and decrease its hydrophobic adsorption on surfaces, we decided to make a hepta-ethoxy substituted DAA, $n = 7$, for which the calculated $\log P$ value becomes -0.18.

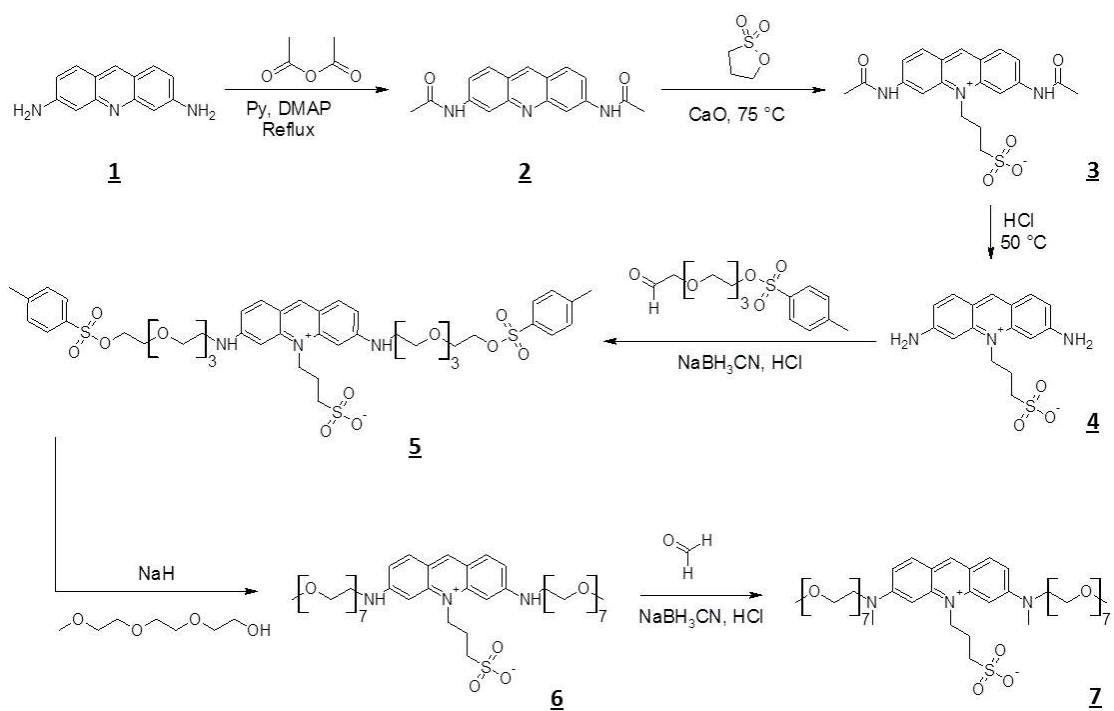


Figure 2.3 Synthesis scheme for making HEG₂Me₂-DAAPS.

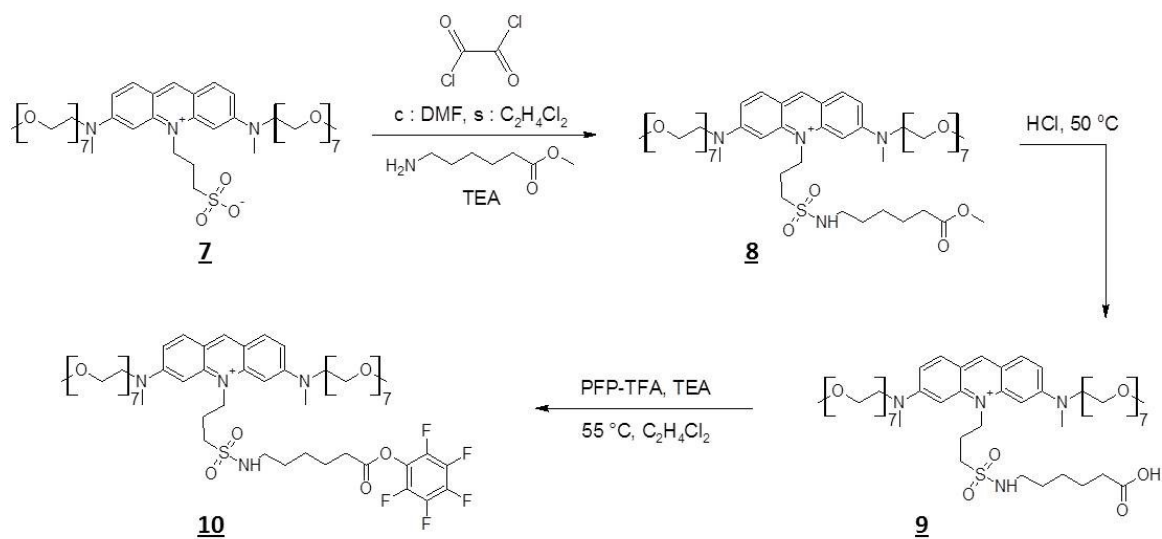


Figure 2.4 Synthesis scheme for elongation of the tether and activation of the HEG₂Me₂-DAA-based amine-reactive fluorescent labeling reagent.

The Me₂HEG₂-DAA-based amine-reactive fluorescent labeling reagent was synthesized according to the reaction schemes shown in Figures 2.3 and 2.4. First, (AcO)₂-DAA was quaternarized with 1,3-propane sultone, followed by the hydrolysis of the amide groups to get DAAPS. Two mono-tosylated tetra(ethylene glycol) groups were connected to DAAPS through reductive amination of DAAPS and the tetra(ethylene glycol) chains were elongated with 2-(2-(2-methoxyethoxy)ethoxy)ethanol to make (HEG)₂-DAAPS. To maintain the desired spectral properties of acridine orange, DAAPS needed to be tetraalkylated. Therefore, formaldehyde was used to alkylate the two secondary amino groups and make Me₂(HEG)₂-DAAPS. The fluorophore was then connected to methyl 6-aminohexanoate, followed by hydrolysis of the ester group to get FL-CA. FL-CA was then activated with pentafluorophenyl trifluoroacetate to form amine reactive FL-CAPFP.

2.1.2 Materials and Method

2.1.2.1 Chemicals and Equipment

3,6-Diaminoacridine (DAA), tetra(ethylene glycol), acetonitrile, dimethyl sulfoxide, dichloromethane, phosphorus pentoxide, triethylamine, sodium cyanoborohydride, 4-dimethylaminopyridine, pyridine, dimethylformamide, hydrochloric acid, sodium hydride, anhydrous tetrahydrofuran, methanol, oxalyl chloride, dichloroethane and pentafluorophenyl trifluoroacetate were purchased from Sigma-Aldrich Co. (St. Louis, MO). Water used in the HPLC and CE experiments was from Mallinckrodt Chemical Co. (St. Louis, MO). The source of calcium hydroxide used in this work was hydrated

lime (Voluntary Purchasing Group, Inc., Bonham, TX). Methyl 6-aminohexanoate used in the synthesis was made in-house by refluxing 6-aminocaproic acid with methanol with a catalytic amount of hydrochloric acid [57]. An HPLC system containing a solvent delivery module Model 126, an auto injector Model 508 and a photodiode array detector Model 168 operating under 32 Karat software control (Beckman-Coulter, Fullerton, CA) was used for reaction monitoring. RP separations were obtained on a 4.6 mm I.D., 75 or 150 mm long analytical column packed with a 3 μm Gemini C18 stationary phase (Phenomenex, Torrance, CA). LC-MS analysis was performed with an ion trap LC-MS 6300 system operating under ChemStation software control (Agilent Technologies, Santa Clara, CA). The column used in the LC-MS analysis was a 2 mm I.D., 150 mm long analytical column packed with a 3 μm Gemini C18 stationary phase (Phenomenex, Torrance, CA). The CE experiments were carried out with a ProteomLab PA 800 system coupled with a LIF detector using a 488 nm argon ion laser module (Beckman-Coulter, Fullerton, CA). Separations were obtained in 50 μm I.D., 360 μm O.D. bare fused silica capillary columns (Polymicro Technologies, Phoenix, AZ) having total and inlet-to-detector lengths of 30 and 20 cm, respectively.

2.1.2.2 Synthesis of Mono-Tosylated Tetra(Ethylene Glycol) (mTs-TEG)

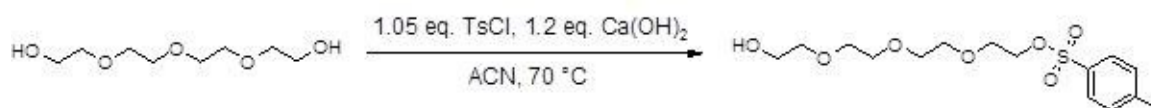


Figure 2.5 Reaction scheme for making mono-tosylated tetra(ethylene glycol).

Reaction scheme for making mono-tosylated tetra(ethylene glycol) is shown in Figure 2.5. An 18.60 g portion of hydrated lime was mixed with 50 ml of acetonitrile and heated at 70 °C with stirring. 38.84 g of tetra(ethylene glycol) and 40.04 g of tosyl chloride were dissolved in 40 ml acetonitrile and carefully added into the heated acetonitrile slurry of lime. The reaction was carried at 70 °C with good stirring for 15 min, then the mixture was cooled with an ice bath. Progress of the reaction was monitored by gradient RP-HPLC with a PDA detector (3 µm, Gemini-C18 stationary phase, 75×4.6 mm column, 1 ml/min flow rate, initial mobile phase composition 60:40 A:B, gradient time 18 min, final mobile phase composition 100 % B, A: water; B: methanol, both with 5 mM ammonium formate, pH 4.5). Based on the integration of the peaks at 260 nm in the chromatogram, approximately 10 % of bis-tosylated tetra(ethylene glycol) was formed. Once the reaction was complete, the solids were removed from the reaction mixture by filtration. Then, the acetonitrile filtrate was diluted sixfold with water and the mixture was centrifuged. Bis-tosylated tetra(ethylene glycol) was separated from the mono-tosylated tetra(ethylene glycol) as an oil phase that formed at the bottom of the centrifuge tube. The tosylation reaction was done with 50 g tetra(ethylene glycol) batches and had a 67 % final, isolated yield with about 99 % purity (based on the integration of the peaks at 260 nm).

The conventional way of making mono-tosylated tetra(ethylene glycol) calls for reacting tosyl chloride with excess tetra(ethylene glycol) at low temperature (0 °C) under basic conditions. The reaction time is hours-to-days long and excess unreacted tetra(ethylene

glycol) makes purification troublesome [58]. In this work, the tosylation reaction was carried out at 70 °C and was completed in 15 min with only 1.05 equivalent of tetra(ethylene glycol). In this work, Ca(OH)₂ from hydrated lime was used as the base, and the reaction byproduct, CaCl₂ remained insoluble in the reaction mixture making for very easy removal by simple filtration. The chromatogram for the reaction mixture is shown in Figure 2.6 (a): about 88 % of the product and 12 % bis-tosylated byproduct were formed after 15 min. The work-up procedure included sixfold dilution of the acetonitrile reaction mixture with water, followed by centrifugation to force phase separation of the approximately 12 % bis-tosylated tetra(ethylene glycol) from the majority of mono-tosylated tetra(ethylene glycol). Both phases from the workup were analyzed by RP-HPLC and the chromatograms are shown in Figure 2.6 (b) and (c), respectively. The ¹H NMR spectrum and EIS mass spectrum of structure of mono-tosylated tetra(ethylene glycol) is shown in Figure 2.7 and 2.8. Mono-tosylated tetra(ethylene glycol) was obtained with approximately 99 % purity. Compared to the conventional methods summarized in Table 2.1, we were able to develop an unique synthesis and purification scheme to obtain mono-tosylated tetra(ethylene glycol) inexpensively, and with high purity.

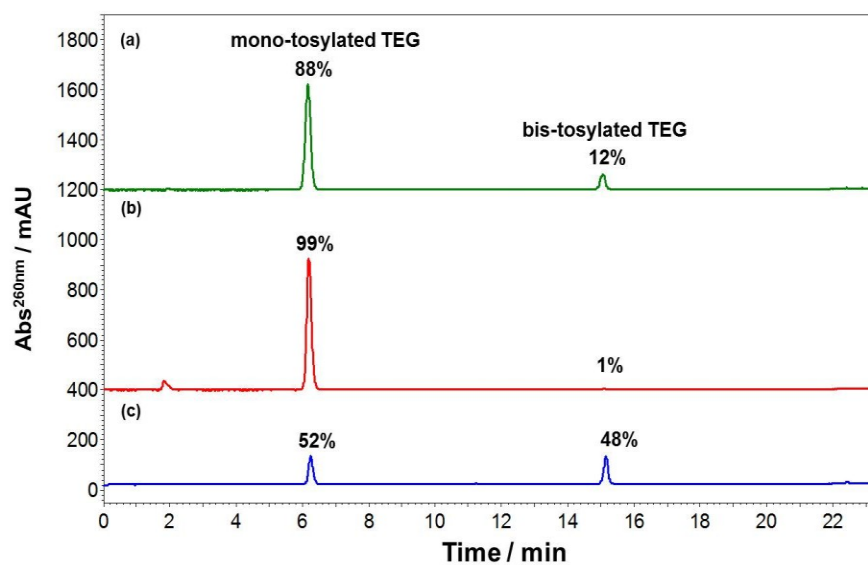


Figure 2.6 RP-HPLC of (a) mono-tosylated TEG reaction mixture, (b) aqueous phase obtained after work-up, (c) oil phase obtained after workup.

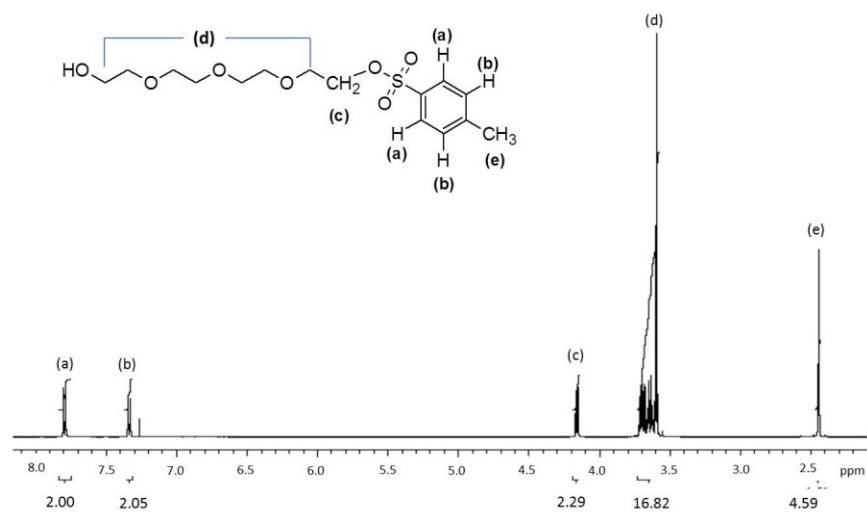


Figure 2.7 ^1H NMR spectrum of mono-tosylated tetra(ethylene glycol) in CDCl_3 .

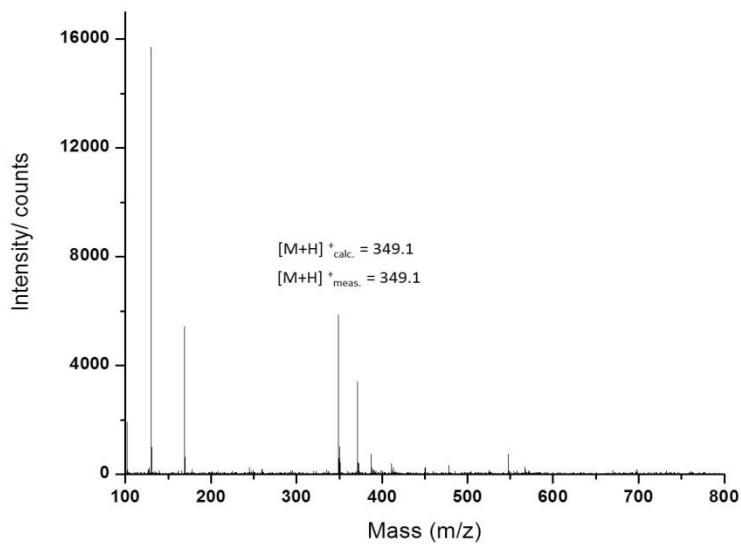


Figure 2.8 ESI mass spectrum of mono-tosylated tetra(ethylene glycol).

Table 2.1 Comparison of the mono-tosylated tetra(ethylene glycol) synthesis and purification methods.

Reaction conditions	Literature[58-61]	This work
Eq of TsCl	0.2	1.05
Base	NaOH, pyridin, Ag ₂ O	Ca(OH) ₂
Reaction temperature	0 °C to RT	70 °C
Reaction time	15 min to 18 h	15 min
Workup	Column chromatography	Filtration, phase separation by centrifugation
Yield (%)	54 to 85	70
Cost	\$ 3,000 / g *	< \$ 0.5 / g

*A quote received on August 28, 2008 from Sinochemexper.

2.1.2.3 Synthesis of Mono-Tosylated Tetra(Ethylene Glycol) -Aldehyde [62]

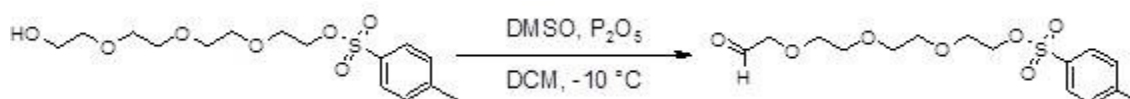


Figure 2.9 Reaction scheme for making mono-tosylated TEG-aldehyde.

Reaction scheme for making mono-tosylated TEG-aldehyde is shown in Figure 2.9.

1.33 g of dimethyl sulfoxide was dissolved in 1 ml of dichloromethane and added into 10 ml dichloromethane with 2.43 g of P_2O_5 under stirring at $-10\text{ }^\circ\text{C}$. Dimethyl sulfoxide was activated by P_2O_5 to form a complex [63] which facilitates the conversion of alcohol to aldehyde. After 1 min, 1.28 g of mono-tosylated tetra(ethylene glycol) in 3 ml dichloromethane was added into the dimethyl sulfoxide / P_2O_5 reaction mixture. After the addition of mono-tosylated tetra(ethylene glycol), the $-10\text{ }^\circ\text{C}$ bath was removed and the reaction mixture was stirred at room temperature. Progress of the reaction was monitored by gradient elution RP-HPLC with a PDA detector (3 μm , Gemini-C18 stationary phase, 75 \times 4.6 mm column, 1 ml/min flow rate, initial mobile phase composition 60:40 A:B, gradient time 18 min, final mobile phase composition 100 % B, A: water; B: MeOH, both with 5 mM ammonium formate). 7 ml of triethylamine was added slowly to the reaction mixture under $-10\text{ }^\circ\text{C}$ to quench the reaction. The final yield of aldehyde was 65 % based on the integration of the peaks at 260 nm in the chromatogram. Aldehyde formation was confirmed by ^1H NMR as shown in Figure 2.10 using the signature chemical shift of the aldehyde group at around 10 ppm.

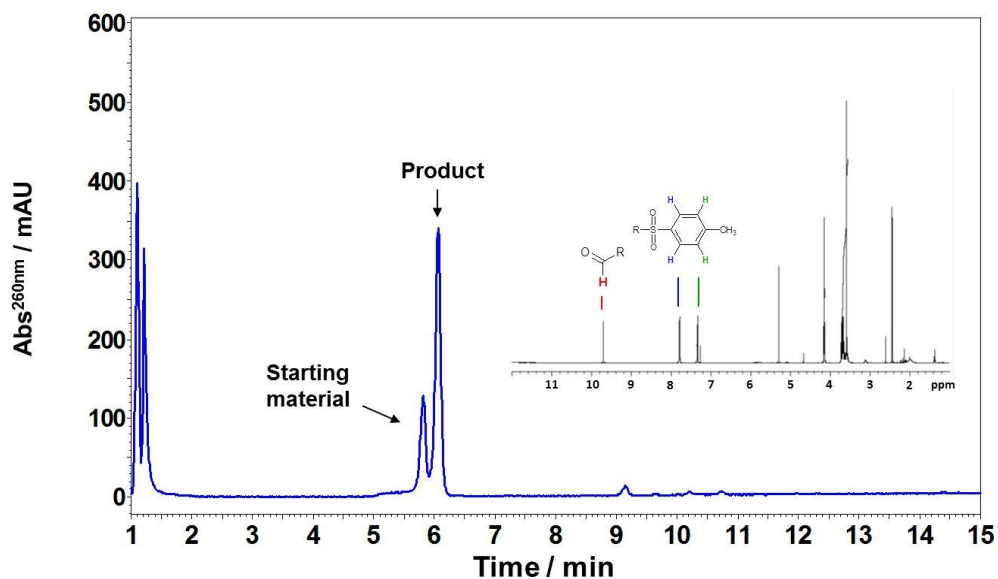


Figure 2.10 RP-HPLC analysis of the mono-tosylated tetra(ethylene glycol)-aldehyde reaction mixture. (Insert: ^1H -NMR spectrum of mono-tosylated tetra(ethylene glycol)-aldehyde).

2.1.2.4 Synthesis of DAAPS (**4**) [64]

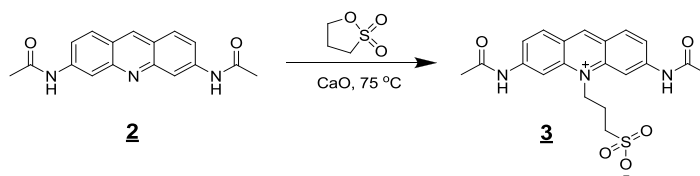


Figure 2.11 Reaction scheme for making $(\text{AcO})_2$ -DAAPS.

Reaction scheme for making $(\text{AcO})_2$ -DAAPS is shown in Figure 2.11. Our first attempt to make Me_2HEG_2 -DAAPS was to quaternarize Me_2HEG_2 -DAA with 1,3-propane

sultone. This route failed to give fair conversion: probably, the oligo(ethylene glycol) groups hindered reaction with the ring nitrogen atom. We took an alternate approach by quaternarizing AcO₂-DAA first, then building the oligo(ethoxy)methyl chains. AcO₂-DAA (**2**) was synthesized by refluxing DAA (**1**) with acetic anhydride, 4-dimethylaminopyridine and pyridine.

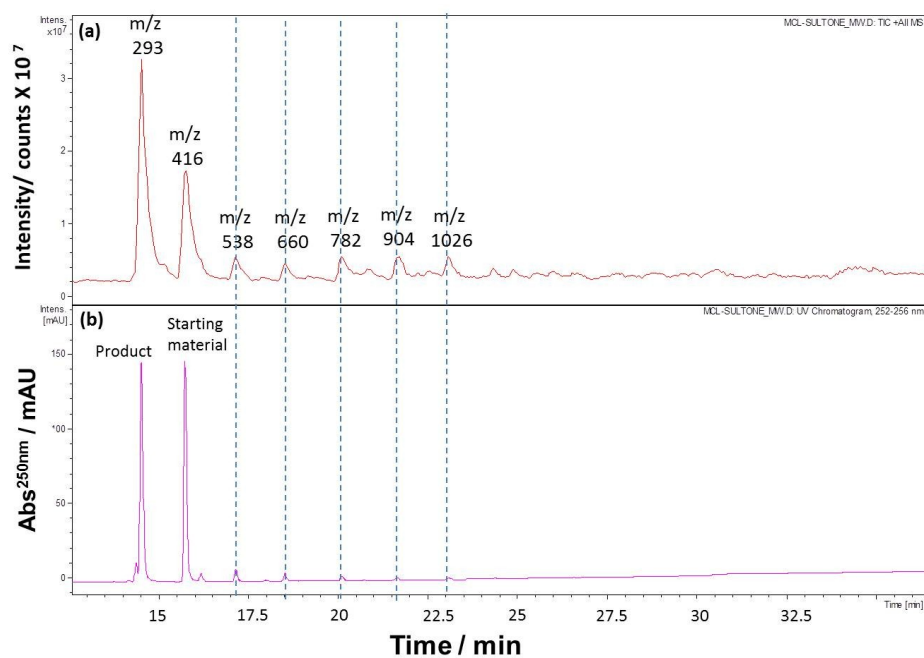


Figure 2.12 LC-MS analysis of the AcO₂-DAA and 1,3-propane sultone reaction mixture after 7 minutes of heating in a microwave oven. (a) TIC, (b) UV absorbance trace at 250 nm.

Quaternarization of AcO₂-DAA was tried in a conventional microwave oven first. After heating the reaction mixture of AcO₂-DAA and 1,3-propane sultone for 7 minutes in the microwave oven, LC-MS analysis as shown in Figure 2.12 indicated that the conversion

rate was only about 50 % and byproducts were formed with repeating $\Delta m/z$ of 122, which indicates oligomerization of 1,3-propane sultone.

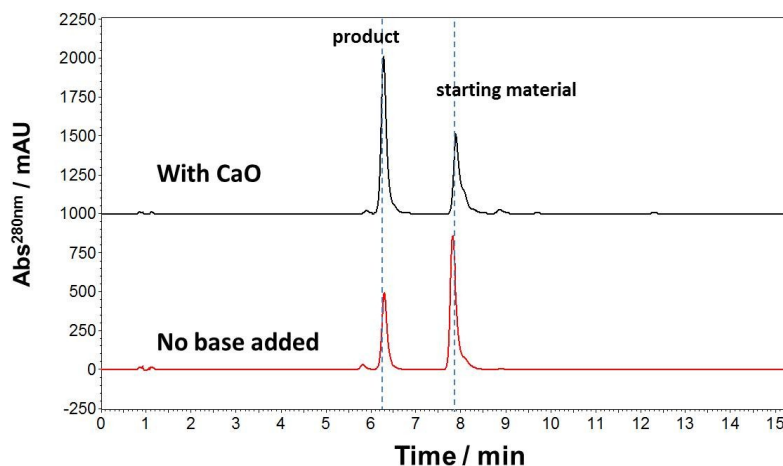


Figure 2.13 RP-HPLC of the reaction mixture of AcO₂-DAA with CaO and without base.

Quaternarization of AcO₂-DAA was improved by base addition as shown in Figure 2.13. K₂CO₃, Cs₂CO₃ and CaO were tested during reaction optimization. CaO gave higher conversion rates than the other two bases tested.

The final optimized quaternarization conditions used 3.5 g of AcO₂-DAA and 0.25 g of calcium oxide in 40 g of melted 1,3-propane sultone at 75 °C with stirring. After 40 min of heating, the reaction mixture was washed 5 times with 80 ml of dichloromethane (total volume of 400 ml) to remove excess 1,3-propane sultone. Next, 100 ml of 0.3 M aqueous solution of acetic acid was added to dissolve CaO, then the reaction mixture

was filtered. The remaining solid was washed three times with 40 ml of dimethylformamide (total volume of 120 ml) to get AcO₂-DAAPS (**3**). Reaction progress and the work-up steps were monitored by RP-HPLC with a PDA detector. Chromatograms for the reaction mixture and the product after work-up are shown in Figure 2.14. ESI mass spectrum of AOC₂-DAAPS is shown in Figure 2.15. AcO₂-DAAPS was hydrolyzed by dissolving it in 1 M HCl and heating the solution at 50 °C for 1 h to get DAAPS (**4**).

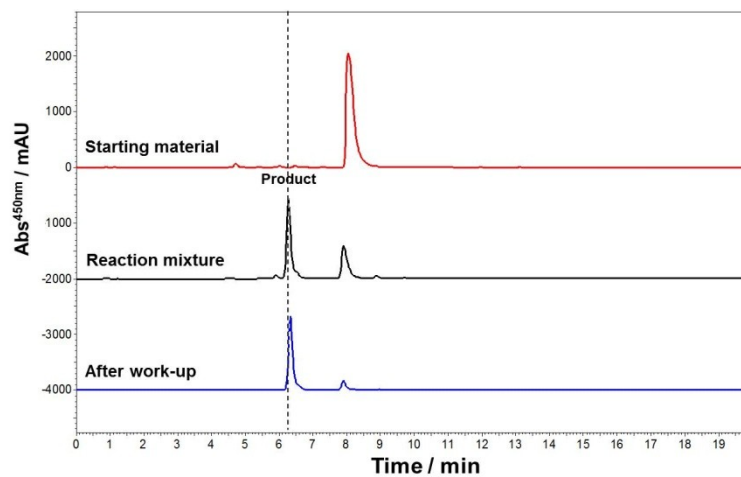


Figure 2.14 RP-HPLC of (a) AcO₂-DAA, (b) quaternarization reaction mixture of AcO₂-DAA, (c) product after workup.

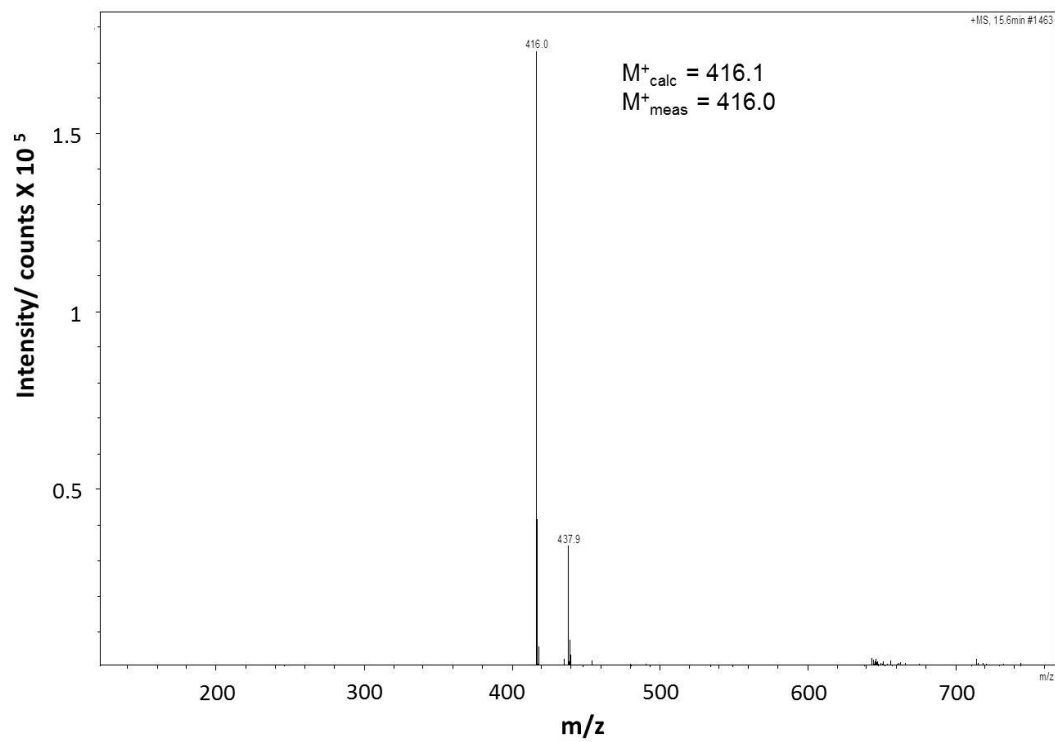


Figure 2.15 ESI mass spectrum of AOC₂-DAAPS.

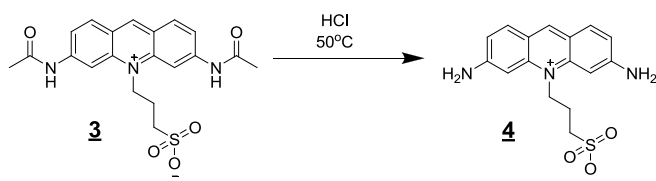


Figure 2.16 Reaction scheme for making DAAPS.

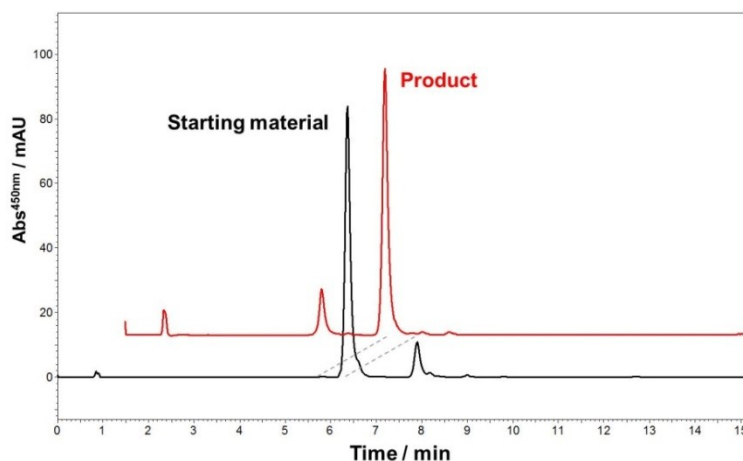


Figure 2.17 RP-HPLC of AcO₂-DAAPS and of the reaction mixture during hydrolysis of AcO₂-DAAPS.

Once AcO₂-DAAPS was made, it was treated with 1 M HCl at 50 °C to get DAAPS as shown in Figure 2.16. The reaction was monitored with RP-HPLC as shown in Figure 2.17. The main byproducts were unreacted AcO₂-DAA and DAA before and after the hydrolysis reaction, respectively.

2.1.2.5 Synthesis of TsTEG₂-DAAPS (**5**)

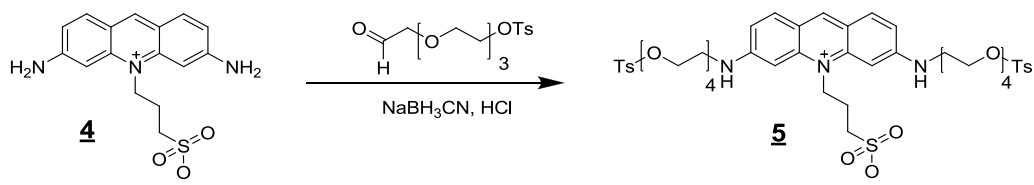


Figure 2.18 Reaction scheme for making TsTEG₂-DAAPS.

Mono-tosylated tetra(ethylene glycol)aldehyde was mixed with DAAPS in a 1 : 1 mixture of dimethylformamide and H₂O that also contained 0.75 M HCl_(aq). The same equivalents of NaBH₃CN and aldehyde were used in the reductive amination reaction. Progress of the reaction was monitored by RP-HPLC with a PDA detector. Figures 2.18 and 2.19 show the reaction scheme and monitoring of the making of TsTEG₂-DAAPS. It required about 15 equivalents of aldehyde and NaBH₃CN to push the formation of TsTEG₂-DAAPS to completion. A small amount of tri-alkylated products was also observed: they were eluted with a retention time of 23 min. TsTEG₂-DAAPS was purified from the reaction mixture by preparative HPLC.

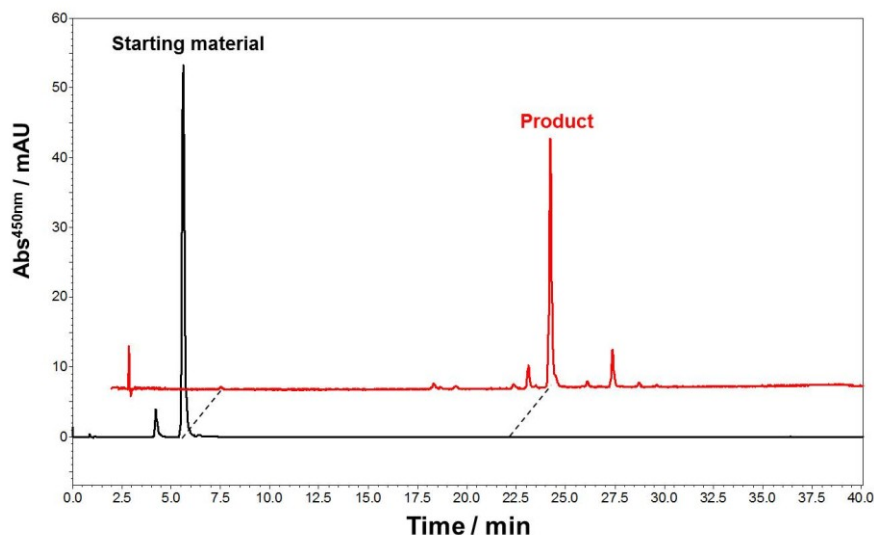
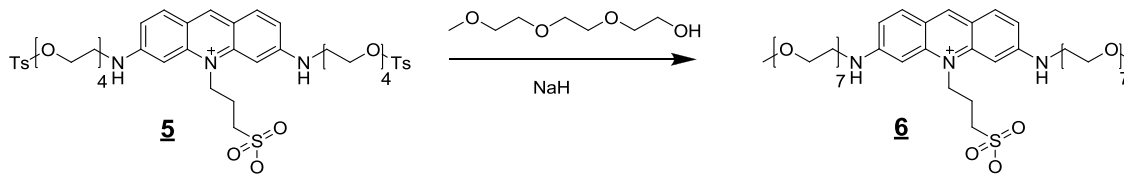


Figure 2.19 RP-HPLC of DAAPS and of the reaction mixture that contains TsTEG₂-DAAPS.

2.1.2.6 Synthesis of HEG₂-DAAPS (**6**)Figure 2.20 Reaction scheme for making HEG₂-DAAPS.

Reaction scheme for making HEG₂-DAAPS is shown in Figure 2.20. 2 ml of 2-(2-(2-methoxyethoxy)ethoxy)ethanol was mixed carefully with 2 g of NaH in 35 ml of anhydrous THF while stirring in an ice bath. After 7 min, TsTEG₂-DAAPS in anhydrous THF was added into the above mixture. Progress of the reaction was monitored by RP-HPLC with a PDA detector: the chromatogram is shown in Figure 2.21. An intermediate appears in the chromatogram with a retention time of 17.5 minutes: it corresponds to (TsTEG)(HEG)-DAAPS. The reaction was carried out at room temperature and went to completion in 4 hours. Unreacted NaH was quenched with excess of methanol.

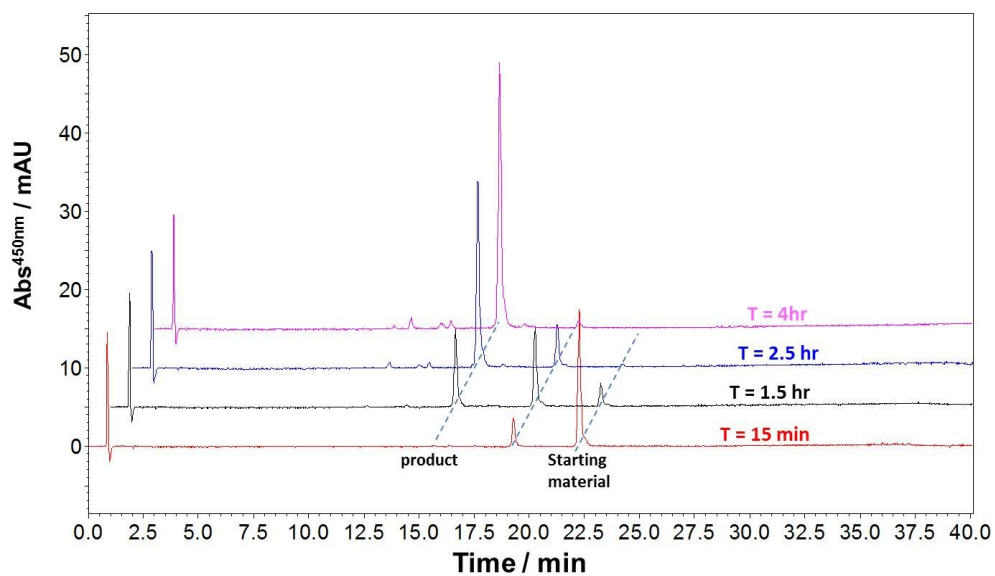


Figure 2.21 RP-HPLC monitoring of the progress of the reaction during making HEG₂-DAAPS.

2.1.2.7 Synthesis of Me₂HEG₂-DAAPS (FL) (**7**)

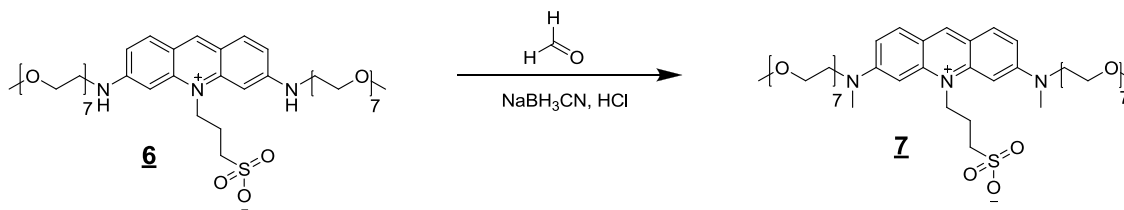


Figure 2.22 Reaction scheme for making Me₂HEG₂-DAAPS (FL).

Formaldehyde is the shortest aldehyde that can be used to alkylate the two secondary amino groups to red-shift the $\lambda^{\text{ex}}_{\text{max}}$ making the fluorophore more compatible with the 488 nm line of the argon ion laser while minimizing the increase in overall

hydrophobicity. Reaction scheme for making Me₂HEG₂-DAAPS (FL) is shown in Figure 2.22. Formaldehyde was mixed with HEG₂-DAAPS in a 1 : 1 mixture of dimethylformamide and H₂O that also contained 0.75 M HCl. The same equivalents of NaBH₃CN and aldehyde were used in the reductive amination reaction. Progress of the reaction was monitored by RP-HPLC with a PDA detector. The insert in Figure 2.23 shows that the spectrum was red-shifted after tetra-alkylation. Figure 2.24 shows the ESI mass spectrum of Me₂HEG₂-DAAPS: it confirms the expected structure.

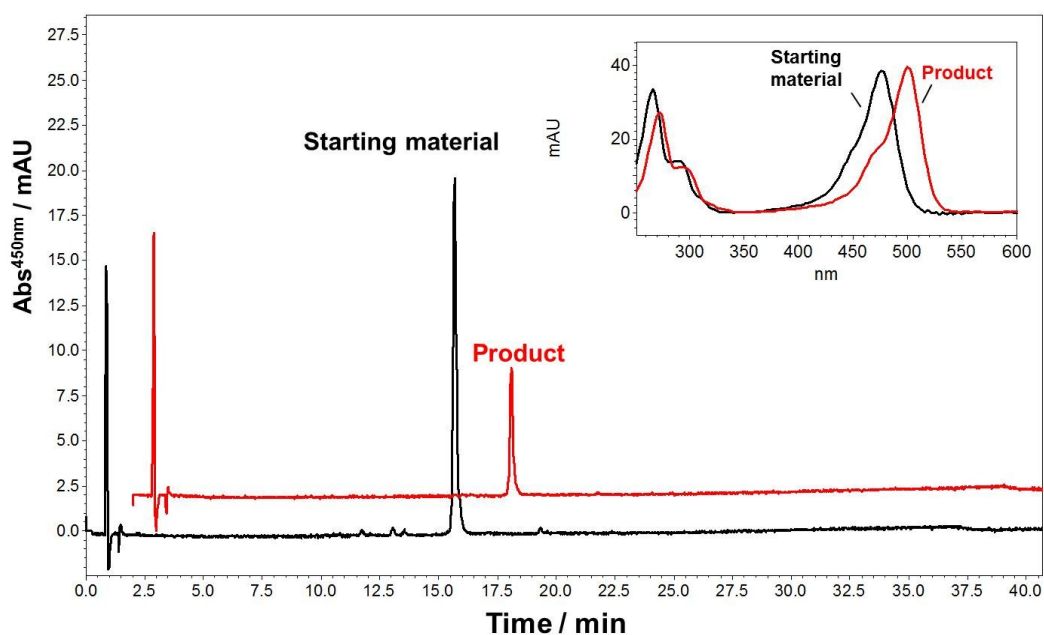


Figure 2.23 RP-HPLC analysis of HEG₂-DAAPS and the reaction mixture of Me₂HEG₂-DAAPS. (Insert: UV absorbance spectra of HEG₂-DAAPS and Me₂HEG₂-DAAPS).

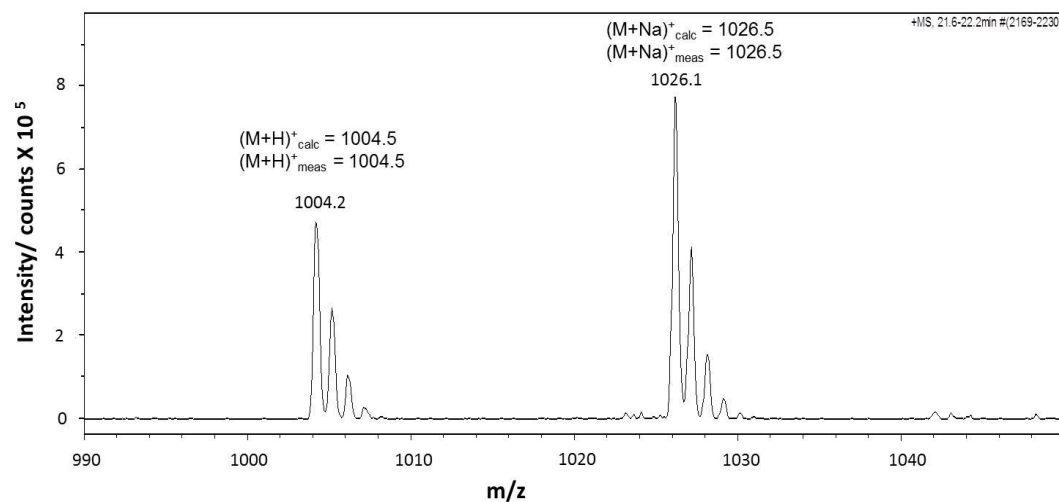


Figure 2.24 ESI mass spectrum of Me₂HEG₂-DAAPS (FL).

2.1.2.8 Synthesis of FL-CA (9)

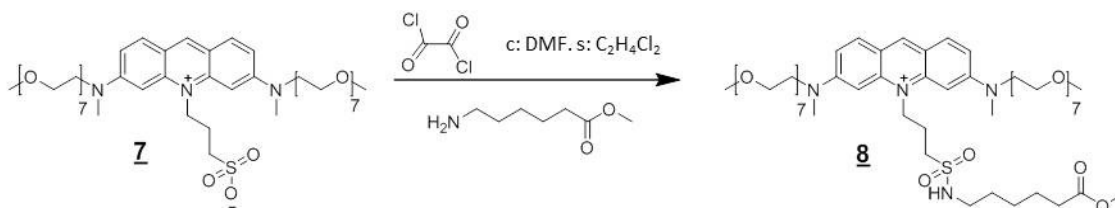


Figure 2.25 Reaction scheme for making FL-Me-CA.

The reactive carboxylic acid group was connected to the core fluorophore by sulfonamide formation between the sulfonyl chloride derivative of FL and methyl 6-aminohexanoate as shown in Figure 2.25. 3 equivalents of oxalyl chloride and a catalytic amount of dimethylformamide were added to FL in dichloroethane while stirring in an ice bath to produce the sulfonyl chloride derivative. The chlorination

reaction was monitored by analyzing a stable sulfonamide product which was formed by reacting the sulfonyl chloride derivative with morpholine. Methyl 6-aminohexanoate and TEA in dichloroethane were mixed with the sulfonyl chloride derivative of FL to form FL-Me-CA (**8**). FL-Me-CA was hydrolyzed by dissolving it in 0.1 M HCl_(aq) at 50 °C for 1 h to obtain FL-CA (**9**). The reaction was monitored by CE with LIF detection. FL was a zwitterion and moved with the electroosmotic flow in the CE analysis and could be differentiated from the cationic FL-Me-CA as shown in Figure 2.26.

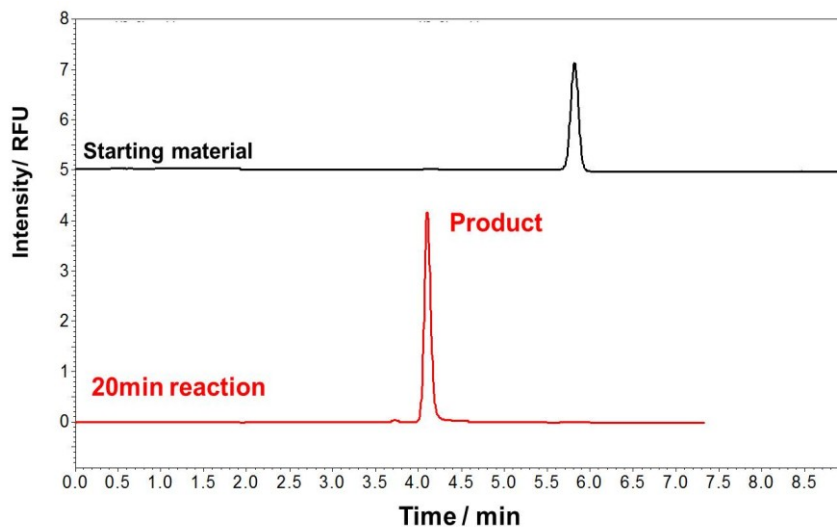


Figure 2.26 CE-LIF analysis of the conversion of FL to FL-Me-CA.

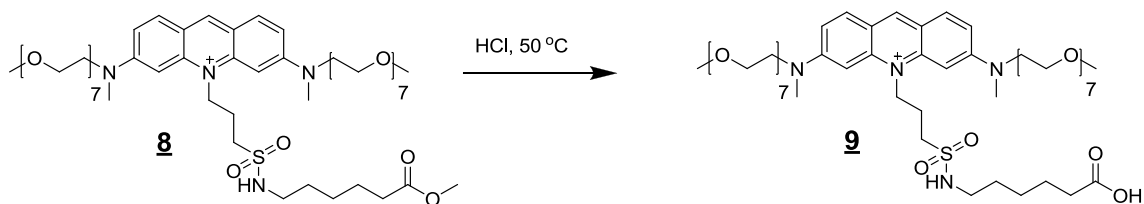


Figure 2.27 Reaction scheme for making FL-CA.

FL-Me-CA was then treated with HCl to get FL-CA as shown in Figure 2.27. Its RP-HPLC analysis and ESI mass spectrum is shown in Figure 2.28 and 2.29.

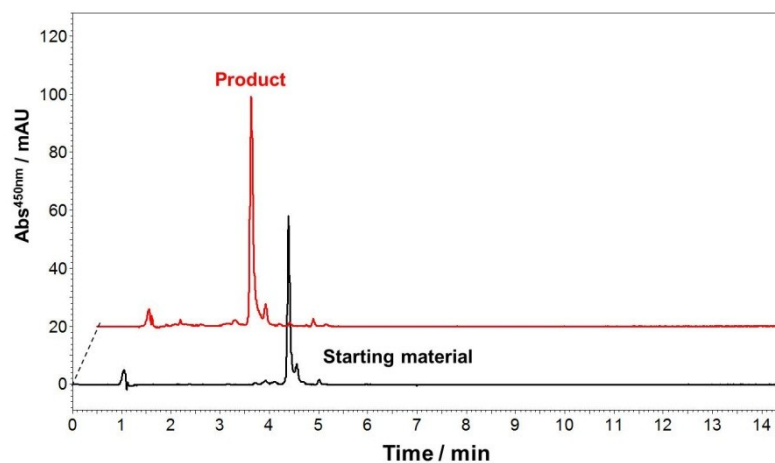


Figure 2.28 RP-HPLC analysis of the reaction mixture during the hydrolysis of FL-Me-CA to FL-CA.

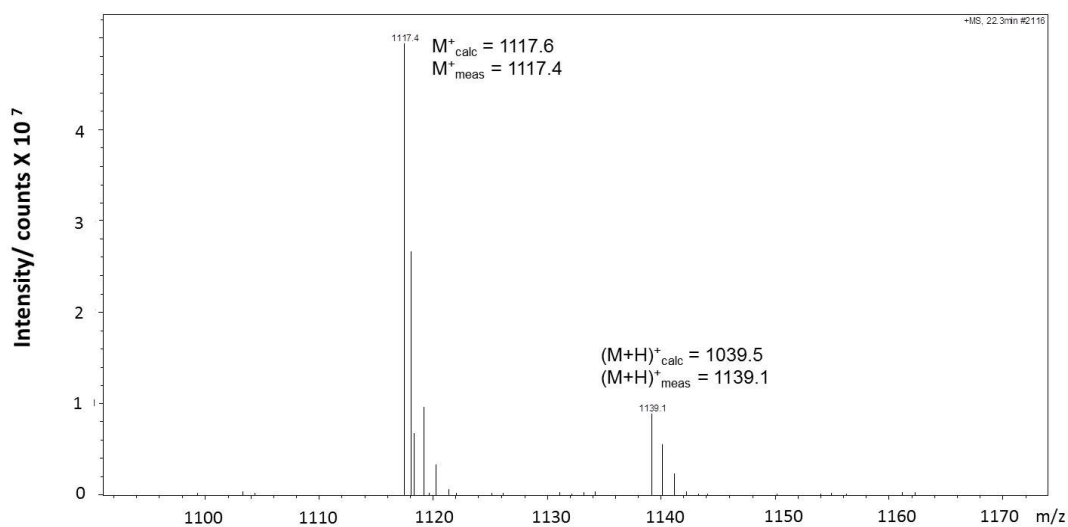


Figure 2.29 ESI mass spectrum of FL-CA.

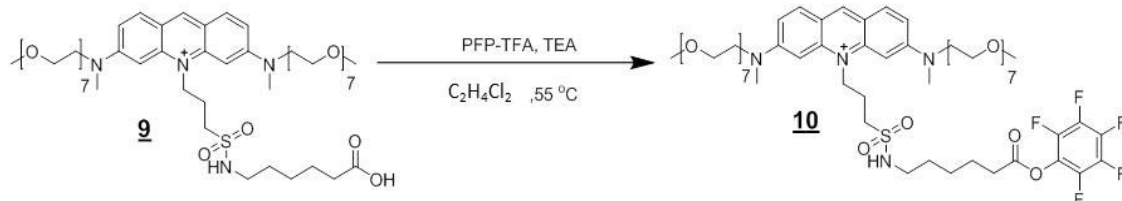
2.1.2.9 Synthesis of FL-CA-PFP (**10**)

Figure 2.30 Reaction scheme for making FL-CA-PFP.

The carboxylic acid group of FL-CA was activated by forming a pentafluorophenyl ester by reacting FL-CA with 5 equivalents of pentafluorophenyl trifluoroacetate (PFP-TFA) in dichloroethane in the presence of triethylamine, at $55\text{ }^\circ\text{C}$ for 30 min as shown in Figure 2.30. The reaction was monitored by RP-HPLC and the target m/z was confirmed with LC-MS as shown in Figure 2.31 and 2.32.

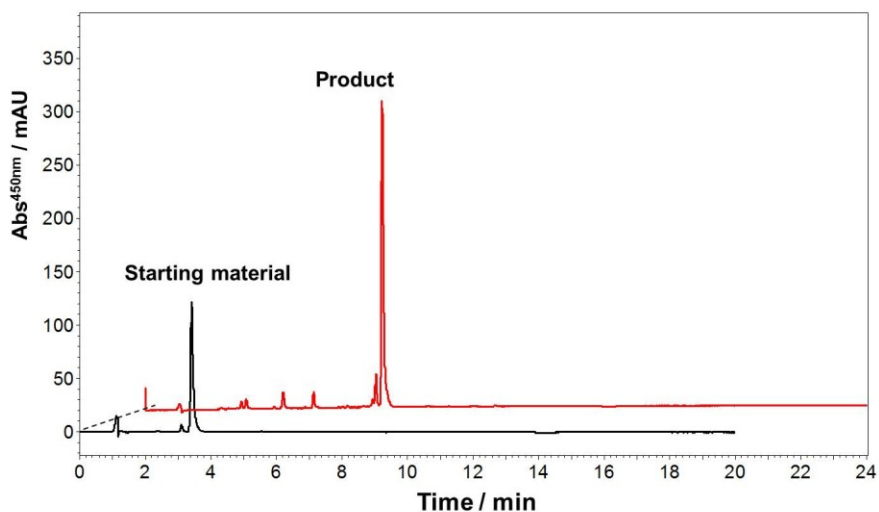


Figure 2.31 RP-HPLC analyses of FL-CA and its activated form, FL-CA-PFP.

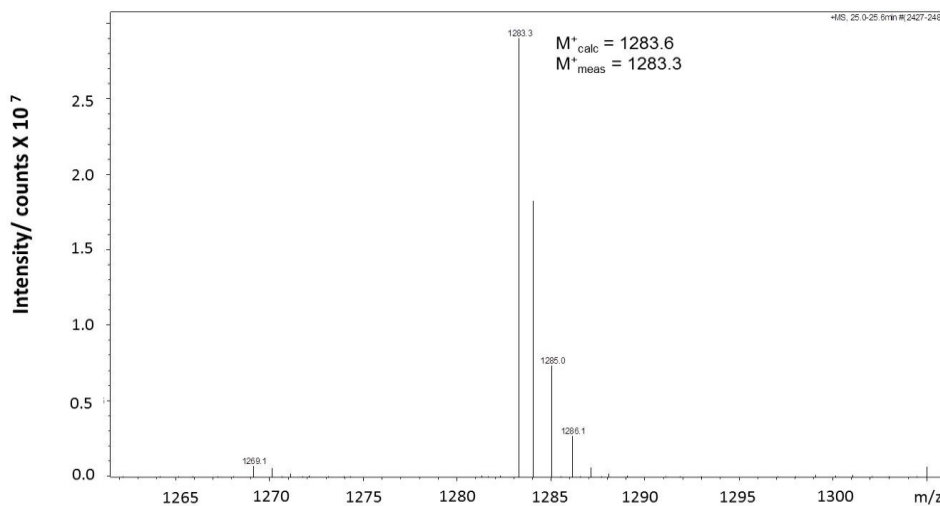


Figure 2.32 ESI mass spectrum of FL-CA-PFP.

2.2 Spectral Properties

2.2.1 Background and Objective

In the visible range, the $\lambda^{\text{ex}}_{\text{max}}$ of acridine orange is around 490 nm making it compatible with the 488 nm line of the argon ion laser. To preserve this advantage in the hydrophilic version of the acridine-based fluorophore, we made the electronic configuration of the fluorescent core as similar as possible by converting both primary amino groups of proflavine into tertiary amino groups.



Figure 2.33 Comparisons of $\lambda^{\text{ex}}_{\text{max}}$ for proflavine, acridine orange and HEG₂Me₂-DAA

Comparisons of $\lambda^{\text{ex}}_{\text{max}}$ for proflavine, acridine orange and HEG₂Me₂-DAA is shown in Figure 2.33. Fluorescent labels used in CE and cIEF usually are subjected to buffers with varied pH values. It is important and necessary to ascertain that the fluorescence properties of the designed label are pH-independent allowing both qualitative and quantitative analysis.

2.2.2 Materials and Method

The UV absorbance spectra were obtained using a Mod 168 photodiode array detector (Beckman-Coulter, Fullerton, CA). Fluorescence spectra at different pH values were taken by using an Aminco Bowman Series 2 Luminescence Spectrometer. Phosphoric acid-based buffers were made by titrating phosphoric acid with sodium hydroxide to make pH 2.4, 7.3 and 10.9 solutions with 10 mM ionic strength for the fluorescence measurements.

2.2.3 Results and Discussion

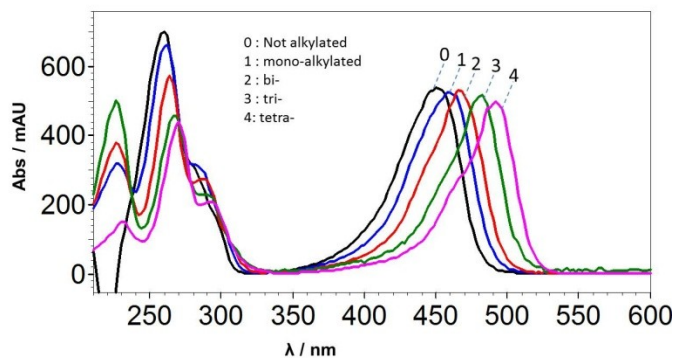


Figure 2.34 UV absorbance spectra of differently alkylated 3,6-diaminoacridines.

Proflavine has its visible-range $\lambda^{\text{ex}}_{\text{max}}$ around 450 nm as shown in Figure 2.34, spectrum number 0. With increasing degree of alkylation on the anilinic amino groups, $\lambda^{\text{ex}}_{\text{max}}$ is red-shifted, on average, by about 10 to 12 nm per alkyl group. For the tetra-alkylated HEG₂Me₂-DAA, $\lambda^{\text{ex}}_{\text{max}}$ reaches 491 nm.

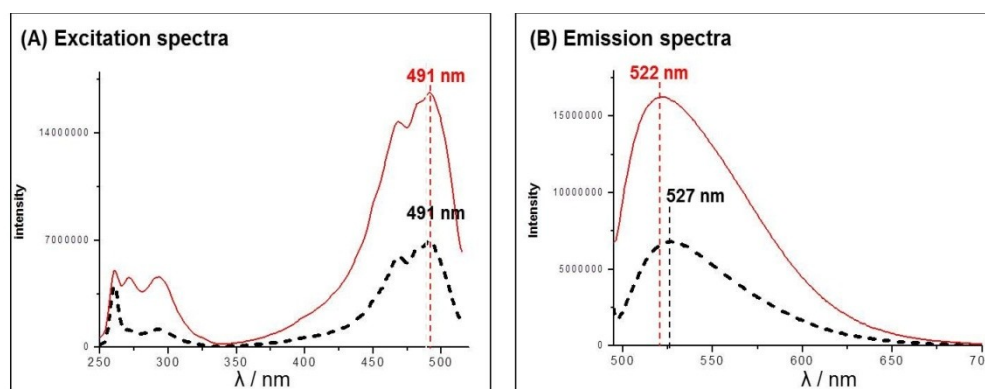


Figure 2.35 Comparison of the fluorescence excitation (A) and emission (B) spectra of acridine orange (dashed line) and HEG₂Me₂-DAA (solid line).

The fluorescence excitation and emission spectra of acridine orange and HEG₂Me₂-DAA are compared in Figure 2.35. Concentrations for both components were adjusted to obtain identical absorbances at $\lambda=280$ nm. $\lambda^{\text{ex}}_{\text{max}}$ remains the same for both the tetramethyl and the tetraTEG substituted proflavines. $\lambda^{\text{em}}_{\text{max}}$ of HEG₂Me₂-DAA is about 5 nm blue-shifted compared to acridine orange. Notice that though the solutions had similar concentrations, HEG₂Me₂-DAA has about two times higher intensity than acridine orange in both the excitation and emission spectra. This result could be due to solvatochromic effects: HEG₂Me₂-DAA has oligo(ethoxy)methyl chains that alter the

hydrophilic/hydrophobic balance around the molecule compared to that of acridine orange.

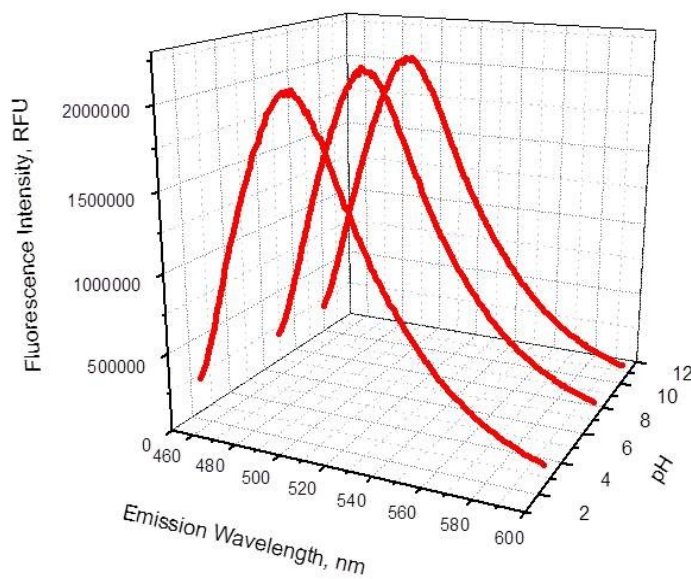


Figure 2.36 Fluorescence emission spectra of HEG₂Me₂-DAA in H₃PO₄/ NaOH aqueous buffers from pH 2.4 to 10.9 with 10 mM ionic strength.

The emission spectra of HEG₂Me₂-DAA were tested in aqueous buffers obtained by titrating H₃PO₄ to pH 2.34, 7.3 and 10.9 with NaOH and an ionic strength of 10 mM. As shown in Figure 2.36, neither the intensity nor $\lambda^{\text{em}}_{\text{max}}$ change throughout the entire pH range.

To sum up the spectral studies of HEG₂Me₂-DAA, we were able to preserve the desirable $\lambda^{\text{ex}}_{\text{max}}$ at about 490 nm, making the fluorophore compatible with the 488 nm

line of the argon ion laser. The emission spectra remain pH-independent and the emission intensities are higher than in acridine orange due, presumably, to the presence of oligo(ethoxy)methyl chains.

2.3 Chromatographic Properties

2.3.1 Background and Objective

In CE, with purely aqueous background electrolytes, acridine orange-based fluorescent reagents exhibit a tailing peak shape indicating hydrophobic interactions with the wall of the bare fused silica capillary. The chromatographic properties of Me₂HEG₂-DAAPS were tested and compared with those of acridine orange propane sulfonate in CE.

2.3.2 Materials and Method

The background electrolyte used in the CE analysis was 10 mM 3-(N-morpholino)propanesulfonic acid (MOPS) titrated with TEA to pH 10.1. A 2 % (w/w) aqueous poly(vinylpyrrolidone) (PVP) solution was used to dynamically coat the wall of the capillary between runs by rinsing the capillary at 30 psi for 2 minutes [65].

Concentrations for both acridine orange propane sulfonate and Me₂HEG₂-DAAPS were adjusted to obtain identical absorbances at $\lambda=280$ nm. The CE experiments were carried out with same instrument and type of capillary as described in 2.2.2.1. CE analysis was run in free zone mode with 30 kV applied potential.

2.3.3 Results and Discussion

CE tests for both acridine orange propane sulfonate and Me₂HEG₂-DAAPS were done with the same capillary as the first and second run. In Figure 2.37, the shape of the Me₂HEG₂-DAAPS peak is Gaussian while the peak of acridine orange propane sulfonate shows a 1.5 minutes long tail. Based on these results, Me₂HEG₂-DAAPS does show improved chromatographic behavior.

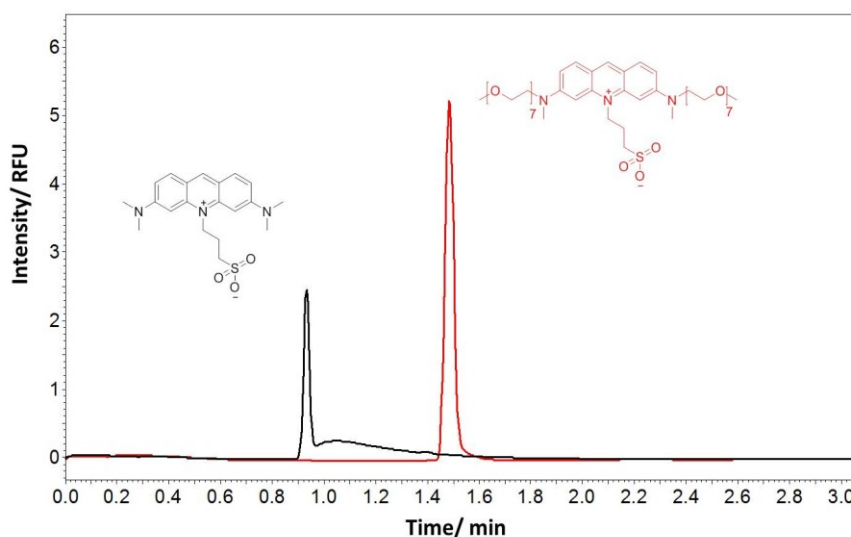


Figure 2.37 CE analyses of acridine orange propane sulfonate and Me₂HEG₂-DAAPS.

2.4 Labeling Reactions Using FL-CA-PFP

2.4.1 Background and Objective

FL-CA-PFP was designed as an amine-reactive fluorescent labeling reagent to tag amines and improve their detection sensitivity in CE analysis. Arginine, histidine, glutamic acid and glycine were labeled with FL-CA-PFP and analyzed by CE-LIF.

Bovine serum albumin and chicken ovalbumin were also labeled with FL-CA-PFP and analyzed by SDS-CEG-LIF and cIEF, respectively.

2.4.2 Materials and Methods

2.4.2.1 Labeling of Amino Acids and Their Analysis by CE-LIF and RP-HPLC.

Arginine, histidine, glutamic acid and glycine were labeled with FL-CA-PFP in a pH 8.2, 0.1 M aqueous sodium bicarbonate buffer. The CE experiments were carried out with the same instrument and type of capillary as described in 2.2.2.1. A 2 % (w/w) aqueous poly(vinylpyrrolidone) (PVP) solution was used to dynamically coat the wall of the capillary between runs by rinsing it at 30 psi for 2 minutes. The pH 2 background electrolyte used in the CE analyses of labeled arginine, histidine and glycine was obtained by adding 15 mmol tetrabutylammonium hydroxide to 5 mmol H₃PO₄ in 1 L water. The background electrolyte used in the CE analyses of labeled glutamic acid was 25 mM boric acid titrated to pH 8.3 with NaOH. HPLC analyses and LC-MS analyses were done with the instrument and column as described in 2.2.2.1.

2.4.2.2 Labeling of Bovine Serum Albumin (BSA) and Its Analysis by SDS-CGE-LIF

Bovine serum albumin was labeled with excess of FL-CA-PFP in a pH 8.2, 0.1 M aqueous sodium bicarbonate buffer at room temperature for 1 hour. An aliquot of the labeling reaction mixture was diluted with the Beckman SDS-MW sample buffer. SDS-CGE was carried out with the same CE instrument and type of capillary as described in 2.2.2.1. The capillary was preconditioned as recommended by Beckman for their SDS-

MW analysis. Briefly, the capillary was rinsed with an aqueous 0.1 M NaOH solution at 50 psi for 5 minutes. This was followed by a rinse with an aqueous 0.1 M HCl solution at 50 psi for 2 minutes, then a rinse with deionized water at 50 psi for 2 minutes. The capillary was then filled with the SDS-MW gel buffer solution at 40 psi for 10 minutes. A 15 kV potential was applied (negative-to-positive polarity), with a ramp-up time of 5 minutes and 20 psi nitrogen blanket on both the inlet and outlet vials.

2.4.2.3 Labeling of Chicken Ovalbumin (Ov) and Its Analysis by cIEF

Chicken ovalbumin was labeled with FL-CA-PFP in a pH 8.2, 0.1 M aqueous sodium bicarbonate buffer with a protein-to-fluorophore ratio of approximately 1 to 7 at room temperature for at 1 hour. The labeling reaction mixture was filtered with a membrane having a 1000 Da cut-off to remove excess FL-CA and NaHCO_3 . An aliquot of the labeled protein solution was serially diluted with the cIEF separation solution which contained 2% of carrier ampholytes $3 < pI < 10$, 15 mM of arginine (cathodic blocker), 2.5 mM of iminodiacetic acid (anodic blocker), 2.5 M urea and the *pI* makers in cIEF gel until the desired LIF signal strength was achieved. The carrier ampholytes and the cIEF gel solution were provided by Beckman-Coulter (Fullerton, CA). The fluorescent *pI* markers used in this work included the acridine orange conjugate of aspartic acid (*pI* 4.11) and the trisulfonamide obtained by reacting 8-hydroxypyrene 1,3,6-trisulfonyl chloride with 4-(2-aminoethyl)morpholine (AEM) (*pI* 6.38), both synthesized earlier in our laboratory [56]. cIEF analyses were carried out with the same CE instrument as described in 2.2.2.1. The 50 μm I.D., 360 μm O.D. capillary columns with a neutral

coating and having total and inlet-to-detector lengths of 30 and 20 cm, respectively, were provided by Beckman-Coulter. The capillary was prepared by rinsing it with 10 mM H_3PO_4 at 30 psi for 2 minutes, followed by a rinse with water at 30 psi for 2 minutes. The capillary was then filled with the mixture of the labeled protein and the cIEF separation solution at 30 psi for 2 minutes. The analyte solution was 200 mM H_3PO_4 in cIEF gel with 2.5 M urea. The catholyte was 300 mM NaOH in deionized water. Focusing was done with an applied potential of 25 kV for 12 minutes and the components were mobilized by applying a 0.5 psi pressure while maintaining a potential at 21 kV. An aqueous solution of 2 mM sodium acetate in 4.3 M urea was used to clean the capillary between runs by applying, simultaneously, 30 psi pressure and 25 kV potential for 5 minutes.

2.4.3 Results and Discussion

2.4.3.1 Labeling of Amino Acids and Their Analysis by CE-LIF

FL-CA-tagged amino acids were analyzed by CE-LIF in the free zone mode: the results are shown in Figure 2.38. For tagged glutamic acid, the CE analysis was done with a pH 8.3 background electrolyte and 30 kV applied potential (negative-to-positive polarity). At pH 8.3, the two carboxylic acid groups of FL-CA-glutamic acid were fully deprotonated making the total charge of FL-CA-glutamic acid equal to -1. FL-CA at pH 8.3 was a zwitterion and appeared as a neutral marker during CE analysis and could be differentiated from the anionic FL-CA conjugate of glutamic acid. Within 15 minutes analysis time, FL-CA had not passed the detector window, because the direction of the

electroosmotic flow pointed away from the detector. For tagged arginine, histidine and glycine, the CE analyses were carried out at pH 2 with 30 kV applied potential (positive-to-negative polarity). In the pH 2 BGE, both FL-CA-glycine and FL-CA appeared to be cationic with a total charge of +1. They could be separated by CE due to their size differences. As shown in Figure 2.38 (c), FL-CA-glycine has a slightly slower mobility than FL-CA. Both FL-CA-arginine and FL-CA-histidine carried a total charge of +2 at pH 2. Thus, they moved faster than FL-CA, as shown in Figure 2.38 (a) and (b).

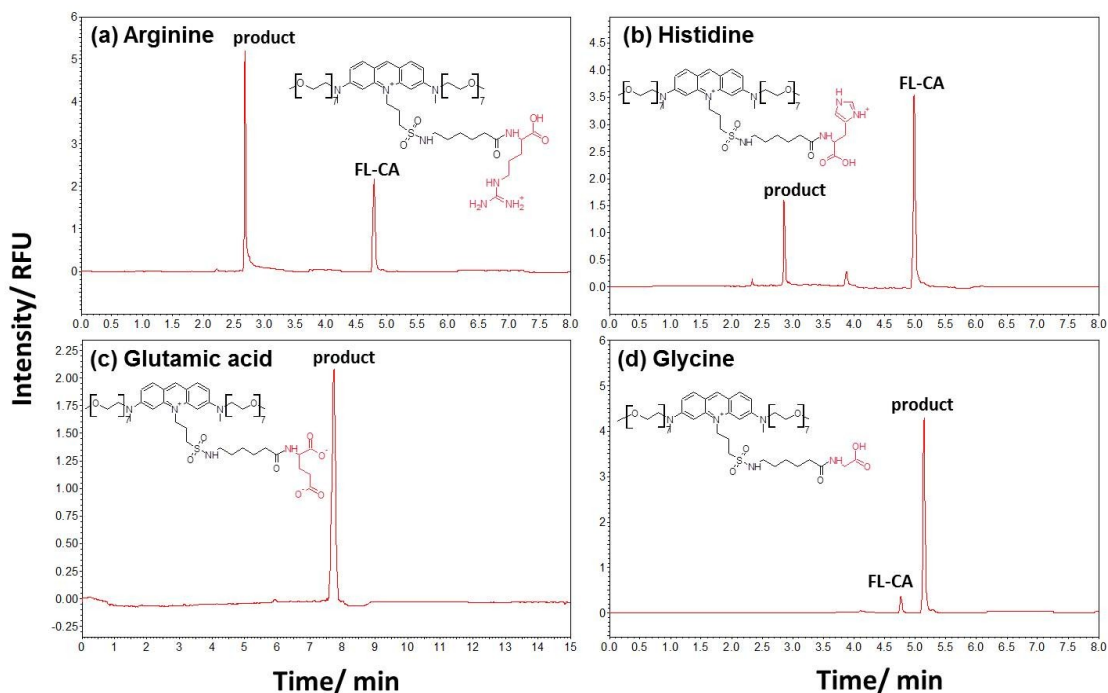


Figure 2.38 CE analyses of FL-CA-PFP tagged amino acids. (a) tagged arginine, (b) tagged histidine, (c) tagged glutamic acid and (d) tagged glycine.

The same set of tagged amino acids was also analyzed by RP-HPLC. The signature UV absorbance spectrum of FL served as a diagnostic tool to help assign the peaks in the chromatograms. The chromatograms shown in Figure 3.39 were acquired at a detection wavelength of 500 nm. Only the FL-related components would appear at this wavelength. The chromatograms shown in Figure 3.39 were acquired at a detection wavelength of 500 nm. Only the FL-related components would appear at this wavelength. FL-CA, a hydrolysis product of FL-CA-PFP, was observed in all the tagging tests as shown in Figure 3.39. At pH 2.7, all four tagged amino acids were retained less in the RP column than FL-CA-PFP. The ESI mass spectra for the four tagged amino acids are shown in Figure 2.40.

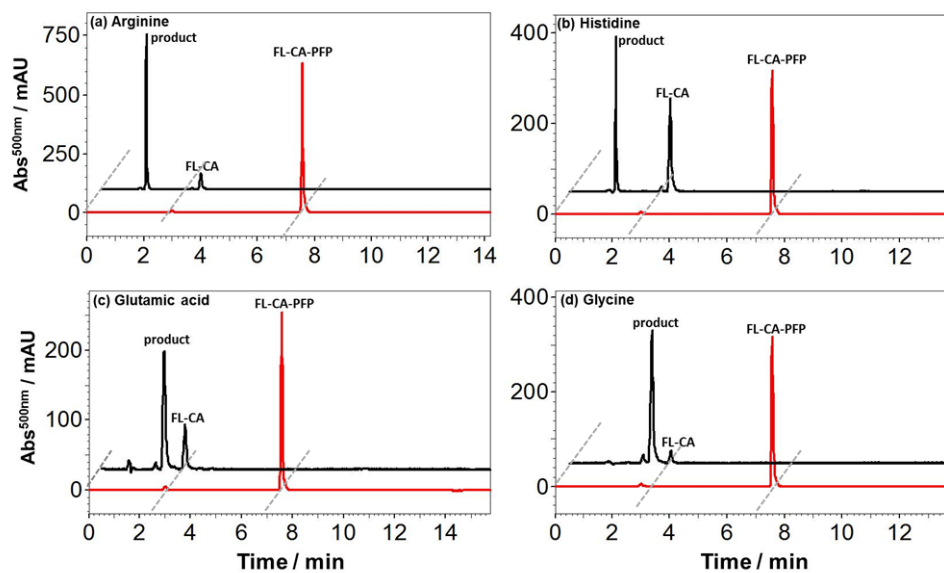


Figure 2.39 RP-HPLC analyses of FL-CA-PFP tagged amino acids. (a) tagged arginine, (b) tagged histidine, (c) tagged glutamic acid and (d) tagged glycine.

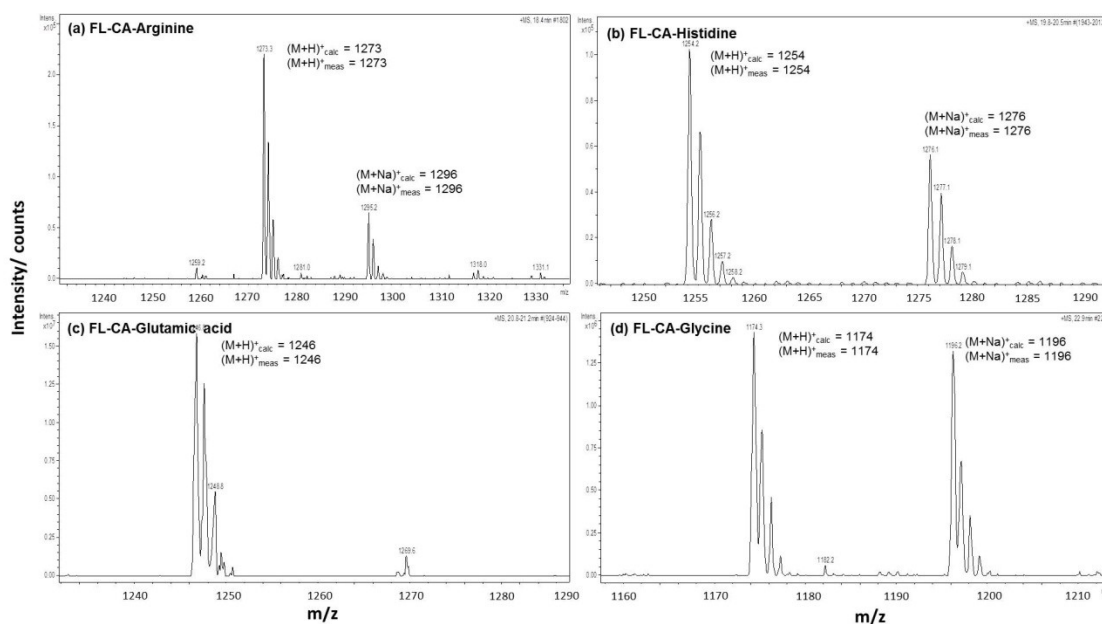


Figure 2.40 ESI mass spectra of FL-CA-PFP tagged amino acids. (a) tagged arginine, (b) tagged histidine, (c) tagged glutamic acid and (d) tagged glycine.

2.4.3.2 Labeling of Bovine Serum Albumin (BSA) and Its Analysis by SDS-CGE-LIF

Bovine serum albumin was labeled with excess of FL-CA-PFP and analyzed by SDS-CGE with LIF detection. As shown in Figure 2.41, the lowest tested concentration for tagged bovine serum albumin was 15 nM which is one-to-two orders of magnitude lower than what can be achieved for the CE system used with UV absorbance detection.

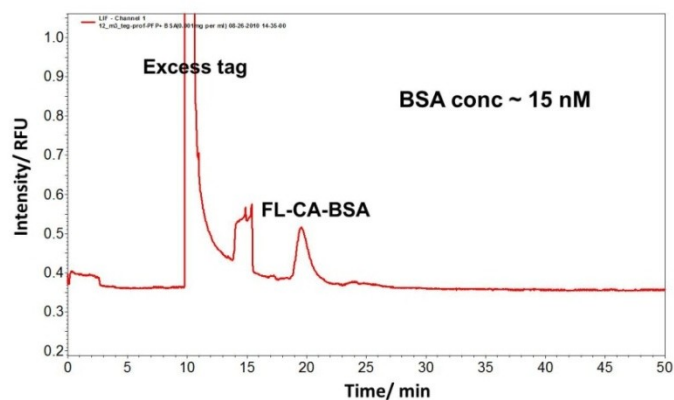


Figure 2.41 SDS-CGE analysis of labeled bovine serum albumin using LIF detection.

2.4.3.3 Labeling of Chicken Ovalbumin (Ov) and Its Analysis by cIEF

Chicken ovalbumin was labeled with FL-CA-PFP with a protein-to-label mole ratio of 1 to 7 in a 0.1 M sodium bicarbonate buffer. The hydrolyzed label and sodium bicarbonate were removed by centrifuging the samples through 10 kD permeation cut-off dialysis membranes in order to avoid interferences during cIEF. The detector traces obtained during cIEF analyses of non-tagged and tagged chicken ovalbumin are overlaid in Figure 2.42 for the UV absorbance and the LIF detectors, respectively. The composition of the cIEF separation solutions (concentrations of pI markers, carrier ampholytes, cathodic and anodic blockers) for both the non-tagged and the tagged samples were the same in order to minimize the changes which are caused by the system but not by the nature of the proteins. The concentration of pI markers needed to get decent signals with the UV absorbance detector overwhelmed the LIF detector. A common problem with amine-reactive protein labels is the acidic shift in the pI value of the protein after labeling due to the loss of a buffering amino group to an amide group.

In the overlay, the pI of the tagged proteins was shifted in the alkaline direction by about 0.02 compared to the non-tagged protein. It is expected that this minimal basic shift in pI caused by tagging with the monocationic FL-CA-PFP is due to the replacement of an amino group with a higher pK_a quaternary ammonium group. The result suggests that derivatization using monocationic FL-CA-PFP does not change the pI of the band of the tagged chicken ovalbumin in a noticeable manner, though the general validity of this assumption over the entire pI range must be experimentally verified once suitable fluorescent pI markers become available. The combined reproducibility of the cIEF analysis and the labeling of chicken ovalbumin was also investigated. As shown in Figure 2.43, the mobilization traces for samples taken from three independent labeling reactions are almost identical demonstrating the reproducibility of the procedure.

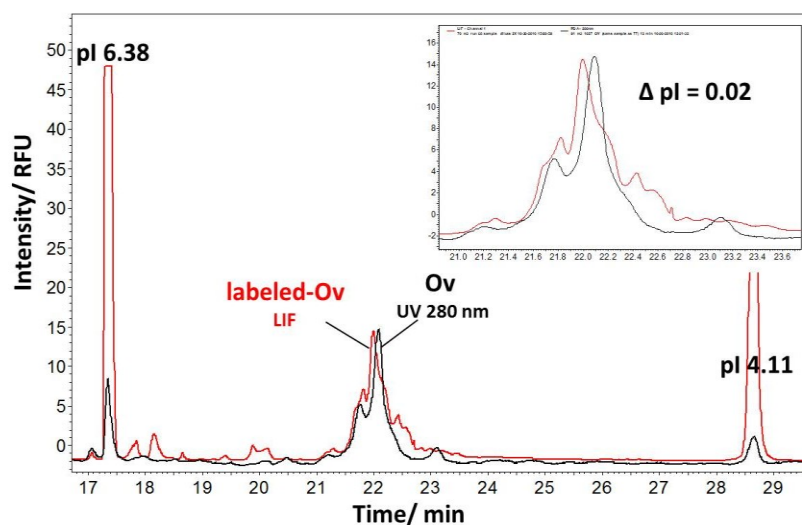


Figure 2.42 Mobilization traces obtained in the cIEF analysis of chicken ovalbumin with UV absorbance detection and labeled chicken ovalbumin with LIF detection.

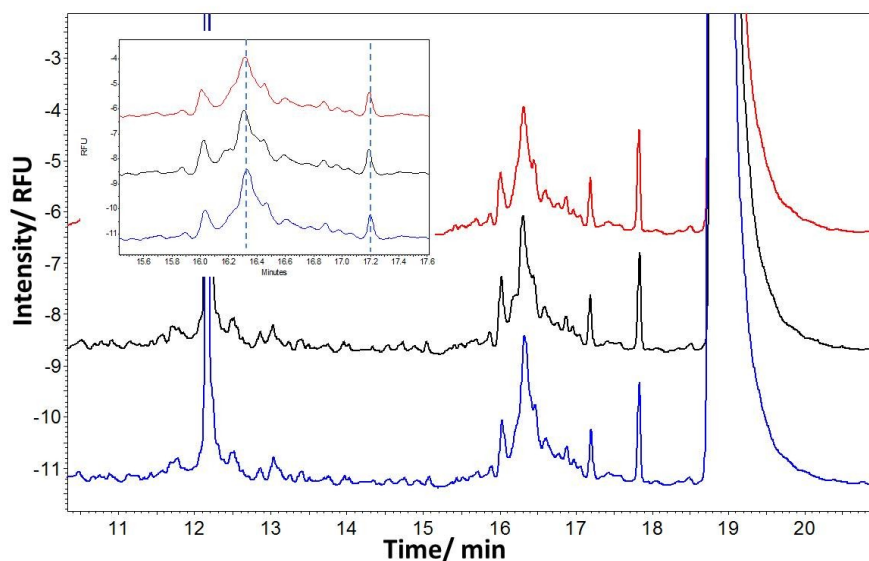


Figure 2.43 Combined reproducibility of the labeling reaction and the cIEF analysis of the same chicken ovalbumin sample.

2.5 Design and Synthesis of a FL-CA-based Trifunctional Probe

2.5.1 Background and Objectives

The objective of this work was to briefly test the feasibility, on a “proof-of-principle” level, of combining biotin, FL-CA and an azide group into a single, quasi-universal probe to facilitate selective enrichment and selective detection of a variety of molecules (*e.g.*, natural products, pharmaceuticals, inhibitors, *etc.*) that carry an alkyne anchoring group that minimally perturbs their biological function. The alkyne anchoring group can be, presumably, readily coupled to the azide-containing trifunctional probe using Cu(I)-mediated click chemistry [66]. Based on $\log P$ values calculated by ALOGPS 2.1 (<http://www.vcclab.org>) [67], the $\log P$ value of our trifunctional probe is about 6 units lower than Tate’s [68]. The 10^6 -fold improvement in hydrophilicity implies better

biocompatibility and hopefully helps to reduce the degree of aggregation and precipitation of the probe-protein conjugates.

The trifunctional probe was synthesized according to the reaction schemes shown in Figures 2.44 and 2.45. The probe was built by a converging approach: a biotin-azide conjugate, compound **6** and FL-CA-PFP were built independently, then connected into one piece via amide formation.

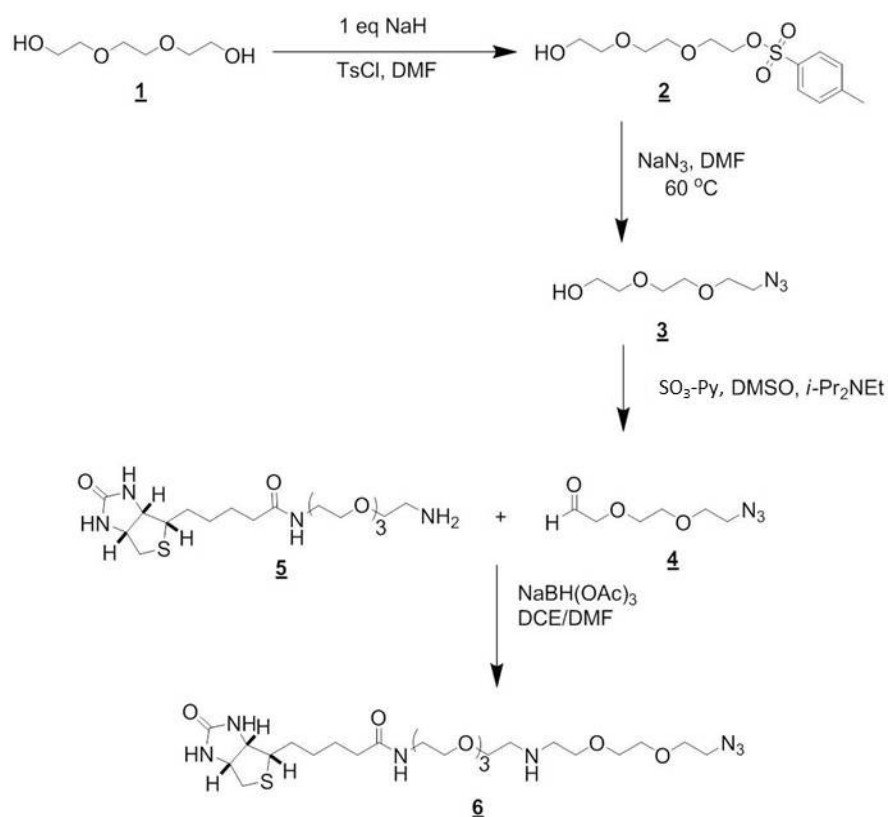


Figure 2.44 Synthesis scheme for making compound **6**.

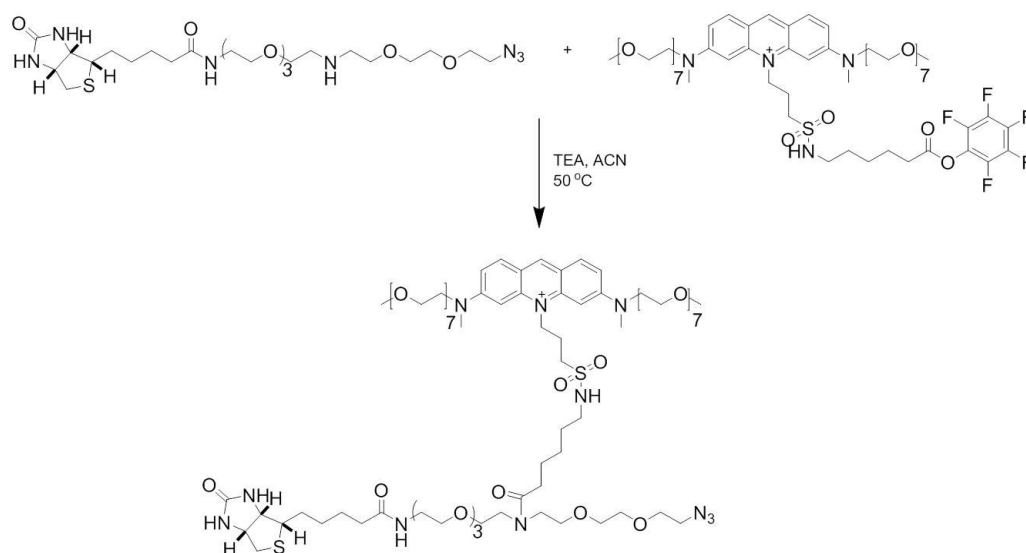


Figure 2.45 Synthesis scheme for making the desired trifunctional probe.

2.5.2 Materials and Method

FL-CA-PFP was made as described in Section 2.1.2. Compound **6** was synthesized by Dr. Robles of Professor Romo's group at TAMU. RP-HPLC and LC-MS analyses were carried out as described in Section 2.1.2.1. Sodium hydride, sulfur trioxide pyridine, diisopropylethylamine and 1H-thieno[3,4-d]imidazole-4-pentanamide were purchased from Sigma-Aldrich Co. (St. Louis, MO).

2.5.2.1 Synthesis of Biotin-Azide Compound **6**

Tetra(ethylene glycol) was mixed with 1 equivalent of sodium hydride and 2 equivalents of tosyl chloride in dimethylformamide and reacted at room temperature. Mono-tosylated tetra(ethylene glycol) was obtained through flash column chromatography with an approximate yield of 76 %, then reacted with sodium azide in dimethylformamide

while heating at 60 °C to make compound **3**, ethanol, 2-[2-(2-azidoethoxy)ethoxy]-. Compound **3** was mixed with sulfur trioxide pyridine and diisopropylethylamine in dimethyl sulfoxide to make compound **4**, acetaldehyde, 2-[2-(2-azidoethoxy)ethoxy]- [69]. After flash column chromatography, compound **4** was reacted with 1H-thieno[3,4-d]imidazole-4-pentanamide in a mixture of dichloroethane and dimethylformamide to make compound **6**. The same equivalents of sodium triacetoxyborohydride [70] and aldehyde were used in the reductive amination reaction. Finally, compound **6** was purified by RP-HPLC using an eluent of 7 % acetonitrile and 93 % water mixture, in isocratic mode. The result of the LC-MS analysis of compound **6** is shown in Figure 2.46.

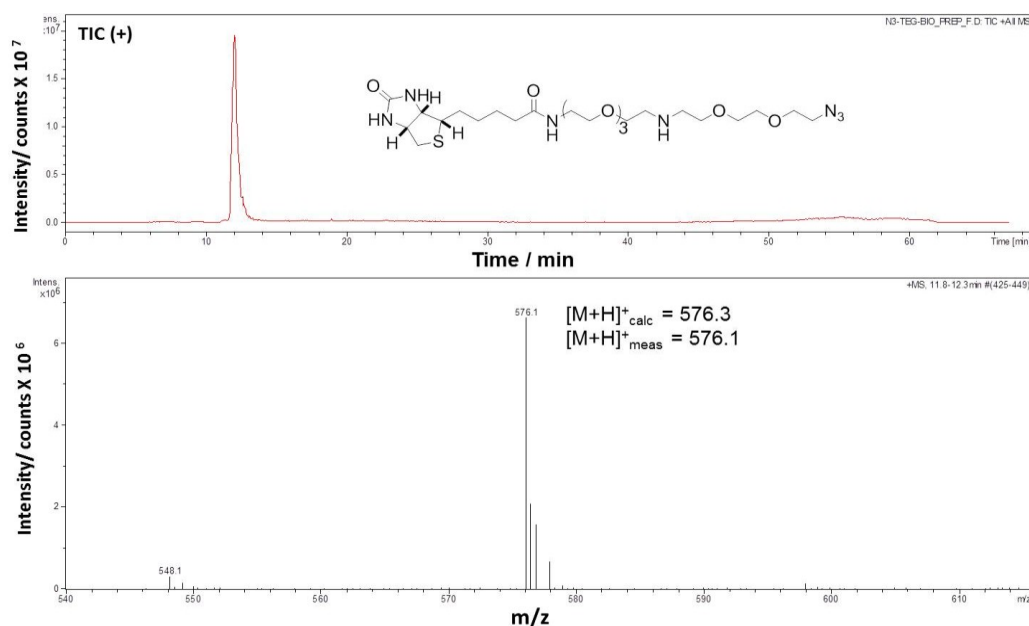


Figure 2.46 LC-MS analysis of compound **6**.

2.5.2.2 Synthesis of the Desired Trifunctional Probe

FL-CA-PFP was mixed with triethylamine and compound **6** in acetonitrile and heated at 50 °C with stirring. After 1 hour, the reaction mixture was analyzed with LC-MS: the results are shown in Figure 2.47. Based on the integration of the peaks at 450 nm in the chromatogram, conversion in this batch was about 35 %. FL-CA was recovered and converted back to FL-CA-PFP. The UV absorbance spectrum of the trifunctional probe, shown in the insert, agrees with that of FL-CA.

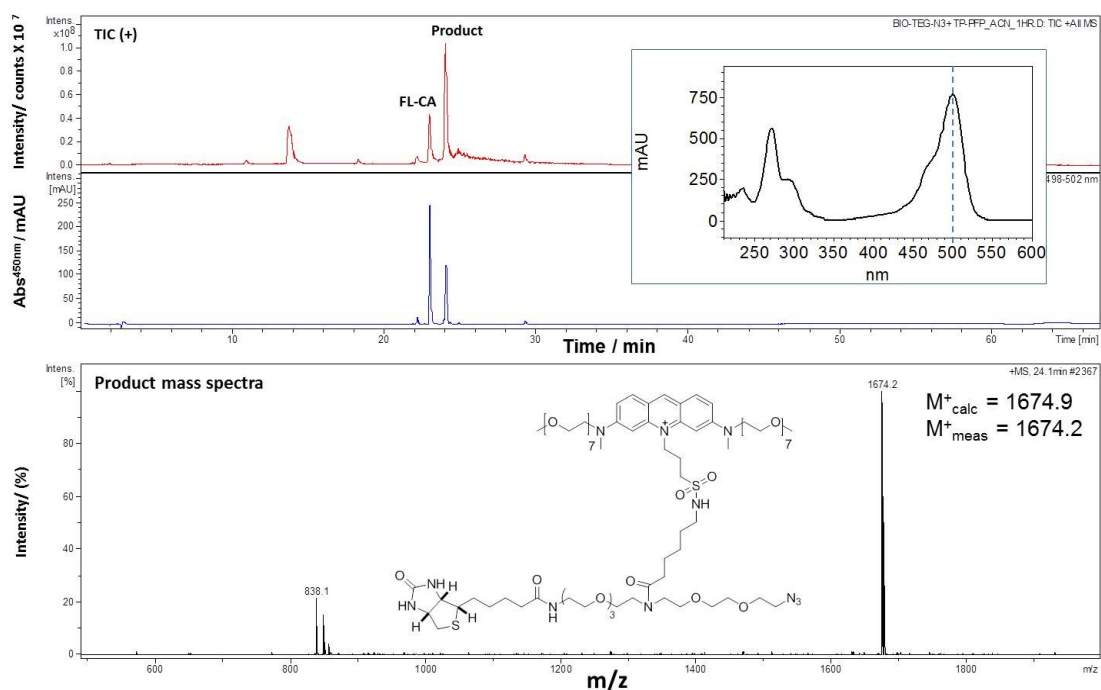


Figure 2.47 LC-MS analysis of the reaction mixture obtained during the final assembly of the trifunctional probe. (Insert: UV absorbance spectrum of the trifunctional probe.)

An attempt was made by Dr. Robles to couple a cyclopropanated derivative of parthenin with the trifunctional probe through click chemistry (reaction scheme shown in Figure 2.48). The reaction mixture was analyzed by LC-MS: its results are shown in Figure 2.49. A small peak with a retention time of 24 minutes was observed in the m/z 2074 extracted ion chromatogram (target m/z) as shown in Figure 2.49(b). It was retained slightly longer than the trifunctional probe itself shown in Figure 2.49(c).

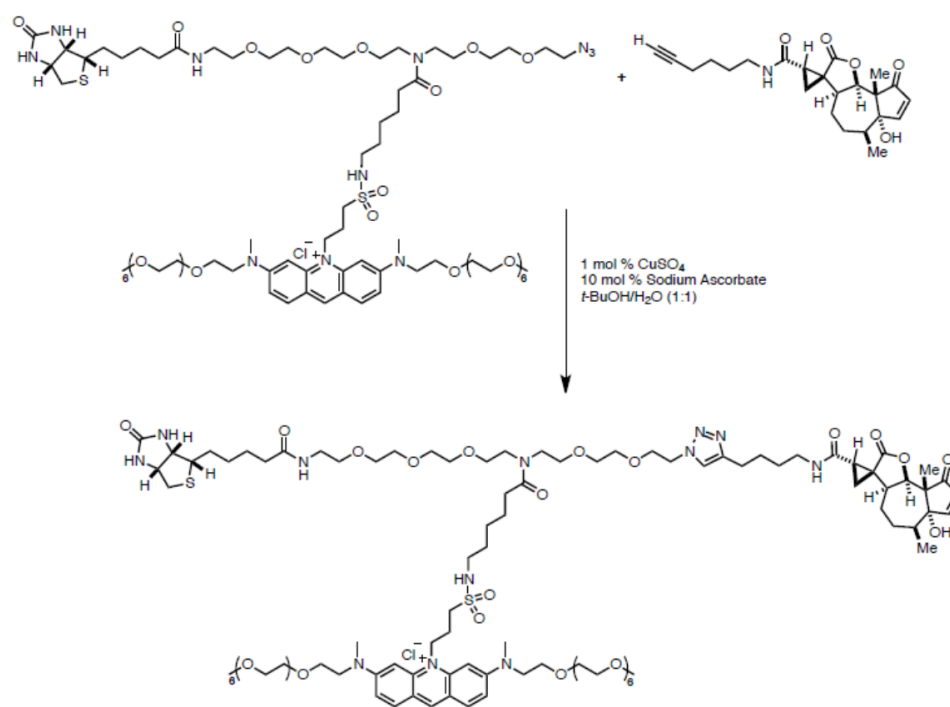


Figure 2.48 Reaction scheme of coupling a cyclopropanated derivative of parthenin with the trifunctional probe.

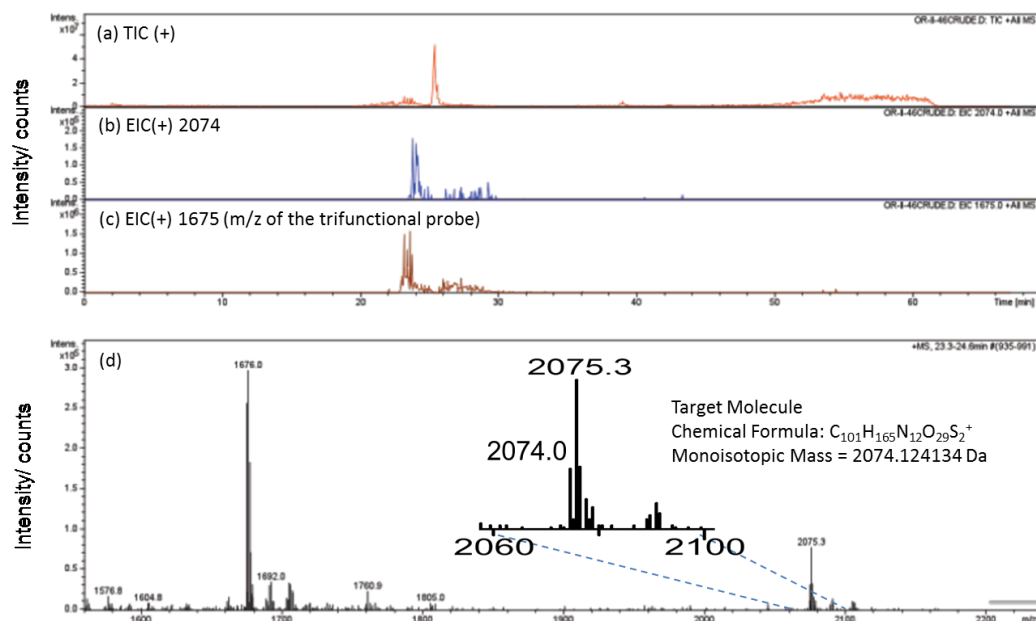


Figure 2.49 LC-MS analysis of the reaction mixture of the trifunctional probe coupled with a cyclopropanated derivative of parthenin: (a) total ion chromatogram in positive ion mode; (b) Extracted ion chromatogram at the target m/z of 2074; (c) Extracted ion chromatogram of the trifunctional probe at m/z = 1675 and (d) calculated average mass spectrum for the 23.3 to 24.6 min retention time range.

2.6 Concluding Remarks

A hydrophilic, monocationic, fluorescent, amine-reactive labeling reagent having pH-independent spectral properties has been made to facilitate the LIF-CE analysis of compounds having primary or secondary amino groups. Each synthetic step was monitored and characterized by RP-HPLC, LC-MS and CE. This hydrophilic version of the acridine orange-based fluorophore is about 30,000 times more water soluble than the original acridine orange-based fluorophore allowing CE analysis with a decent peak

shape under purely aqueous conditions. FL-CA has its visible-range $\lambda^{\text{ex}}_{\text{max}}$ around 490 nm making it compatible with the 488 nm line of the argon ion laser. The spectral properties of FL-CA were independent of pH in the $2.4 < \text{pH} < 11$ range. The monocationic charge of FL-CA helped to minimize the change in the pI value of chicken ovalbumin after derivatization. In a proof-of-principle experiment, FL-CA was incorporated into a trifunctional probe that contained FL-CA to facilitate selective, sensitive LIF detection, a biotin group to permit selective enrichment from dilute solutions (via affinity interactions with avidine), and an azido group to facilitate coupling to target molecules labeled with a minimally disruptive alkyne group. The trifunctional probe was successfully synthesized and Cu(I)-mediated coupling to an alkyne-labeled cyclopropanated derivative of parthenin had been tried on a microgram scale and the reaction mixture was analyzed by LC-MS.

Though traditional gel-based electrophoresis suffers from low resolution and low sensitivity compared to CE-based separations, it has been widely used in proteomics [71]. Because of the selection of the unique reporting group, the trifunctional probe has the potential to become a quasi-universal affinity probe in CE-mediated analysis. Its compatibility with cIEF is especially significant considering that cIEF is one of the widely used techniques for pI characterization and simultaneous sample concentration in bio-analysis. We demonstrated that labeling of chicken ovalbumin with FL-CA-PFP lead to a pI shift of only 0.02 after derivatization. The designed FL-CA-PFP is a suitable derivatizing agent for cIEF-LIF due to its high water solubility, pH-independent spectral

properties and the minimal shift it caused in the pI value of the test protein, chicken ovalbumin. However, the validity of this claim could not be demonstrated across the entire pI range, because the number of available LIF-compatible pI markers having reasonably narrow pI gaps and allowing the accurate determination of pI values is very limited. The lack of this experimental proof currently prevents the widespread use of FL-CA-PFP in cIEF and renders it to the status of just another “me too” derivatizing agent. Another important reason why fluorescent pI markers are necessary is that the low sensitivity of UV absorbance detection requires the use of very high (at least three orders of magnitude higher) sample loadings than LIF detection. Too high analyte concentration alters the pH gradient locally in an uncontrolled manner and leads to false pI values. Very low sample loads that do not distort the pH gradient and do not cause loss of resolution are only possible when highly sensitive detection methods, such as LIF are available. In order to facilitate and maximize the application of FL-CA-PFP in highly sensitive and accurate cIEF-LIF analysis, it is necessary to develop optimized, closely-spaced fluorescent pI markers. Consequently, we decided to work on the design and synthesis of LIF-compatible pI markers as discussed in Chapter 3.

3. DESIGN AND SYNTHESIS OF A FAMILY OF PYRENE-BASED FLUORESCENT *pI* MARKERS

3.1 Design and Synthesis

3.1.1 Background and Objective

According to one of the cIEF reviews written by Righetti [22], “in cIEF, there is no other way for charting the course of pH than to use *pI* markers.” Proteins with known *pI* values can be used as *pI* markers in cIEF with UV absorbance detection. Ten commercially available protein *pI* markers and seven UV-absorbing tryptic digest peptides derived from cytochrome c were used as *pI* markers in cIEF by Mohan and Lee [72]. These proteins and peptides cover a *pI* range from 3.67 to 10.25. Native protein *pI* markers have disadvantages: their solubility is low in isoelectric state, they tend to aggregate, denaturing reagents can not be present in the cIEF system, their purity is often insufficient and the choice of their *pI* values is limited by nature [54]. To avoid the disadvantages of using proteins as *pI* markers, modifications and synthetic approaches had been tried. Arai *et al.* [27] labeled both tryptic peptides and ampholytes with dansyl chloride to enhance their detectability at 280 nm to profile the pH gradient. Synthetic oligopeptides as *pI* markers had also been designed by Shimura *et al.* [26, 27]. The C-terminal carboxyl group, and the side chains of aspartic acid and glutamic acid were utilized to obtain acidic *pI* markers. On the other hand, tyrosine and lysine were essential constituents for markers in the alkaline *pI* region. For *pI* markers around the neutral pH, the N-terminal amino group and the histidine residues were utilized.

Moreover, each peptide was designed to contain a tryptophan residue to facilitate detection by UV absorbance at 280 nm. The pI values were determined by slab-gel IEF: the pH values of the focused bands were measured directly with a microprobe glass electrode. Some characteristic properties of the synthetic peptide pI markers are summarized in Figure 3.1. The 16 pI markers cover the 3.38 to 10.17 range and the measured pI values are reasonably close to the calculated ones. Their focusing behavior was characterized by the $[-dz/d(pH)]_{pI}$ and Vh/cm values (the integral of the required focusing potential and time for unit gel length). The $[-dz/d(pH)]_{pI}$ value is inversely proportional to Vh/cm . Rapid focusing was achieved with less than 120 Vh/cm for the markers whose $[-dz/d(pH)]_{pI}$ values were greater than 1.

No.	Peptides	pI det. ^{a)}	SD ^{b)}	pI cal. ^{c)}	ΔpI ^{d)}	$-dz/dpH$ ^{e)}	Vh/cm ^{f)}
28	H-Trp-Tyr-Lys-Arg-OH	10.17	0.019	10.02	0.15	1.11	95
29	H-Trp-Tyr-Lys-Lys-OH	9.99	0.025	9.76	0.23	1.49	95
30	H-Trp-Tyr-Tyr-Lys-Lys-OH	9.68	0.029	9.52	0.16	1.73	95
31	H-Trp-Tyr-Tyr-Tyr-Lys-Lys-OH	9.50	0.022	9.36	0.14	1.90	95
32	H-Trp-Tyr-Lys-OH	8.40		8.62	-0.22	0.37	
33	H-Trp-Glu-Tyr-Tyr-Lys-Lys-OH	8.40	0.028	8.46	-0.06	0.52	270
34	H-Trp-Glu-His-His-His-Arg-OH	7.27	0.012	7.34	-0.07	1.23	120
35	H-Trp-Glu-His-Arg-OH	7.00	0.015	7.04	-0.04	0.77	120
36	H-Trp-Glu-His-His-OH	6.66	0.024	6.42	0.24	1.31	120
37	H-Trp-Glu-Arg-OH	5.91	0.078	6.06	-0.15	0.12	520
38	H-Trp-Glu-His-OH	5.52	0.025	5.48	0.04	0.43	270
39	H-Trp-Asp-Asp-His-His-OH	5.31	0.022	5.24	0.07	0.53	320
40	H-Trp-Glu-Glu-His-OH	4.28	0.035	4.54	-0.26	1.38	70
41	H-Trp-Asp-Asp-Arg-OH	4.05	0.038	4.16	-0.11	1.48	70
42	H-Trp-Glu-Glu-OH	3.78	0.038	3.82	-0.04	1.25	70
43	H-Trp-Asp-Asp-Asp-OH	3.38	0.041	3.38	0.00	1.70	120

a) pI det., determined pI values (average of five independent experiments)

b) SD, standard deviations of determined pI values

c) pI cal., calculated pI values using Eq. (1)

d) ΔpI , differences between pI det. and pI cal

e) $-dz/dpH$, $[-dz/d(pH)]_{pI}$ values calculated using Eq. (2)

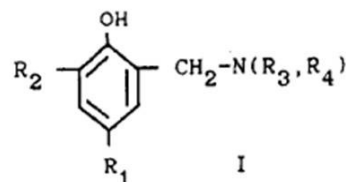
f) Vh/cm , the sum of the products of time and applied field strength required for focusing (see Section 3.2)

Figure 3.1 Peptide sequences and characteristic properties of the synthetic peptide pI markers [27].

Compared to protein and peptide pI markers, it is easier to obtain synthetic low-molecular-mass markers in pure form and they are less susceptible to change over time. The pI values of a series of ampholytic dyes (Patent Blue V, Fast Green FCF, Methyl Blue, Evan's Blue and Congo Red) were measured in gel IEF: they range from 3 to 5.8 [73]. They were used as internal pH standards to obtain the pI of bovine serum albumin, ovalbumin and bovine insulin which resulted in a good agreement with the literature values. Four different colored ferrous complexes of phenanthroline [74] were tested in gel IEF. It was reported that they focused relatively sharply in the gel and had a pI range from 5.45 to 6.82. In 1994, Slais *et al.* [54] designed 19 UV absorbing pI markers by varying the substituents on an aminomethylphenol core. The structures of these pI markers are listed in Figure 3.2. The substitution patterns were selected to optimize the $[-dz/d(pH)]_{pI}$ values and minimize the hydrophobicities of the markers. The properties of these markers are summarized in Figure 3.3. The pI values were determined by potentiometric titration: they ranged from pI 5.3 to 10.4. As for $[-dz/d(pH)]_{pI}$, all markers had a value greater than 0.045, except markers numbered 6 and 7, and thus were acceptable focusers. The pI markers also had satisfactory molar absorbance values in both the UV and the visible regions. $\log P$ is an indication of how hydrophobic a molecule is. Most of the pI makers had good water solubilities with calculated $\log P$ values below 1. The design took the acid-base, spectroscopic and hydrophobic properties into consideration and set an example of how to build desirable pI markers.

STRUCTURES OF SUGGESTED *pI* MARKERS OF GENERAL FORMULA I

No.	R ₁	R ₂	N(R ₃ , R ₄) ^a	M _r
1	NO ₂	CH ₂ N(R ₃ , R ₄)	PIP	406
2	CH ₂ N(R ₃ , R ₄)	NO ₂	PIP	406
3	NO ₂	CH ₂ N(R ₃ , R ₄)	MPIPE	509
4	CH ₂ N(R ₃ , R ₄)	NO ₂	MPIPE	509
5	CH ₂ N(R ₃ , R ₄)	NO ₂	HPIPE	569
6	NO ₂	H	DEA	261
7	NO ₂	H	PIP	273
8	NO ₂	CH ₂ N(R ₃ , R ₄)	MOR	435
9	CH ₃	NO ₂	MPIPE	338
10	CH ₃	NO ₂	HPIPE	368
11	CH ₂ N(R ₃ , R ₄)	NO ₂	MOR	410
12	Cl	NO ₂	MPIPE	359
13	CH ₃	NO ₂	MOR	289
14	Cl	NO ₂	HPIPE	389
15	NO ₂	H	MOR	275
16	Cl	NO ₂	MOR	309
17 ^b	4-CH ₂ N(R ₃ , R ₄)	2-Cl-6-NO ₂	MPIPE	359
18 ^b	4-CH ₂ N(R ₃ , R ₄)	2-Cl-6-NO ₂	HPIPE	389
19 ^b	4-CH ₂ N(R ₃ , R ₄)	2-Cl-6-NO ₂	MOR	309



^a PIP = 1-piperidyl; MPIPE = 1-(4-methylpiperazinyl); HPIPE = 1-(4-hydroxyethylpiperazinyl); DEA = diethylamino; MOR = 4-morpholinyl.

^b Aminomethyl group in position 4- and substituents R₁ and R₂ in position 2- and 6-, respectively.

Figure 3.2 List of the structures of the 19 UV absorbing *pI* markers designed by Slais *et al.* [54].

IEF, SPECTRAL AND LIPOPHILIC CHARACTERISTICS OF PROPOSED pI MARKERS

No.	pI	$ (dz/dpH)_{pI} $	λ_{max} (nm) ^a	$A^{1\%}$ ^b	Log P_{ow} ^c
1	10.4	0.76	403	617	1.08
2	10.1	0.60	412	374	0.64
3	8.6	0.74	420	102	-0.02
4	8.5	0.72	419	131	-0.78
5	8.4	0.60	417	80	-1.30
6	8.1	0.01	392	744	0.38
7	8.0	0.02	392	661	0.62
8	7.9	0.45	403	698	0.43
9	7.9	0.27	425	165	0.79
10	7.7	0.19	423	119	0.31
11	7.5	0.43	416	115	-0.19
12	7.4	0.17	428	156	0.58
13	7.2	0.15	416	162	1.05
14	7.0	0.14	423	139	0.02
15	6.6	0.15	400	526	0.49
16	6.5	0.07	421	142	0.88
17	6.4	0.09	416	131	-0.94
18	6.2	0.10	415	133	-2.18
19	5.3	0.12	409	142	-0.16

^a Wavelength of absorption maximum in UV-Vis spectrum of aqueous buffer solution at pH equal to the pI value.

^b Absorptivity of a 1% aqueous buffer solution at pH equal to the pI value.

^c Partition coefficient between 1-octanol and water at 25°C.

Figure 3.3 Characteristic properties of the synthetic UV absorbing pI markers [54].

There is a significant limitation of using UV absorbance as the detection method in cIEF: the detection sensitivity is poor because the currently available carrier ampholytes also have absorbance in the UV range. Using laser induced fluorescence (LIF) as the detection method can improve the detection sensitivity in cIEF; mass detection limits in cIEF coupled with LIF detection had reached the attomole range [75]. Only a few fluorescent pI markers are available, they are (1) fluorescent proteins, (2) fluorophore-labeled ampholytes, and (3) fluorescent small organic molecules. The problem with fluorescent proteins as pI markers is that the choices are very limited by the low numbers of proteins that can be excited with visible-range lasers.

Shimura and Kasai made 5 fluorescent *pI* markers ranging from *pI* 3.95 to 8.20 by labeling peptides with 5-carboxytetramethylrhodamine succinimidyl ester on the N-terminal amino group [75]. The spectral properties of 5-carboxytetramethylrhodamine are pH independent: fluorescence can be excited with the green light (543.5 nm) from an He-Ne laser. The potential detection limit of the labeling dye was reported to be 10^{-21} mol in capillary zone electrophoresis [76]. The problem with the fluorophore-labeled ampholytes as *pI* markers is that the presence of multiple labeling sites leads to a mixture of products with different *pI* values. Reversed phase HPLC was used to purify the labeled peptides with a recovery rate of 40% - 70% (based on the initial number of moles of peptides used in the synthesis). Shimura *et al.* [77] continued the work of making tetramethylrhodamine-labeled peptides as fluorescent *pI* markers in 2002. In this work, each peptide was designed to include a cysteine residue which was coupled with an iodoacetylated derivative of tetramethylrhodamine to avoid multiple labeling. 19 fluorescent *pI* markers were made covering the pH range from 3.64 to 10.12. The maximum *pI* gap was 0.68 as shown in Figure 3.4. To mitigate the effects of microbial or enzymatic degradation, the peptide-based *pI* markers were stored under acidic conditions: this, in turn, caused hydrolytic degradation after 3 days under a fluorescent lamp.

Table 1. Summary of *pI* Determination of Tetramethylrhodamine-labeled Peptide *pI* Markers

no. ^a	peptides ^b	<i>pI</i> (obs) ^c	SD	<i>N</i> ^d	V h cm ^{-1e}	<i>pI</i> (calc) ^f	-dz/dpH ^g
46	Gly-Cys-Tyr-Lys-Arg	10.12	0.05	4	113	10.02	1.108
47	Gly-Cys-Tyr-Lys-Lys	9.94	0.02	3	113	9.76	1.490
48	Gly-Cys-Tyr-Tyr-Lys-Lys	9.70	0.02	3	113	9.52	1.725
45	Gly-Cys-Tyr-Tyr-Tyr-Lys-Lys	9.56	0.03	3	113	9.36	1.896
73	Gly-Cys-Lys-Lys-Lys-Tyr-Tyr-Glu-Glu-Tyr-Arg-Tyr-Tyr	9.22	0.02	3	163	9.10	2.134
67	Gly-Cys-Tyr-Tyr-Tyr-Lys-Tyr-Tyr-Tyr-Lys-Tyr-Tyr-Tyr	insoluble				8.88	2.290
49	Gly-Cys-Tyr-Lys	slow focusing			>213	8.62	0.375
74	Lys(Gly)-Cys-Glu-Tyr-Tyr-Lys-Lys-Tyr	8.77	0.04	5	113	8.56	0.867
76	Lys(Gly)-Cys-Glu-Lys(Gly)-Tyr-Tyr-Tyr-Lys-Lys-Tyr-Tyr	8.68	0.05	3	163	8.56	1.308
44	Gly-Cys-Glu-Tyr-Tyr-Lys-Lys	8.71–8.93			>113	8.46	0.519
68	Gly-Cys-Tyr-Tyr-Tyr-His-Tyr-Tyr-His-Tyr-Tyr-Lys	insoluble				8.28	0.880
75	Lys(Gly)-Cys-Lys-Lys(Gly)-Glu	8.21	0.03	3	113	7.90	1.547
69	Gly-Cys-His-His-His-His-His-His-His-His	7.74	0.03	4	113	7.66	1.710
50	Gly-Cys-Glu-His-His-His-Arg	7.58	0.03	4	113	7.34	1.229
51	Gly-Cys-Glu-His-Arg	7.38	0.04	4	113	7.04	0.771
52	Gly-Cys-Glu-His-His	6.86	0.04	4	113	6.42	1.311
53	Gly-Cys-Glu-Arg	slow focusing			>113	6.06	0.125
70	Gly-Cys-His-Glu-His-Glu-His-Glu-His	6.18	0.02	3	113	6.02	2.060
54	Gly-Cys-Glu-His	slow focusing			>113	5.48	0.428
71	Gly-Cys-His-Glu-His-Glu-His-Glu-His-Glu	5.53	0.02	3	113	5.46	1.570
55	Gly-Cys-Asp-Asp-His-His	slow focusing			>113	5.24	0.526
72	Gly-Cys-Glu-His-Glu-His-Glu-His-Glu-Lys-Glu	4.99	0.01	3	113	5.02	2.240
56	Gly-Cys-Glu-Glu-His	4.50	0.08	3	113	4.54	1.381
57	Gly-Cys-Asp-Asp-Arg	4.23	0.02	3	113	4.16	1.477
58	Gly-Cys-Glu-Glu	3.99	0.01	3	113	3.82	1.249
59	Gly-Cys-Asp-Asp-Asp	3.64	0.02	3	113	3.38	1.695

^a The numbers of the peptides used for the mixture of 12 *pI* markers are underlined. ^b The peptides were labeled at the cysteine residues with iodoacetylated tetramethylrhodamine. The amino termini are shown on the left side. Lys(Gly) represents N^ε glycyL-lysine. L isomers were used, except for glycine. ^c Determined *pI* values. ^d The number of determinations. ^e The labeled peptides were focused within the listed values under the conditions used for *pI* determinations. ^f Calculated *pI* values. ^g Calculated -dz/dpH values at pH=*pI*.

Figure 3.4 Peptide sequences and characteristic properties of the tetramethylrhodamine-tagged peptide *pI* markers [77].

Slais *et al.* [39] synthesized four fluorescein-based *pI* markers by reacting fluorescein methylester with mono-alkylated piperazines at 80°C for 20-60 hours under reflux. The reaction scheme is shown in Figure 3.5. This series of low-molecular-mass markers covers a relatively narrow *pI* range from 5.4 to 6.6. Fluorescein-based *pI* markers are compatible with argon ion laser-induced fluorescence detection. However, their spectral properties are pH dependent: the detection limits are more favorable in the basic pH region.

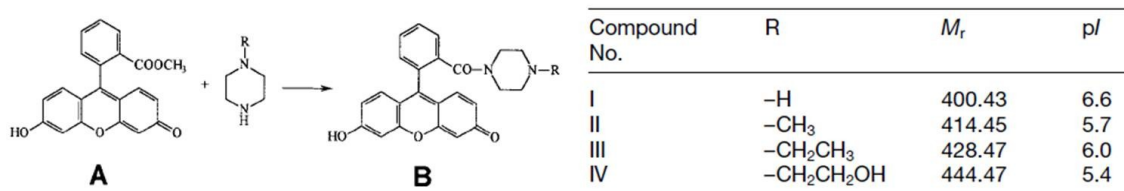


Figure 3.5 Synthetic scheme (left) and the summarized properties (right) of fluorescein-based pI markers [39].

The need for LIF-compatible pI markers remains unsatisfied. Slais [78] summarized the criteria a good colored pI marker should fulfill as follows: (1) high color intensity in the visible range, (2) good focusing ability, (3) high water solubility, (4) chemical and hydrolytic stability, (5) purity and (6) accessibility.

Up to now, compounds selected as pI markers had to be found via extensive screening [79], because there were no known correlations between the structure of an ampholyte and its pI value. It was discovered in our laboratory that the pK_a values of two identical protic groups used as substituents of the sulfonamido groups on a pyrene core structure differ by about 0.7. The same was found for protic groups attached to bis-sulfonamido groups of certain other aryl core structures as well. The significance of this finding is that it permits the development of ampholytes with $[-dz/d(pH)]_{pI}$ values greater than 0.9 in a methodical and systematic way. (The significance of the $[-dz/d(pH)]_{pI}$ value of an ampholyte was discussed in Chapter 1.4.)

The generic structure of the rationally designed pyrene-based fluorescent *pI* markers is shown in Figure 3.6. The *pI* markers contain two identical buffering groups as part of the sulfonamido substituents attached at the 1 and 3 positions and a charge-balancing (titrating) group attached as part of an alkoxy substituent at the 6 position of the pyrene core.

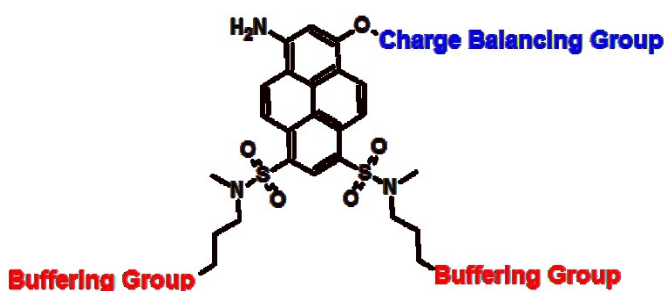


Figure 3.6 One of the possible generic structures of the pyrene-based *pI* markers.

The effective charge versus pH curve of a designed *pI* marker can be calculated using the SPARC software, Ver. 4.6 (available at sparc.chem.uga.edu/sparc/index.cfm). The calculated *pI* value can be found at the pH where the effective charge of the molecule equals zero as in the example shown in Figure 3.7. A large set of pyrene-based fluorescent *pI* markers with predicted excellent focusing properties covering the *pI* range 3 to 10 is listed in Tables 3.1 to 3.7.

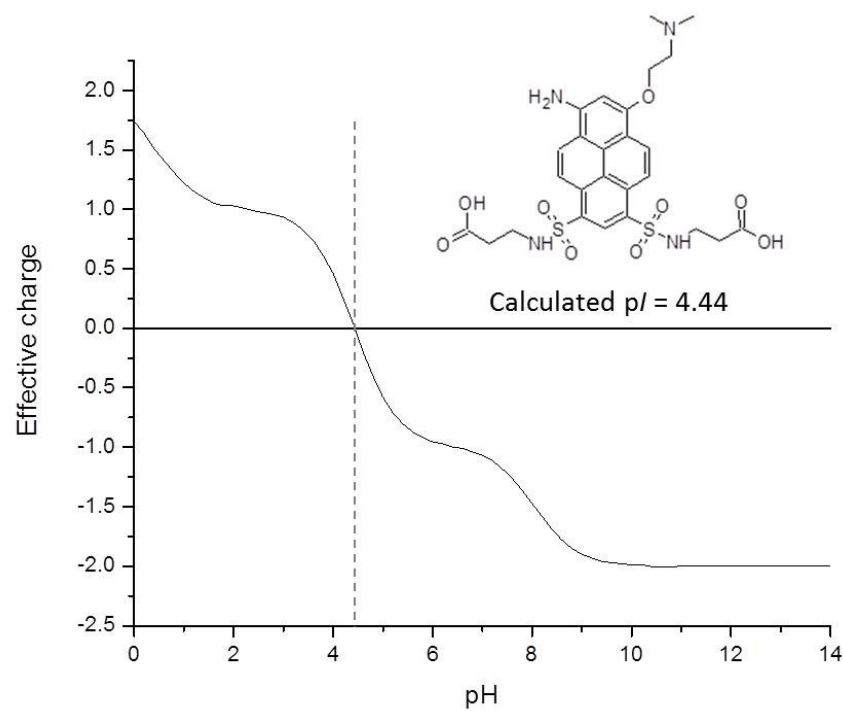


Figure 3.7 An effective charge versus pH curve generated by SPARC for a pI marker utilizing β -alanine as the source of the buffering groups and N,N -dimethylamino bromoethane as the source of the titrating group.

Table 3.1 A list of the possible pyrene-based fluorescent pI markers ($3 < pI < 4$)

pI	Sulfonamido buffering group derived from	Titrant group derived from	$[-dz/dpH]_{pI}$
3.04	Aminomalonic acid	Dimethylaminopropanol	1.17
3.04	Aminomalonic acid	Choline	1.16
3.05	3-Aminopentanedicarboxylic acid	Isethionic acid	1.21
3.09	Iminodipropionic acid	Isethionic acid	1.26
3.10	Aspartic acid	Ethylene glycol	0.56
3.10	Glutamic acid	Ethylene glycol	0.79
3.32	4-Imidazoleacetic acid	Isethionic acid	1.17
3.39	2-Hydroxy-4-aminobutyric acid	Isethionic acid	1.10
3.40	4-Aminoheptanedicarboxylic acid	Isethionic acid	1.21
3.50	Iminodipropionic acid	Ethylene glycol	1.30
3.55	3-Aminopentanedicarboxylic acid	Ethylene glycol	1.22
3.60	3-Aminopentanedicarboxylic acid	Dimethylaminopropanol	1.19
3.60	N-(Acetic)-3-aminopropionic acid	Choline	1.19

Table 3.1 (continued)

<i>pI</i>	Sulfonamido buffering group derived from	Titration group derived from	$[-dz/dpH]_{pI}$
3.63	β -Alanine	Isethionic acid	1.15
3.65	2-Hydroxy-4-aminobutyric acid	Choline	1.16
3.66	Aspartic acid	Choline	1.19
3.77	Iminodi(4-butyric acid)	Isethionic acid	1.17
3.85	Iminodi(3-propionic acid)	Choline	1.26
3.90	Iminodi(3-propionic acid)	Dimethylaminopropanol	1.26
3.92	4-Aminoheptanedicarboxylic acid	Ethylene glycol	1.19
3.92	Glutamic acid	Choline	1.19
3.95	Glutamic acid	Dimethylaminopropanol	1.20

Table 3.2 A list of the possible pyrene-based fluorescent pI markers ($4 < pI < 5$)

pI	Sulfonamido buffering group derived from	Titrant group derived from	$[-dz/dpH]_{pI}$
4.04	3-Aminopentanedicarboxylic acid	Dimethylaminopropanol	1.22
4.04	3-Aminopentanedicarboxylic acid	Choline	1.22
4.06	Iminodiacetic acid	Choline	1.22
4.10	3-Hydroxy-4-aminobutyric acid	Choline	1.15
4.17	Aspartic acid	Dimethylaminopropanol	1.16
4.18	Aspartic acid	Choline	1.17
4.26	β -Alanine	Choline	1.15
4.26	Iminodi(3-propionic acid)	N,N'N'-trimethylpiperazine	1.30
4.32	5-Aminocaproic acid	Isethionic acid	1.15
4.52	4-Aminoheptanedicarboxylic acid	Choline	1.11
4.53	4-Aminobutyric acid	Choline	1.15
4.55	4-Aminoheptanedicarboxylic acid	Dimethylaminopropanol	1.13
4.56	Iminodiacetic acid	N,N'N'-trimethylpiperazine	1.23
4.65	Glycine	Choline	1.15

Table 3.3 A list of the possible pyrene-based fluorescent pI markers ($5 < pI < 7$)

pI	Sulfonamido buffering group derived from	Titrant group derived from	$[-dz/dpH]_{pI}$
5.06	Piperazine-N-ethanesulfonic acid	N-(2-hydroxyethyl)-N-methyl-N'(2-sulfoethyl)-N'-methylethylenediamine	0.73
5.52	N-(2-Hydroxyethyl-(ethoxy(ethoxy))-piperazine	Isethionic acid	1.13
5.61	Piperazine-N-ethanesulfonic acid	N-(2-hydroxyethyl)-N-methyl-N'(2-sulfoethyl)-N'-methyl-propylenediamine	1.19
5.69	Histidine	Isethionic acid	0.76
5.98	Piperazine-N-3-propanesulfonic acid	N-(2-hydroxyethyl)morpholine	0.74
6.09	Piperazine-N-3-propanesulfonic acid	N-(2-hydroxyethyl)-N-methyl-N'(2-sulfoethyl)-N'-methyl-propylenediamine	0.90
6.20	Piperazine-N'-ethanesulfonic acid	Dimethylaminopropanol	0.93
6.20	5-Hydroxymethyl imidazole	Isethionic acid	1.15
6.25	4-Hydroxymethyl imidazole	Isethionic acid	1.15
6.29	Aminomethylphosphonic acid	Dimethylaminopropanol	1.14
6.46	Imino (diethylene glycol)	Isethionic acid	1.15
6.47	2-Hydroxypropylmorpholine	Isethionic acid	1.15
6.53	Imidazole	Isethionic acid	1.15

Table 3.3 (continued)

pI	Sulfonamido buffering group derived from	Titration group derived from	$[-dz/dpH]_{pI}$
6.73	Morpholine	Isethionic acid	1.15
6.75	4-Imidazolecarboxylic acid	Dimethylaminopropanol	1.15
6.87	4-Imidazoleacetic acid	Dimethylaminopropanol	1.17

Table 3.4 A list of the possible pyrene-based fluorescent pI markers ($7 < pI < 9$)

pI	Sulfonamido buffering group derived from	Titration group derived from	$[-dz/dpH]_{pI}$
7.01	2-Aminoethylmorpholine	Isethionic acid	1.15
7.31	Histidine	Ethylene glycol	0.39
7.50	N-(2-Aminoethyl)-tris(hydroxymethyl)aminomethane	Isethionic acid	1.14
7.78	Tris(hydroxymethyl)amino methane	Isethionic acid	1.15
8.00	N,N-di(2-hydroxyethyl)-N'-methyl-ethylenediamine	Isethionic acid	1.14
8.23	Diethanolamine	Isethionic acid	1.15
8.38	Lysine	Isethionic acid	1.15
8.66	(2-Hydroxyethyl-(ethoxy-(ethoxy))amine	Isethionic acid	1.15
8.70	Glycine	Dimethylaminopropanol	1.20
8.87	N-Ethyl-N-(2-Hydroxyethyl-(ethoxy-(ethoxy))amine	Isethionic acid	1.14
8.89	5-Aminocaproic acid	Dimethylaminopropanol	0.48
8.93	N-Propyl(β -alanine)	Dimethylaminopropanol	0.68

Table 3.5 A list of the possible pyrene-based fluorescent pI markers ($9 < pI < 10$)

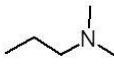
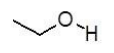
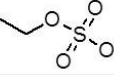
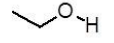
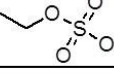
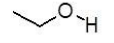
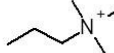
pI	Sulfonamido buffering group derived from	Titration group derived from	$[-dz/dpH]_{pI}$
9.04	Di(3-propanol)amine	Isethionic acid	1.15
9.09	Glycine	Choline	1.10
9.13	2-Hydroxy-4-aminobutyric acid	Dimethylaminopropanol	0.92
9.20	N,N-(Di(2-hydroxyethyl)ethylenediamine	Isethionic acid	1.17
9.26	Dimethylamine	Isethionic acid	1.15
9.27	2-Hydroxy-4-aminobutyric acid	Dimethylaminopropanol	0.36
9.31	Iminodi(4-butyric acid))	Dimethylaminopropanol	0.34
9.33	N-ethyl-N-(2-hydroxyethyl)amine	Isethionic acid	1.14
9.39	Diethylamine	Isethionic acid	1.15
9.43	N-Methyl-N',N'(dimethyl)ethylenediamine	Isethionic acid	1.15
9.45	Lysine	Dimethylaminopropanol	0.75
9.48	N,N'-Di(2-hydroxyethyl)ethylenediamine	Isethionic acid	1.17
9.59	N-Propylamine	Isethionic acid	1.15
9.61	Lysine	Dimethylaminopropanol	0.75

Table 3.5 (continued)

pI	Sulfonamido buffering group derived from	Titration group derived from	$[-dz/dpH]_{pI}$
9.63	Ethanolamine	Isethionic acid	1.15
9.65	Piperazine	Isethionic acid	1.17
9.80	3-Hydroxy-4-aminobutyric acid	Choline	1.09

Seven pyrene-based *pI* markers with the highest structural complexity were chosen to demonstrate that the proposed synthetic approach is feasible and that the *pI* markers are good focusers, as predicted. Three amino acids (aspartic acid, histidine and lysine) were used to introduce the buffering groups and amino, alcohol and sulfate functional groups were selected as the charge balancing (titrating) groups (see Table 3.6). A general synthetic scheme of making the pyrene-based fluorescent *pI* markers is shown in Figure 3.8. The final *pI* marker structures are shown in Figure 3.9.

Table 3.6 Seven synthesized pyrene-based *pI* markers.

<i>pI</i>	Buffering Group	Titrating Group
3.07	Asp	
4.16	Asp	
5.73	His	
7.45	His	
8.34	Lys	
9.42	Lys	
10.50	Lys	

* *pI* values were calculated using SPARC (SPARC Performs Automatic Reasoning in Chemistry) Online Calculator v4.6.

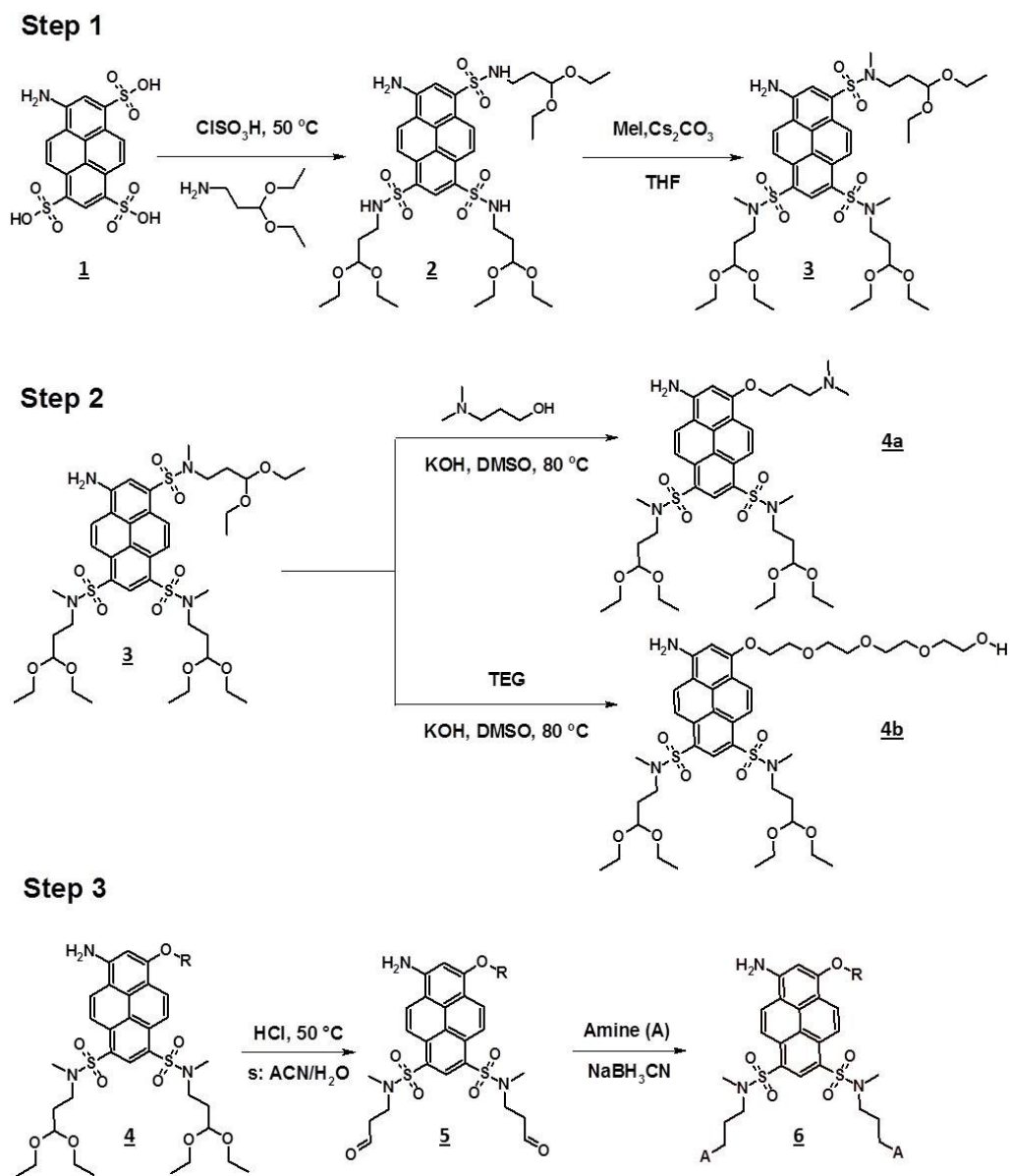


Figure 3.8 Synthesis scheme of making the pyrene-based fluorescent pI markers.

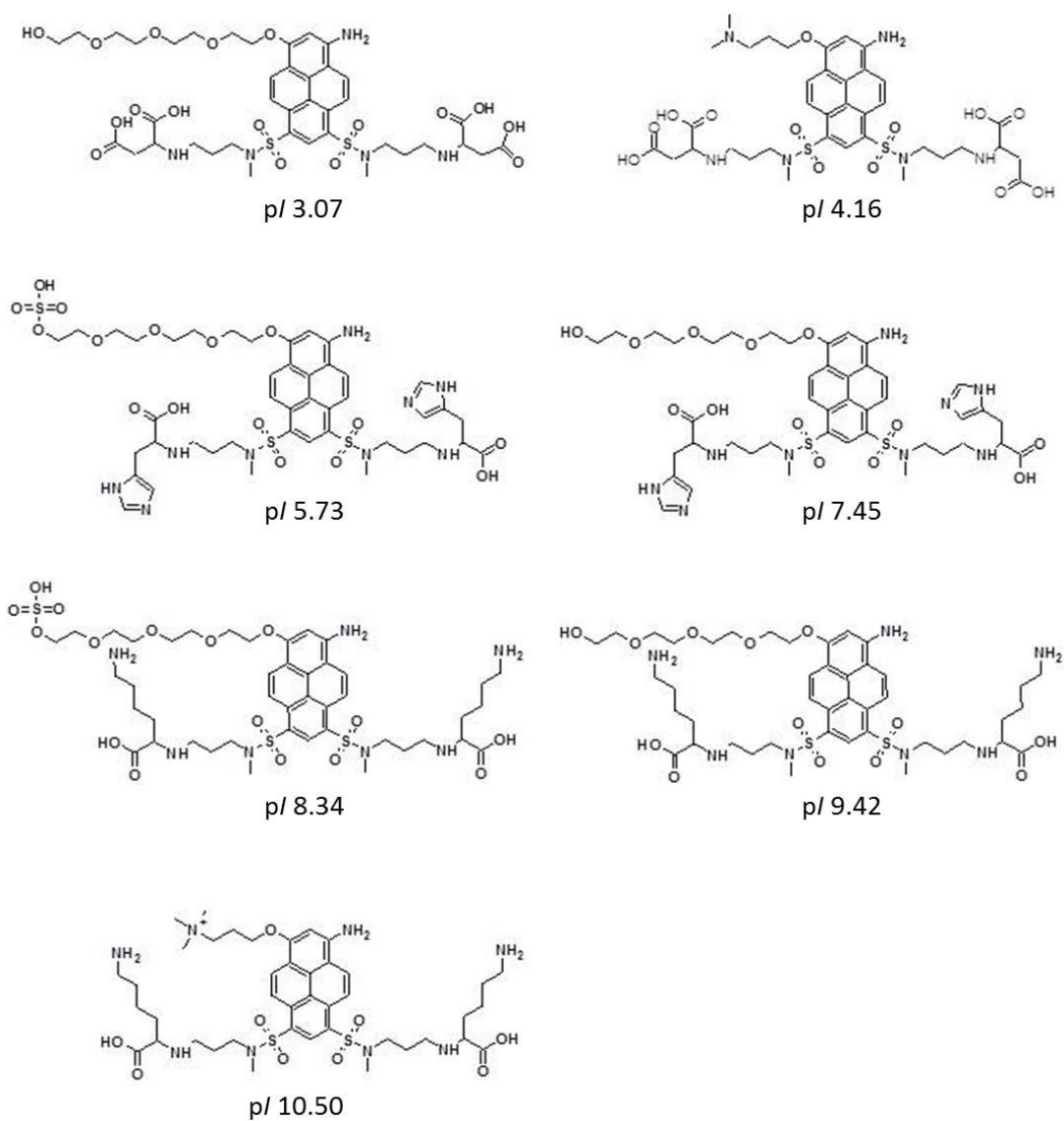


Figure 3.9 Structures of the pyrene-based pI markers synthesized in this work and their calculated pI values.

3.1.2 Materials and Method

3.1.2.1 Chemicals and Equipment

8-Amino-1,3,6-pyrenetrisulfonic acid (APTS), trisodium salt was provided by Beckman Coulter Inc. (Fullerton, CA). 3-Aminopropionaldehyde diethyl acetal, *N*-Boc-L-lysine methyl ester hydrochloride and dimethyl-L-aspartate hydrochloride were purchased from TCI America Co. (Portland, OR). Chlorosulfonic acid, methyl iodide, cesium carbonate, *N,N*-dimethyl propanolamine, histidine methyl ester dihydrochloride, tetrahydrofuran, acetonitrile, dimethyl sulfoxide, tetra(ethylene glycol), triethylamine, sodium cyanoborohydride, potassium hydroxide, sodium sulfate, hydrochloric acid and sulfur trioxide pyridine complex were purchased from Sigma-Aldrich Co. (St. Louis, MO). HPLC analyses and LC-MS analyses were done with the instrument and column described in 2.1.2.1.

3.1.2.2 Synthesis of Compound **2** [56]

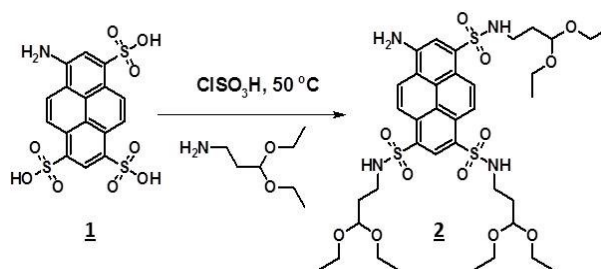


Figure 3.10 Reaction scheme for making compound **2**.

Reaction scheme for making compound **2** is shown in Figure 3.10. A 60 mg portion of APTS was mixed with chlorosulfonic acid at a rate of 18 ml acid per gram of APTS in a dry round bottom flask, placed into an ice bath, then heated to 50°C with stirring. After 20 minutes, the reaction mixture was removed from the 50°C oil bath and carefully added into 20 mL of iced water forming a red precipitate, chlorinated APTS. The slurry was centrifuged and the supernatant was decanted to get a pasty solid. 250 μ L (15 equivalents) of 3-aminopropionaldehyde diethyl acetal and 810 μ L (50 equivalents) of triethylamine were premixed in 2 mL acetonitrile and the solution was mixed with chlorinated APTS at room temperature for 5 minutes. The insert in Figure 3.11 shows that the absorbance maximum of the product was red-shifted compared to that of APTS as a result of sulfonamidation. Work-up of the reaction mixture containing compound **2** was done by concentrating the reaction mixture about tenfold, then mixing it with a 20 times larger volume of water to precipitate out the target. The precipitate was used in the following methylation step without further purification.

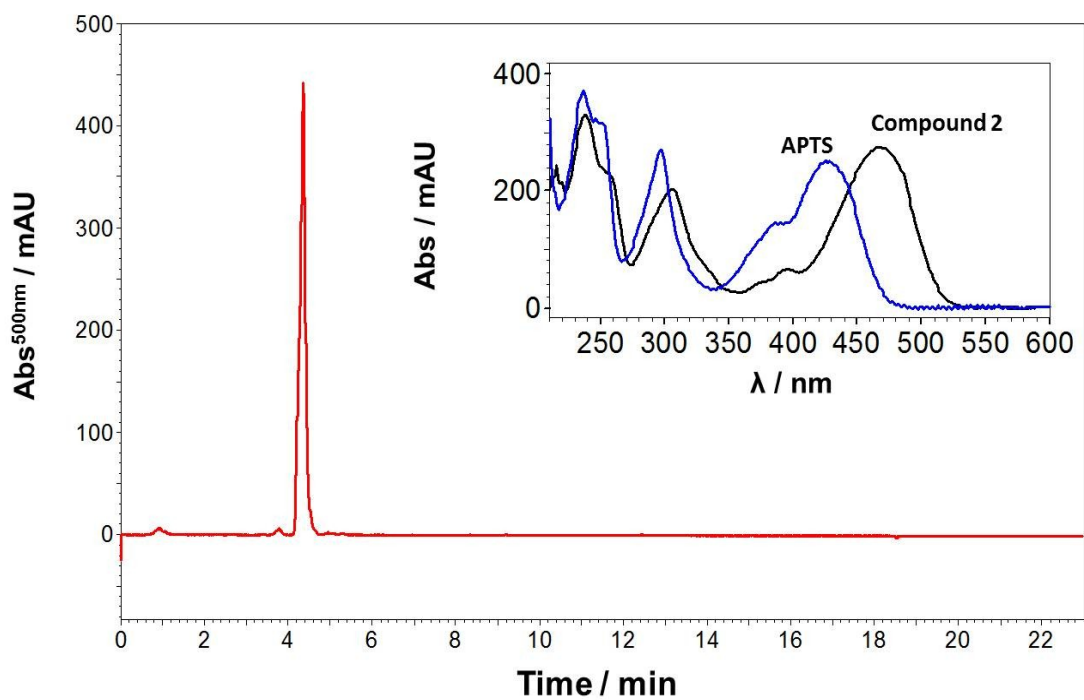


Figure 3.11 RP-HPLC analysis of compound 2. (Insert: overlay of the UV absorbance spectra of APTS and compound 2).

3.1.2.3 Synthesis of Compound 3

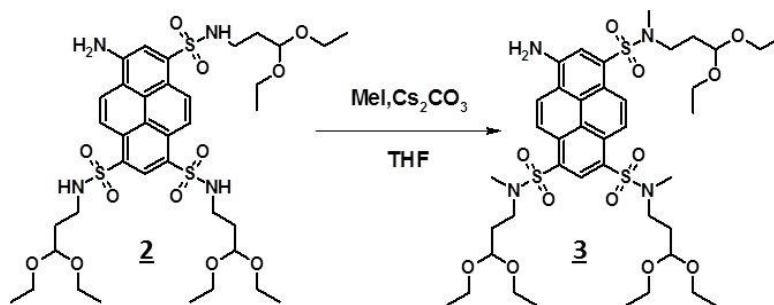


Figure 3.12 Reaction scheme for making compound 3.

Reaction scheme for making compound **3** is shown in Figure 3.12. Methylation of compound **2** was done by mixing 17.4 mg of compound **2** with methyl iodide in the presence of 80 mg (12 equivalents) of cesium carbonate in 100 μ L tetrahydrofuran. The extent of methylation of compound **2** was monitored by RP-HPLC as shown in Figure 3.13. Methylation was complete after adding 20 equivalents of methyl iodide. The residues of 3-aminopropionaldehyde diethyl acetal, triethylamine and water from the previous synthetic steps and the work-up procedures consumed the excess amount of methyl iodide. An overmethylated byproduct was also found during LC-MS analysis of the methylation reaction mixture. Work-up of the reaction mixture containing compound **3** was achieved by removing most of the left-over methyl iodide and tetrahydrofuran with a stream of nitrogen gas, followed by addition of 200 μ L of water to precipitate out the methylated target.

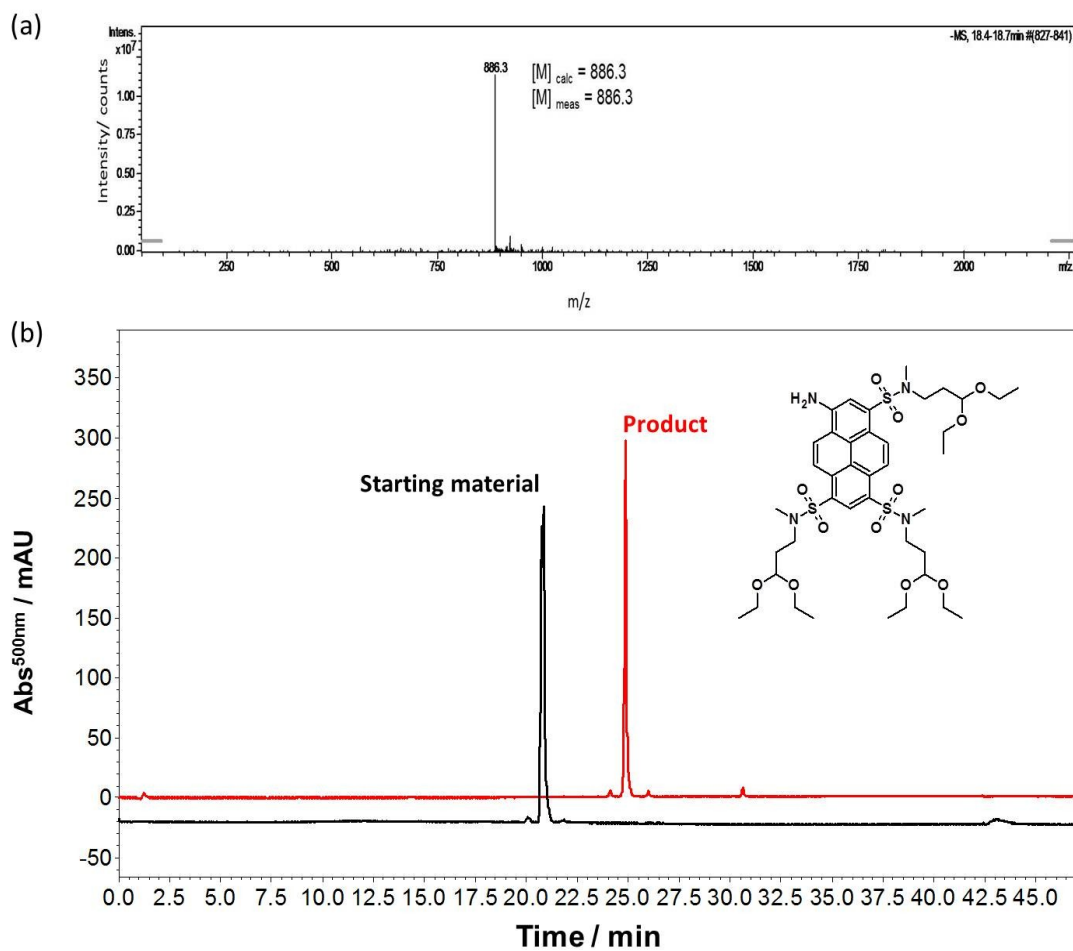
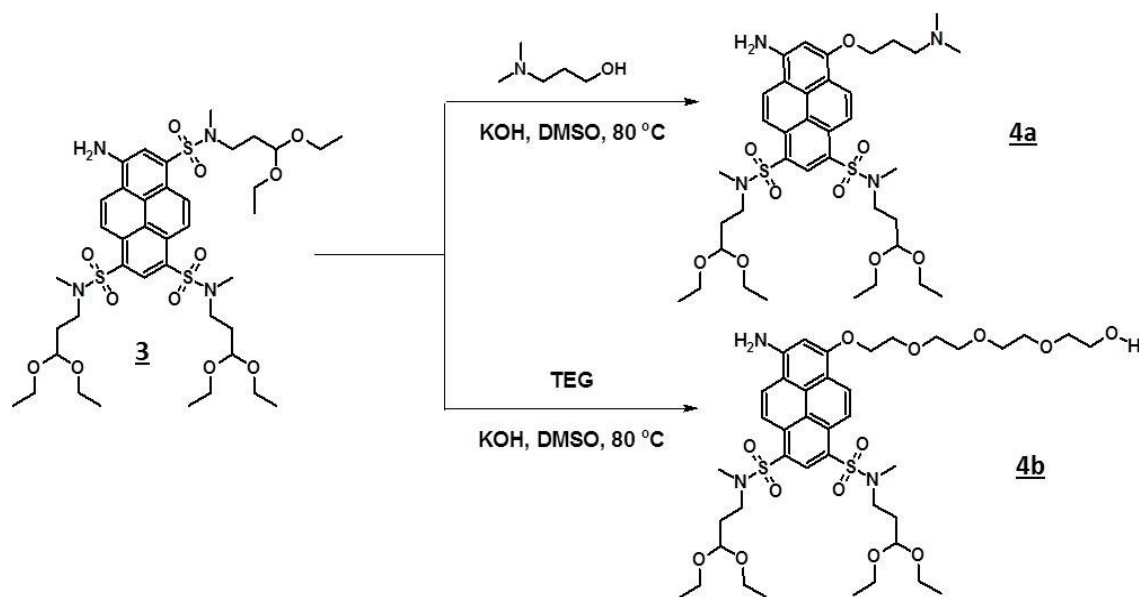


Figure 3.13 (a) ESI mass spectrum (negative ion mode) of compound **3** and (b) RP-HPLC analysis of the reaction mixture and compound **3**.

3.1.2.4 Synthesis of Compound **4**Figure 3.14 Reaction scheme for making compound **4**.

It was discovered earlier in our laboratory that when trisulfonamido APTS was treated with sodium hydroxide in a 50% solution of alcohols in dimethyl sulfoxide [56], one of the sulfonamido groups was replaced by an alkoxy group causing a 10 nm red shift in $\lambda^{\text{ex}}_{\text{max}}$ compared to that of the trisulfonamido APTS. Therefore, dimethylamino propanol and tetra(ethylene glycol) were used to react with compound **3** to make the corresponding alkoxy derivatives as shown in Figure 3.14. Both alcohols were mixed with dimethyl sulfoxide at a 1 to 1 volume ratio and mixed with compound **3**. Finely ground potassium hydroxide was added to the reaction mixture as a base depot. The reactions were carried out at 80 °C overnight with good stirring. The alkoxy substituted

reaction products and the starting material were analyzed by RP-HPLC as shown in Figure 3.15. The UV absorbance spectra of both derivatives were the same and agreed with the reported analogous spectra [56]. ESI mass spectra of compounds **4a** and **4b** are shown in Figure 3.16. The work-up procedure included a tenfold dilution of both reaction mixtures with water, followed by three successive extractions of the solution with equal volumes of ethyl acetate. Compounds **4a** and **4b** were obtained as oily concentrates after solvent removal and used, without further purification, in the next step.

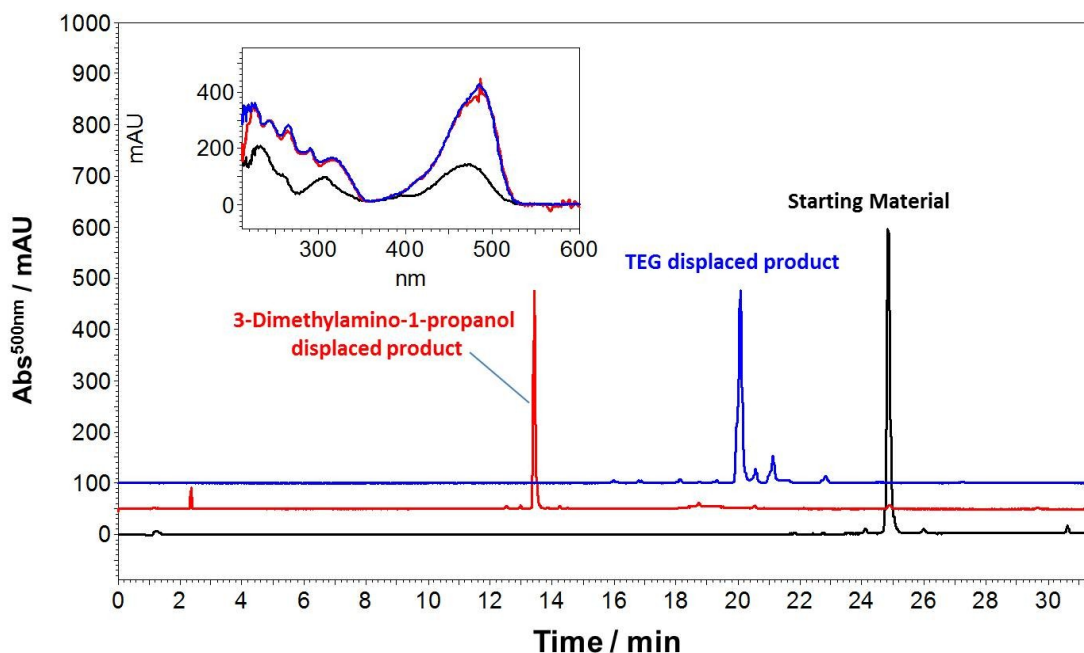


Figure 3.15 RP-HPLC analysis of compound **3** and its alkoxy derivatives. (Insert: UV/VIS absorbance spectra of compounds **3**, **4a** and **4b**.)

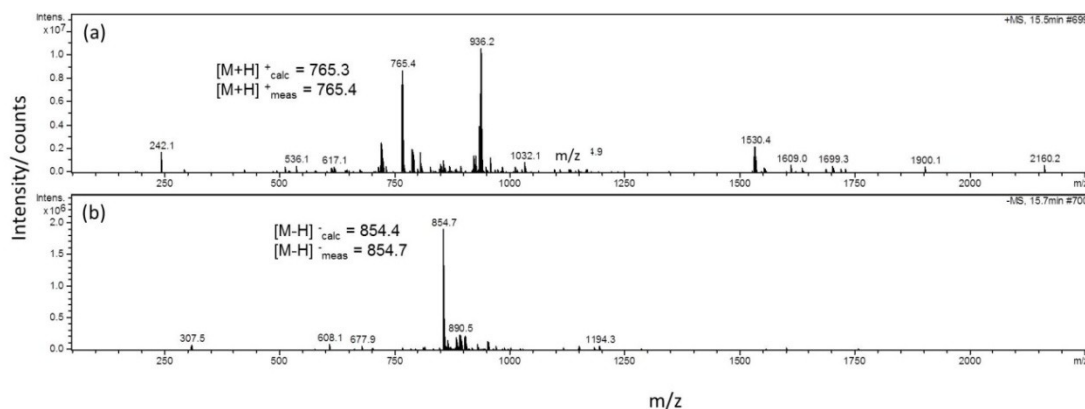


Figure 3.16 ESI mass spectra of compounds **4a** and **4b**.

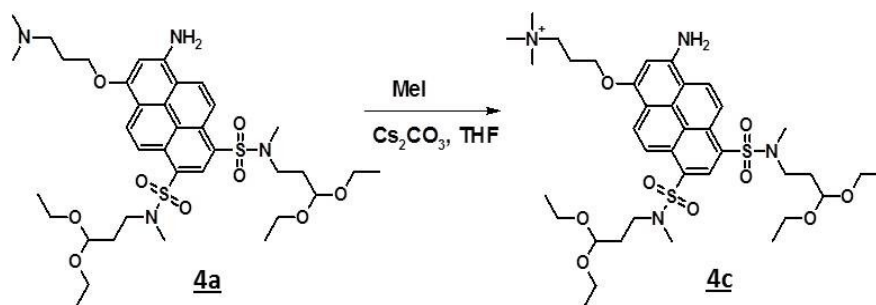


Figure 3.17 Reaction scheme for making compound **4c**.

To make the desired *pI* marker with a calculated *pI* value of 10.5 as described in Figure 3.9, compound **4c** carrying an alkoxy substituent with a terminal quaternary ammonium group was synthesized by methylating the dimethylamino group of compound **4a** as shown in Figure 3.17. 10 mg of compound **4a** was dissolved in 100 μ L of tetrahydrofuran with a depot of cesium carbonate and 2 μ L (3 equivalents) of methyl iodide were added at room temperature. The reaction mixture was analyzed by LC-MC after 2 hours. The results are shown in Figure 3.18. Cesium carbonate was removed

from the reaction mixture by centrifugation and the solution obtained was used, without further purification, in the next step.

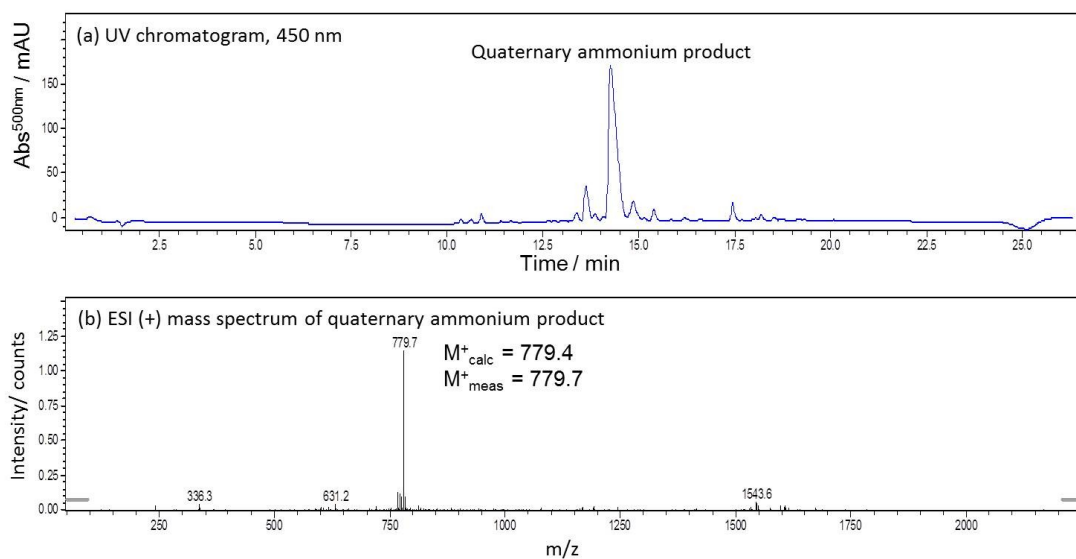


Figure 3.18 LC-MS analysis of the reaction mixture of compound **4c**.

3.1.2.5 Synthesis of Compounds **5** and **6**

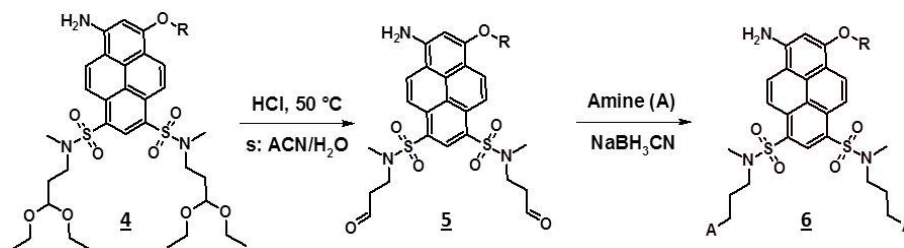


Figure 3.19 Reaction scheme for making compounds **5** and **6**.

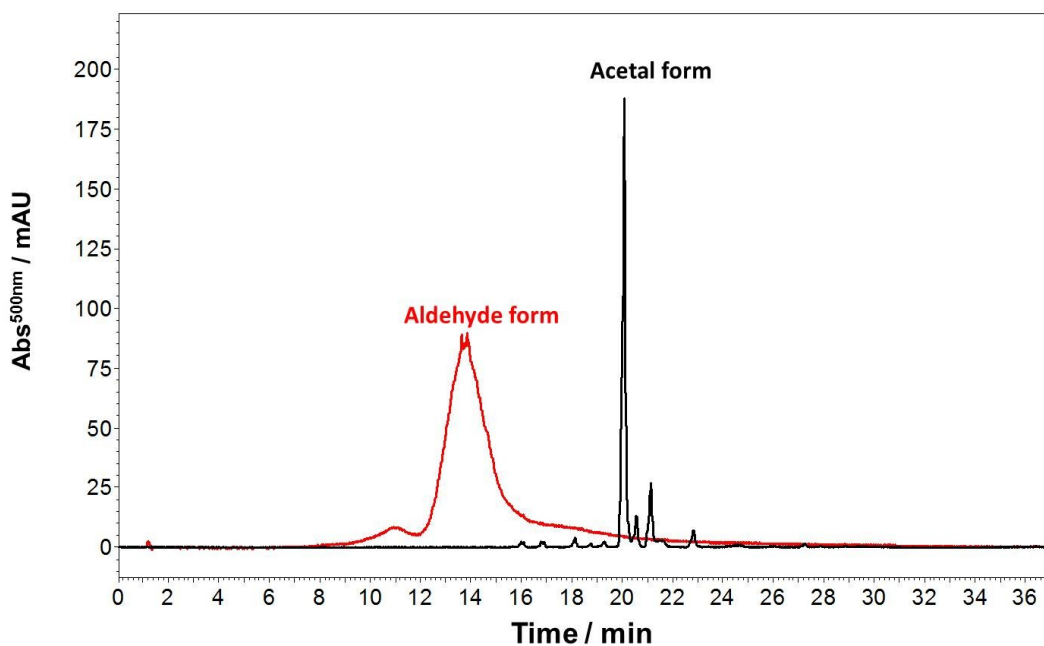


Figure 3.20 Overlaid chromatograms of compounds 4 and 5.

The conversion of compound 4 (diacetal) to 5 (aldehyde) as shown in Figure 3.19 was performed on the 10 mg scale by adding 2.2 equivalents of hydrochloric acid to compound 4 which was dissolved in a mixture of 75% (v/v) acetonitrile and 25% (v/v) water. Conversion to the aldehyde form was monitored by RP-HPLC. The conversion reaction was complete within 15 minutes at 50°C for the tetra(ethylene glycol) derivative and 30 to 45 minutes for both the dimethylamino propanol and quaternary ammonium derivatives. As shown in Figure 3.20, the peak of the aldehyde compound was broadened by the moderately fast (on the time scale of the separation) equilibration rate between the diol and aldehyde forms of compound 4 in the column. Once compound 4 was converted into 5, an aldehyde, the pH of the solution was adjusted to around 4~6

with acetic acid and a 5% sodium bicarbonate solution. Water from the reaction mixture was then removed by passing the mixture through, twice, a Pasteur pipet column that was packed with about 1 gram of anhydrous sodium sulfate, using acetonitrile as the eluent. Compound **5** in acetonitrile was then concentrated and used in the following reductive amination step. The free base form of dimethyl-L-aspartate was obtained by neutralizing dimethyl-L-aspartate hydrochloride with sodium hydroxide in water, then extracting it into dichloromethane. The same procedure was used to get *N*-Boc-L-lysine methyl ester from its hydrochloride salt. Histidine methyl ester dihydrochloride was neutralized with 2 equivalents of sodium hydroxide in methanol and used directly in the reductive amination step.

The general reductive amination procedure was to mix compound **5** with the corresponding amino acid esters at a mole ratio of 1 to 20 in acetonitrile or methanol with a depot of anhydrous sodium sulfate, at room temperature, followed by, after 30 minutes, the addition of sodium cyanoborohydride in tetrahydrofuran as the reducing agent. RP-HPLC analysis of the reaction mixtures obtained during reductive amination to make the respective compound **6** derivatives are shown in Figure 3.21.

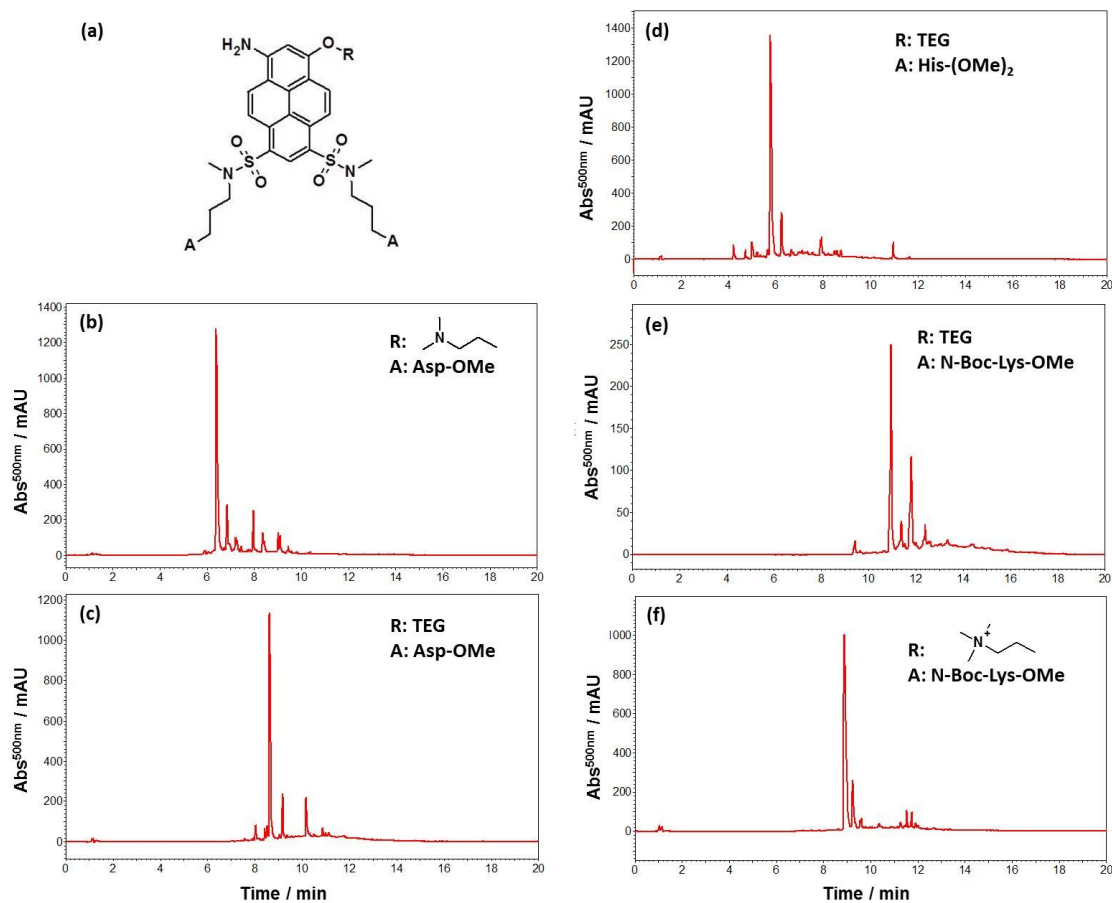


Figure 3.21 RP-HPLC analysis of the reaction mixtures obtained during reductive amination to make the respective compound **6** derivatives. (a) general structure of compound **6**, (b) to (f) chromatograms.

3.1.2.6 Sulfation of the TEG Derivatives of Compound **6**

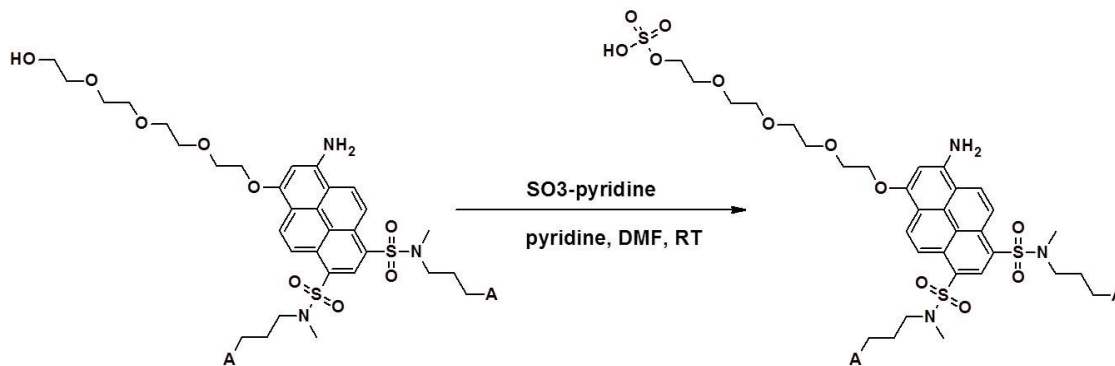


Figure 3.22 Sulfation of the TEG derivative of compound **6**.

The APTS-based pI markers with calculated pI values of 5.73 and 7.45 have the same buffering groups (histidine) on the APTS, but the charge-balancing (titrating) groups are different: by changing the charge-balancing group from a neutral alcohol group to a sulfate group shifts the pI value from 7.545 to 5.73. The same is true for the markers with pI values of 9.42 and 8.34. The sulfation reaction was done by reacting both the histidine and lysine derivatives of compound **6** with excess sulfur trioxide pyridine complex in dimethylformamide in the presence of a catalytic amount of pyridine as shown in Figure 3.22. LC-MS analysis of the sulfation reaction mixture of the histidine derivative of compound **6** is shown in Figure 3.23.

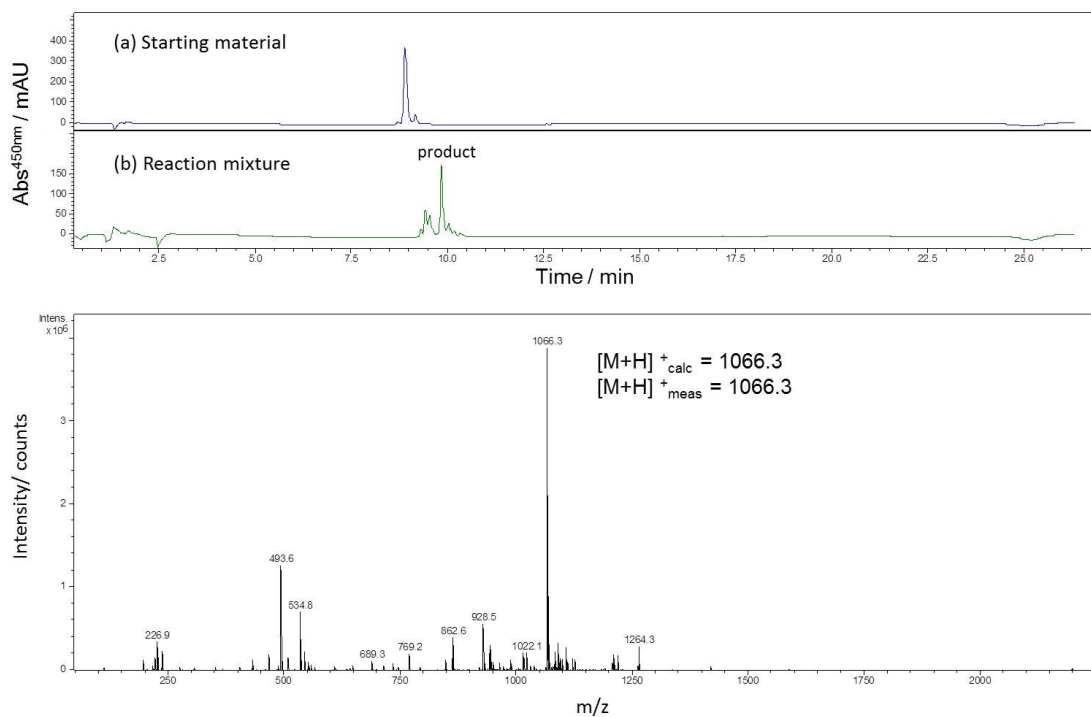


Figure 3.23 LC-MS analysis of the sulfation reaction mixture of the histidine derivative of compound **6**.

3.1.2.7 LC-MS Analysis of APTS-Based *pI* Makers after Purification

5 to 10 mg amounts of all 7 APTS-based *pI* makers were purified with semipreparative-scale RP-HPLC to get the final products and analyzed by LC-MS as shown in Figures 3.24 to 3.30.

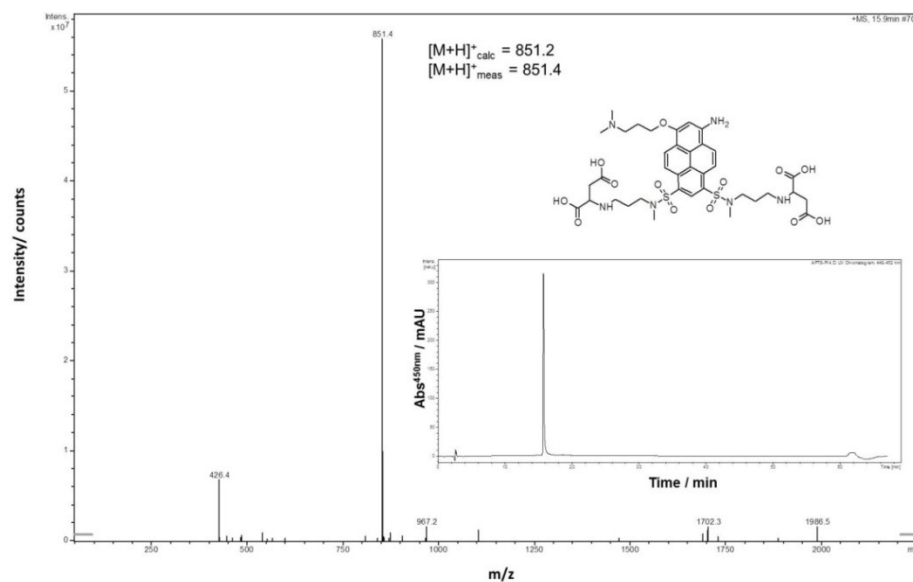


Figure 3.24 ESI mass spectrum of the APTS-based pI marker having a calculated pI value of 3.07 (Insert: chromatogram of the purified compound)

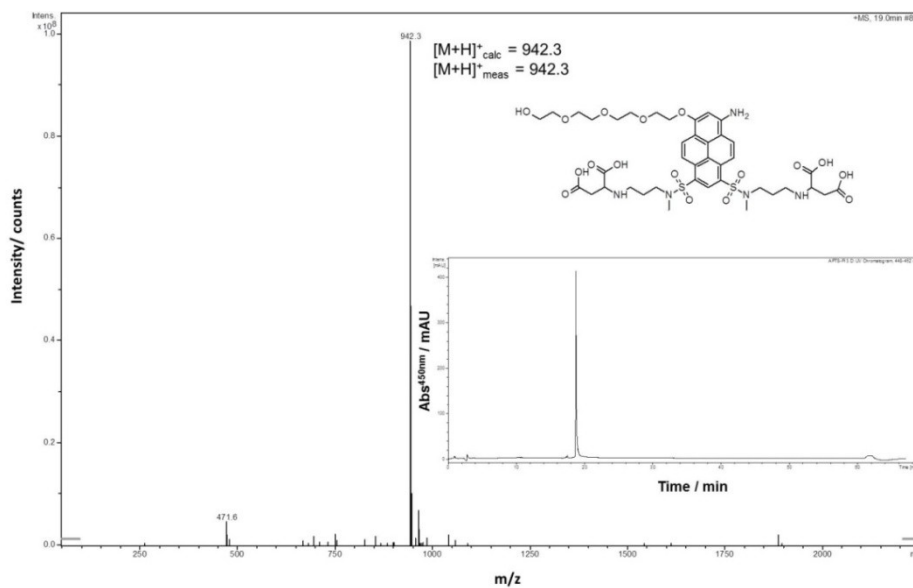


Figure 3.25 ESI mass spectrum of the APTS-based pI marker having a calculated pI value of 4.16 (Insert: chromatogram of the purified compound)

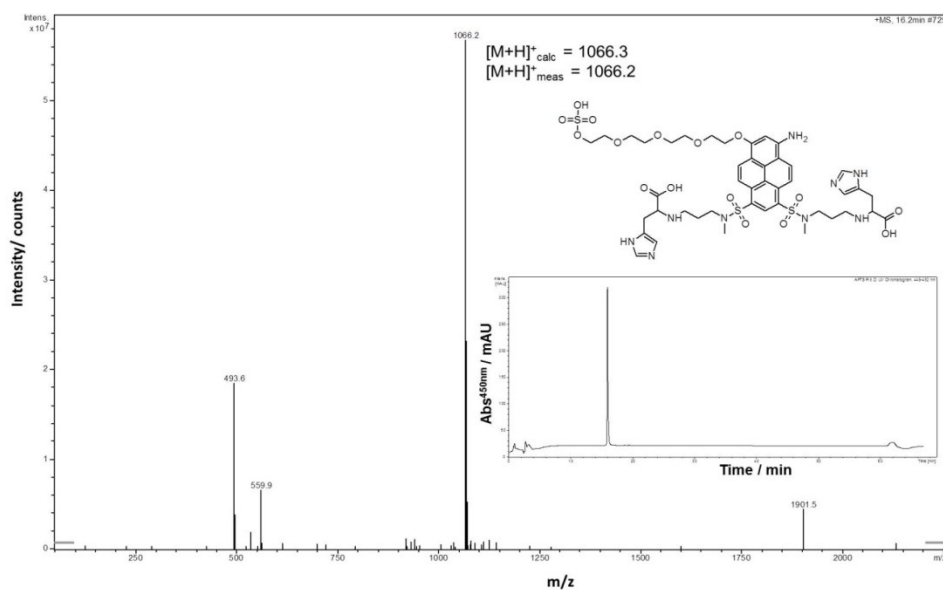


Figure 3.26 ESI mass spectrum of the APTS-based pI marker having a calculated pI value of 5.73 (Insert: chromatogram of the purified compound)

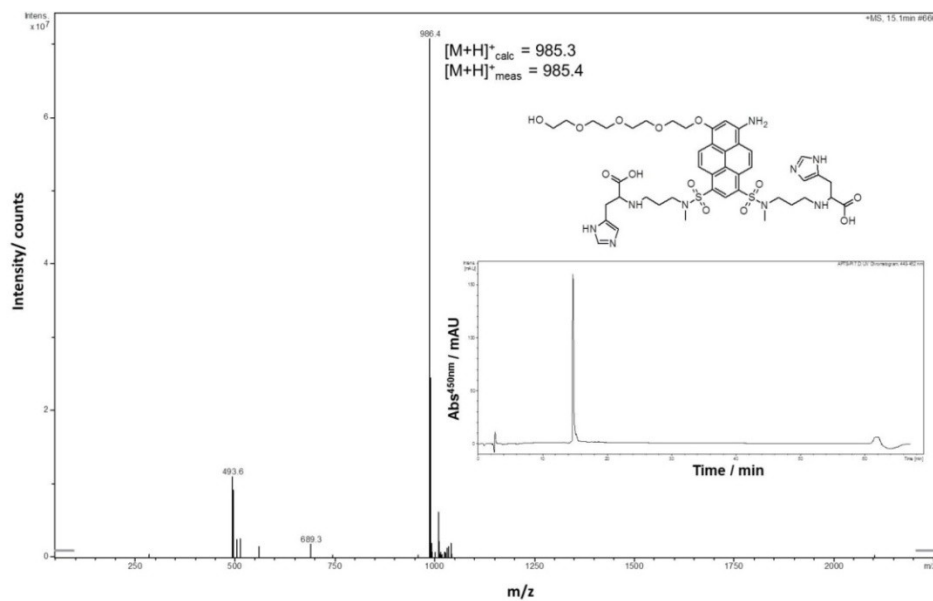


Figure 3.27 ESI mass spectrum of the APTS-based pI marker having a calculated pI value of 7.45 (Insert: chromatogram of the purified compound)

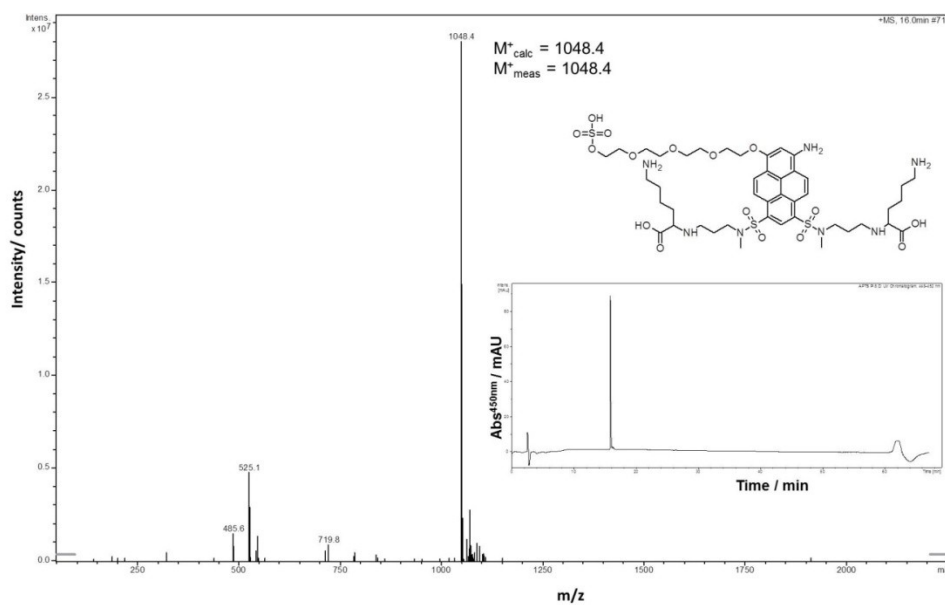


Figure 3.28 ESI mass spectrum of the APTS-based pI marker having a calculated pI value of 8.34 (Insert: chromatogram of the purified compound)

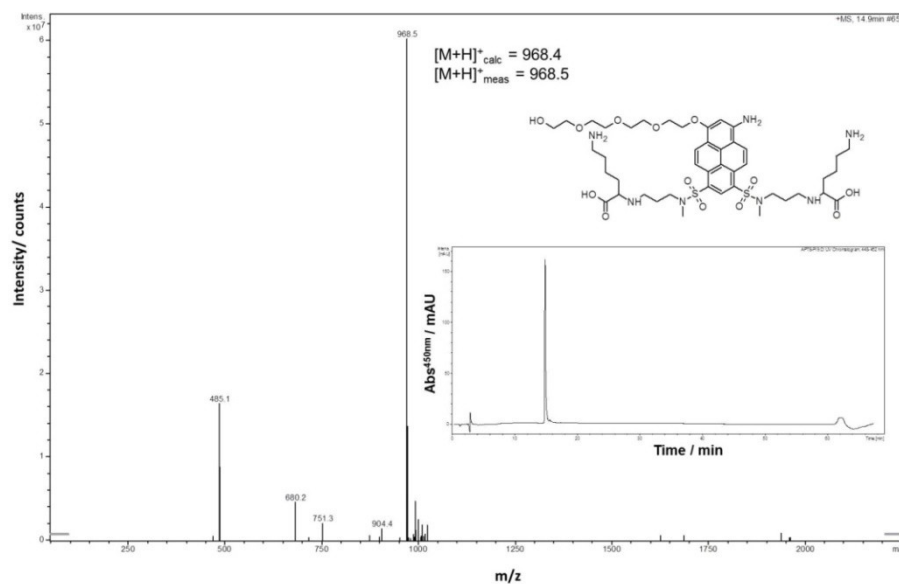


Figure 3.29 ESI mass spectrum of the APTS-based pI marker having a calculated pI value of 9.42. (Insert: chromatogram of the purified compound.)

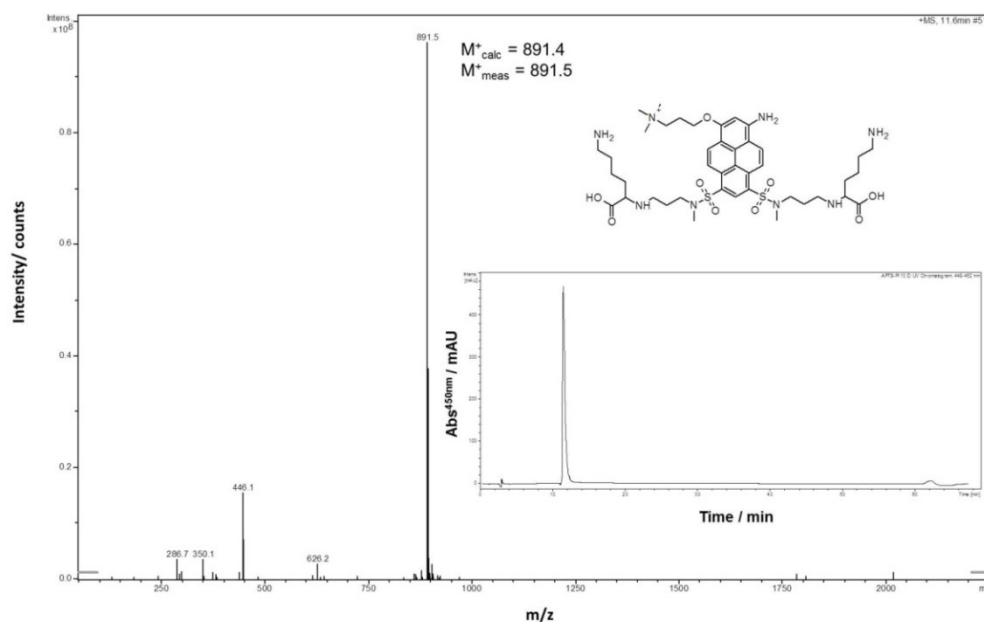


Figure 3.30 ESI mass spectrum of the APTS-based pI marker having a calculated pI value of 10.15. (Insert: chromatogram of the purified compound.)

3.2 pI Value Determination

3.2.1 Background and Objective

There are basically two ways of determining the pI values of ampholytic compounds: directly, by isoelectric focusing (IEF) or by indirectly, finding the respective pK_a values and calculating the pI value. IEF can be performed in a slab-gel format and the pH of the carrier ampholyte-filled gel segment where the analyte is focused can be measured directly with a miniaturized glass electrode. The main disadvantage of this method is that a large sample amount is needed. Performing IEF in a capillary [25] helps solve the problems encountered in slab-gel IEF and allows the use of higher applied potential for better separation efficiency. Factors affecting the measurement and pros and cons of the

cIEF determination of the pI values were discussed clearly in one of Righetti's IEF reviews [22]. Poor engineering of the pH gradient and instability of the pH gradient are the major problems in cIEF. Shimura *et al.*[27] found that the calibration curve obtained by plotting the pH values as a function of detection time was not linear in most cases and pointed out that “ pI values of samples should be estimated by assuming a linear relationship for pH against detection time only between two flanking marker peptides.” Another approach to determine the pI value is, in principle, to obtain the respective pK_a values since the pI value can be calculated as $pI = 1/2 (pK_{a1} + pK_{a2})$ where pK_{a1} and pK_{a2} are the neighboring pK values and $pK_{a1} < pI < pK_{a2}$, for a diprotic ampholyte [80]. In capillary zone electrophoresis (CZE), the pK_a value of an analyte can be obtained by appropriately fitting the curve of the effective mobilities of the analyte as a function of the pH of the background electrolytes [81-83]. The pI values of the APTS based pI markers synthesized in this work were determined by pressure-mediated capillary electrophoresis (PreMCE) [84] and cIEF.

3.2.2 Materials and Method

An APTS-based molecule used as fluorescent electroosmotic flow marker (neutral marker) and hydroxypyrenetrisulfonate-based (HPTS-based) pI makers were synthesized in our laboratory [56]. Dextran sulfate sodium salt ($M_w \sim 500,000$), 25% (w/w), poly(vinylsulfonic acid, sodium salt), hexadimethrin bromide (Polybrene) were purchased from Sigma-Aldrich Co. (St. Louis, MO). Pharmalyte pI 3-10 carrier ampholytes and the cIEF kit were purchased from Beckman-Coulter (Fullerton, CA).

Both PreMCE and cIEF experiments were carried out with a ProteomLab PA 800 system coupled with a LIF detector using a 488 nm argon ion laser module (Beckman-Coulter, Fullerton, CA).

3.2.2.1 Pressure-Mediated Capillary Electrophoresis (PreMCE)

The Polybrene (PB)-coated capillary used in PreMCE experiment was prepared from 25 μm I.D., 360 μm O.D. bare fused silica capillary column stock (Polymicro Technologies, Phoenix, AZ). The capillary was first rinsed with methanol for 3 minutes, water for 3 minutes and then with 1 M sodium hydroxide for 45 minutes, at 70 psi pressure. After this preconditioning step, the capillary was treated with a 10 % (w/w) Polybrene solution for 15 minutes to form the first cationic layer. A 3 % (w/w) dextran sulfate (DS) or 25 % (w/w) poly(vinylsulfonate) solution was next rinsed through the PB-coated capillary for 15 minutes to form an anionic layer on top of PB. The final PB-coated capillary had a total of 3 PB layers deposited by sequential rinses with PB and DS [85]. The same preconditioning procedure was used to make the anionic poly(vinylsulfonate)-coated capillary. After depositing the first layer of PB onto the capillary, a poly(vinylsulfonate) solution was rinsed through the capillary twice, with water rinses in between. The BGEs were prepared with HPLC grade water and the details of their preparations are listed in Table 3.7. The pH values of the BGEs were measured at 25 °C with a sympHony pH meter (VWR International, Radnor, PA) and a MicroProbe pH sensor (Thermo Fisher Scientific Inc., Waltham, MA).

Table 3.7 Background electrolytes used in the PreMCE experiments

pH	Compositions
2.5-3.0	H ₃ PO ₄ – LiOH (Ionic strength = 5 mM)
3.5-4.0	β-alanine – MSA (Ionic strength = 5 mM)
4.3	13 mM HOAc and 5 mM LiOH
4.7	6.5 mM HOAc and 5 mM LiOH
6.2	9 mM MES and 5 mM LiOH
6.9	14 mM MOPS and 5 mM LiOH
8.1	10 mM TRIS and 5 mM MSA
8.8	20 mM morpholine and 5 mM MSA
9.9	9 mM β-alanine and 5 mM LiOH
11.4	0.45 mM H ₃ PO ₄ and 4.5 mM LiOH

*The ionic strength of all listed BGEs was 5 mM.

PreMCE was performed according to the procedures described by Williams and Vigh [84]. The programmed potential (V_{prog}) was set at 30 kV with normal or reversed polarity, depending on the surface coating of the capillary. Electrophoretic separation times were varied from 2 to 3.5 minutes with linear voltage ramp-up and ramp-down times of 0.17 minutes each. The pressure mobilization velocity was about 0.1 cm/sec. Injection times (t_{inj}) were 4 seconds, and transfer times (t_{tr}) were set for 45 seconds, both at 4 psi. The analyte tested was injected first and transferred a distance into the capillary

by applying 4 psi pressure for time t_{tr} . Second, the EOF marker was injected and transferred a distance into the capillary by applying 4 psi pressure for the same time t_{tr} . Third, another EOF marker was injected and transferred, again for time t_{tr} . After loading the analyte and EOF markers, a potential V_{prog} was applied to cause electrophoretic migration. Finally, a neutral marker was injected into the capillary at the end of the electrophoretic process and the bands were mobilized with 4 psi pressure to pass them by the detector. Examples of the detector traces obtained for both the load and the electrophoretic experiments are shown in Figure 3.31. The effective mobility (μ_{eff}) values of the analyte can be determined accurately with PreMCE.

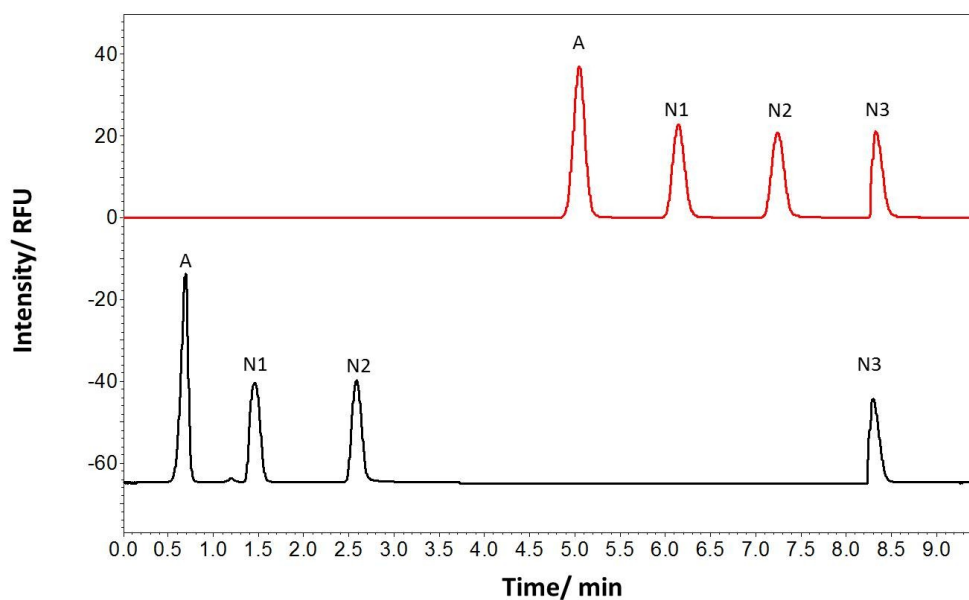


Figure 3.31 Detector traces obtained in a PreMCE experiment.

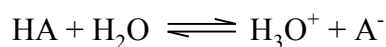
3.2.2.2 Effective Mobility of a Polyprotic Electrolyte as a Function of pH

The pI value of an ampholyte can be determined by measuring and analyzing its effective mobility versus pH curve. According to Tiselius [22], the effective mobility of an analyte, μ_{eff} is calculated as [86]:

$$\mu_{eff} = \sum_i \alpha_i \mu_i \quad (3.1)$$

where α_i is the mole fraction and μ_i is the ionic mobility of the i th species of the analyte.

For a monoprotic weak acid, the acid dissociation equilibrium can be schematically described by:



The corresponding concentration-based equilibrium coefficient K_a is:

$$K_a = \frac{[A^-][H_3O^+]}{[HA]} \quad (3.2)$$

The analytical concentration of HA is:

$$C_{HA} = [A^-] + [HA] \quad (3.3)$$

From Equation 3.2, the molar concentration of A^- can be expressed as Equation 3.4 and substituted in Equation 3.3:

$$[A^-] = \frac{K_a}{[H_3O^+]} [HA] \quad (3.4)$$

$$C_{HA} = [A^-] + [HA] = \frac{K_a}{[H_3O^+]} [HA] + [HA] = [HA] \left(\frac{K_a}{[H_3O^+]} + 1 \right) \quad (3.5)$$

With Equation 3.4 and 3.5, the mole fraction α_{HA} of HA can be expressed as:

$$\alpha_{HA} = \frac{[HA]}{C_{HA}} = \frac{[HA]}{[HA] \left(\frac{K_a}{[H_3O^+]} + 1 \right)} = \frac{[H_3O^+]}{K_a + [H_3O^+]} \quad (3.6)$$

Similarly, the mole fraction α_{A^-} of A^- is expressed as in Equation 3.9:

$$[HA] = \frac{[H_3O^+]}{K_a} [A^-] \quad (3.7)$$

$$C_{HA} = [A^-] + [HA] = [A^-] + \frac{[H_3O^+]}{K_a} [A^-] = [A^-] \left(1 + \frac{[H_3O^+]}{K_a} \right) \quad (3.8)$$

$$\alpha_{A^-} = \frac{[A^-]}{C_{HA}} = \frac{[A^-]}{[A^-] \left(1 + \frac{[H_3O^+]}{K_a} \right)} = \frac{K_a}{K_a + [H_3O^+]} \quad (3.9)$$

For a polyprotic acid, H_nA , all α_i values can be expressed as:

$$\alpha_0 = \frac{[H_nA]}{C_{HA}} = \frac{[H_3O^+]^n}{D} \quad (3.10)$$

$$\alpha_1 = \frac{[H_{n-1}A^-]}{C_{HA}} = \frac{K_{a1}[H_3O^+]^{n-1}}{D} \quad (3.11)$$

...

$$\alpha_n = \frac{[A^{n-}]}{C_{HA}} = \frac{K_{a1}K_{a2}\dots K_{an}}{D} \quad (3.12)$$

where the denominator D is:

$$D = [H_3O^+]^n + K_{a1}[H_3O^+]^{n-1} + K_{a1}K_{a2}[H_3O^+]^{n-2} + \dots + K_{a1}K_{a2}\dots K_{an} \quad (3.13)$$

Therefore, the effective mobility of a polyprotic acid varies with the molar concentration of hydronium as:

$$\mu_{eff} = \frac{K_{a1}[H_3O^+]^{n-1}}{D}\mu_1 + \frac{K_{a1}K_{a2}[H_3O^+]^{n-2}}{D}\mu_2 + \dots + \frac{K_{a1}K_{a2}\dots K_{an}}{D}\mu_n \quad (3.14)$$

3.2.2.3 Capillary Isoelectric Focusing (cIEF)

Two different ways of performing cIEF were tested in this work. In the conventional cIEF runs, the settings followed the instructions of the cIEF kit from Beckman-Coulter.

A cIEF mixture containing 2 % carrier ampholytes (CAs), 15 mM arginine, 2.5 mM

iminodiacetic acid as the anodic and the cathodic blocker, respectively, and 7 APTS-based *pI* markers dissolved in Beckman Coulter's cIEF polymer solution was prepared. 200 mM H₃PO₄ and 300 mM NaOH were used as the anolyte and the catholyte. Once the capillary was filled with the cIEF mixture, focusing was done by applying 25 kV potential for 9 minutes, followed by mobilization of the content of the capillary by 0.5 psi pressure while maintaining 21 kV potential. The other way of performing cIEF was tested when we tried to optimize the cIEF runs. Instead of mixing the two blockers with CAs, they were loaded into the respective ends of the capillary sequentially. Arginine and triethanolamine were both tested as cathodic blockers, and IDA and acetic acid as anodic blockers. Lengths and concentrations of the blockers and the CAs were optimized as stated in the results and discussions section. Focusing was done by applying 30 kV potential for 9 minutes, followed by 1 psi pressure mobilization.

3.2.3 Results and Discussion

3.2.3.1 *pI* Value Determinations by PreMCE

We planned to determine the *pI* values of the APTS based *pI* markers by first obtaining the effective mobilities of the APTS based *pI* markers in background electrolytes of different pH values using pressure-mediated capillary electrophoresis (PreMCE) described in 3.3.2.1. The *pKa* values of the APTS based *pI* markers were then to be determined by nonlinear curve fitting to Equation 3.14 described in 3.3.2.2.

Unfortunately, we encountered severe adsorption due to electrostatic and hydrophobic interactions between the APTS based *pI* markers and the capillary wall in the low ionic

strength background electrolytes, which makes accurate measurement of the effective mobilities in certain pH ranges impossible. A detector trace obtained in a PrEMCE experiment where no chromatographic retention is evident is shown in Figure 3.32: the distance between the analyte and the first neutral marker (d_{AN}) is equal to the distance between the first and second neutral marker (d_{NN}).

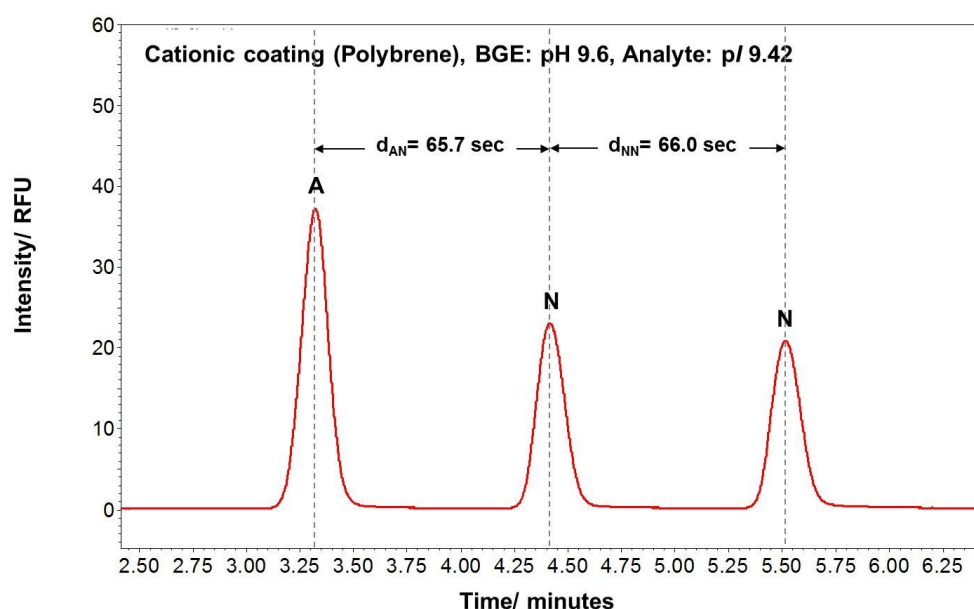


Figure 3.32 The LIF detector trace recorded in a PrMCE experiment with the *pI* marker having a calculated *pI* value of 9.42 and loaded as the first band in a background electrolyte of pH 9.6, in a Polybrene-coated capillary.

Based on its structure, the APTS-based *pI* marker with a calculated *pI* value of 4.16 is considered to have the weakest chromatographic retention from among all the seven markers synthesized in this work. The *pI* 4.16 (calculated) marker was loaded as the

first band in a PreMCE experiments carried out in a background electrolyte of pH 3.6 in four capillaries that had different surface coatings: a cationic coating (Polybrene), an anionic coating (poly (vinylsulfonate)) and two types of hydrophilic neutral coating (cross-linked polyacrylamide and GuarantTM). The respected detector traces are shown in Figures 3.33 to 3.36. At pH 3.6, all three of the amino groups of the *pI* marker are protonated and at least two of its carboxylate groups are dissociated. This makes the *pI* marker having a calculated *pI* value of 4.16 a cation. Due to the presence of multiple anionic and cationic groups on the *pI* marker, the marker was chromatographically retained on both the cationic and the anionic surface coatings via electrostatic interactions. The APTS based *pI* marker having a calculated *pI* value of 4.16 was then tested in two other capillaries that had different types of neutral surface coatings. In these capillaries, retention was reduced but not eliminated. We also checked the behavior of the APTS based *pI* marker having a calculated *pI* value of 7.45 (considered to be the most hydrophobic APTS-based *pI* marker among all seven of the markers synthesized in this work due to the presence of the two histidine-derived buffering groups). As shown in Figures 3.37 to 3.40, chromatographic retention was found in all four of the coated capillaries at pH 9.0, even though the pH of the BGE was at least 1.5 pH units above its calculated *pI* value.

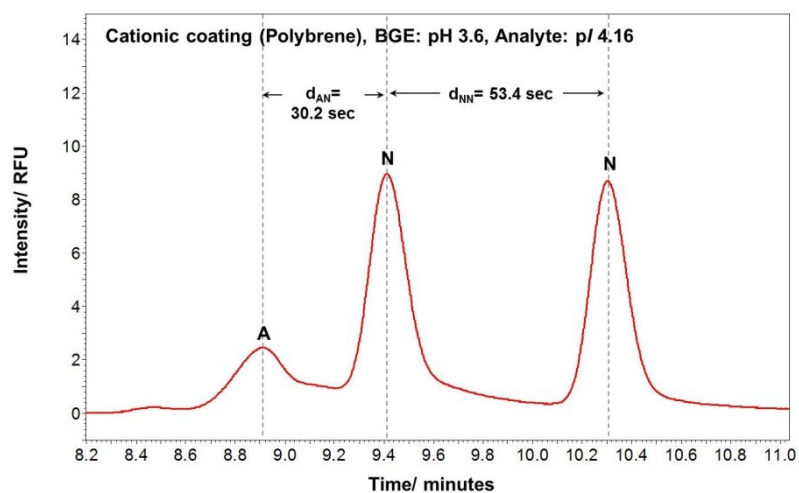


Figure 3.33 The LIF detector trace recorded in a PrMCE experiment with the pI marker having a calculated pI value of 4.16 and loaded as the first band in a background electrolyte of pH 3.6, in a Polybrene-coated capillary.

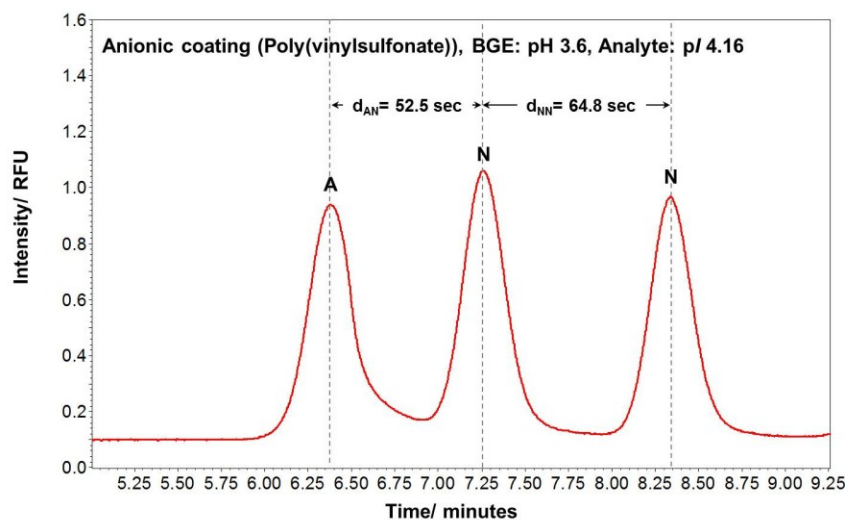


Figure 3.34 The LIF detector trace recorded in a PrMCE experiment with the pI marker having a calculated pI value of 4.16 and loaded as the first band in a background electrolyte of pH 3.6, in a poly (vinylsulfonate)-coated capillary.

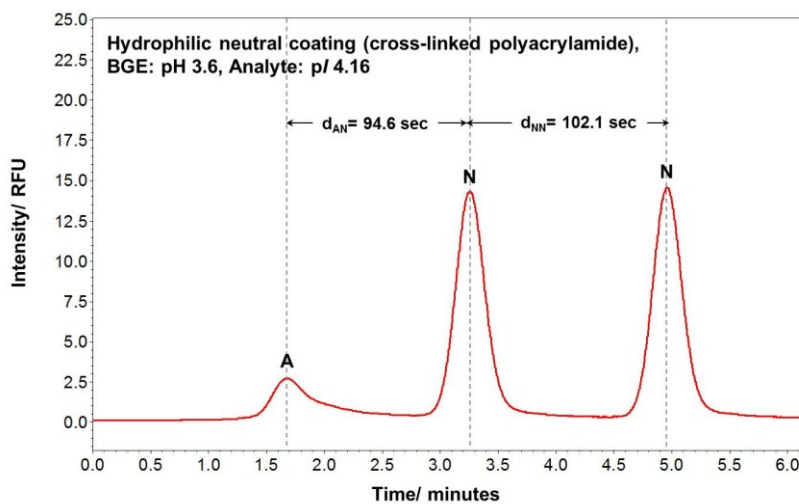


Figure 3.35 The LIF detector trace recorded in a PrMCE experiment with the pI marker having a calculated pI value of 4.16 and loaded as the first band in a background electrolyte of pH 3.6, in a cross-linked polyacrylamide coated capillary.

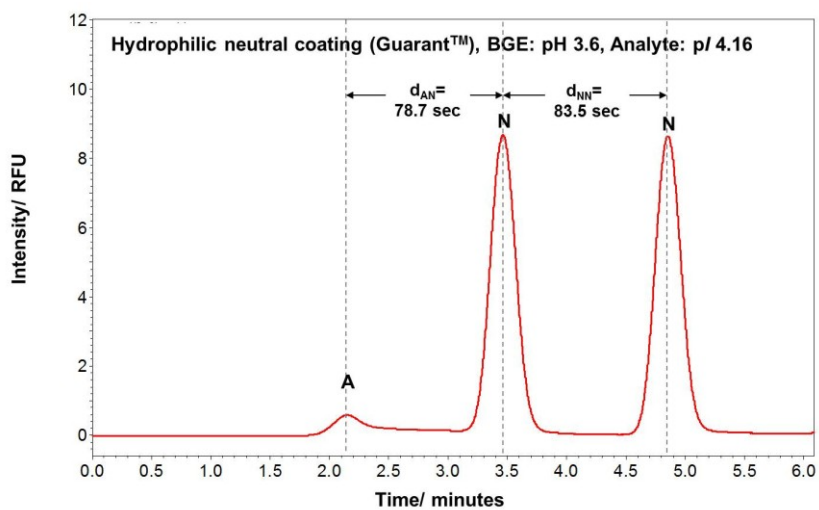


Figure 3.36 The LIF detector trace recorded in a PrMCE experiment with the pI marker having a calculated pI value of 4.16 and loaded as the first band in a background electrolyte of pH 3.6, in a Guarant™ capillary (ALCOR Biosystems).

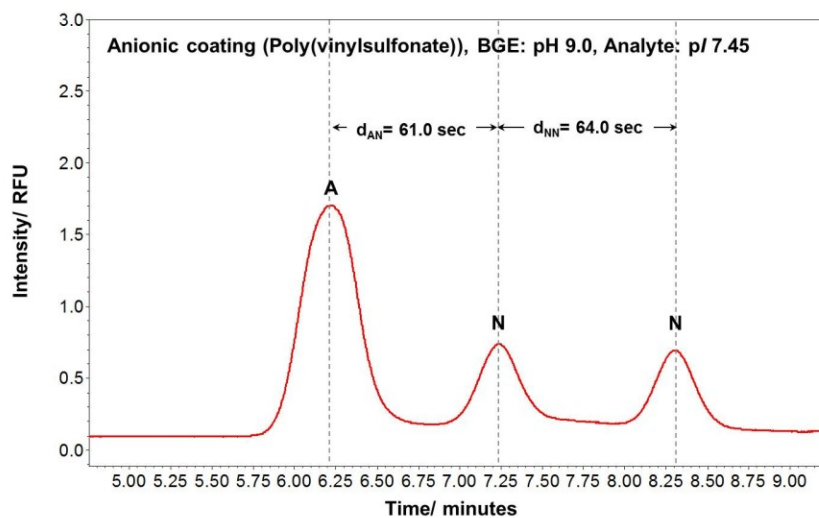


Figure 3.37 The LIF detector trace recorded in a PrMCE experiment with the pI marker having a calculated pI value of 7.45 and loaded as the first band in a background electrolyte of pH 9.0, in a poly (vinylsulfonate)-coated capillary.

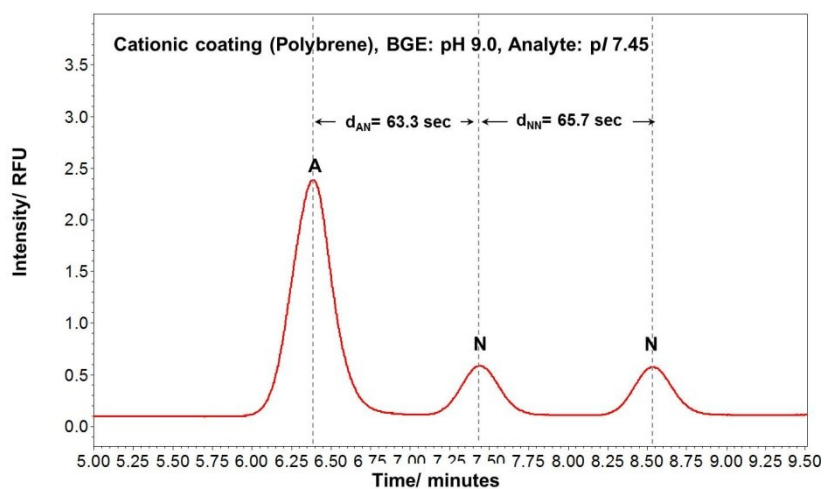


Figure 3.38 The LIF detector trace recorded in a PrMCE experiment with the pI marker having a calculated pI value of 7.45 and loaded as the first band in a background electrolyte of pH 9.0, in a Polybrene-coated capillary.

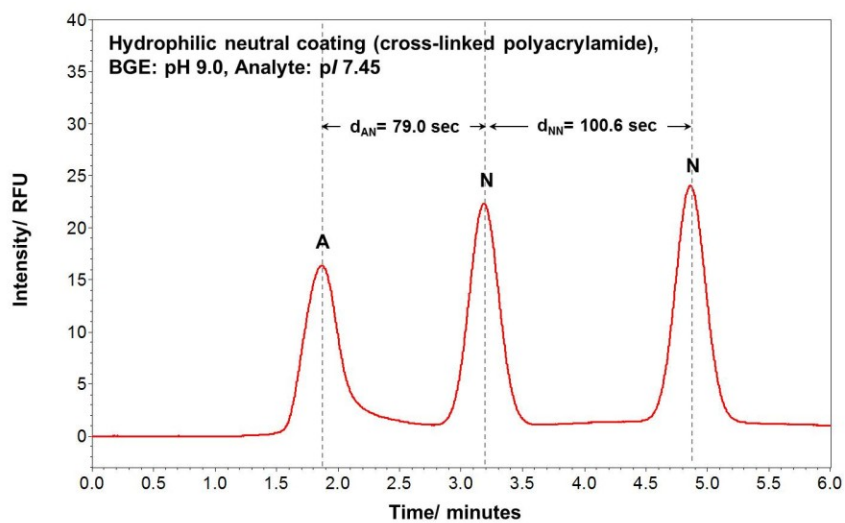


Figure 3.39 The LIF detector trace recorded in a PrMCE experiment with the *pI* marker having a calculated *pI* value of 7.45 and loaded as the first band in a background electrolyte of pH 9.0, in a cross-linked polyacrylamide coated capillary.

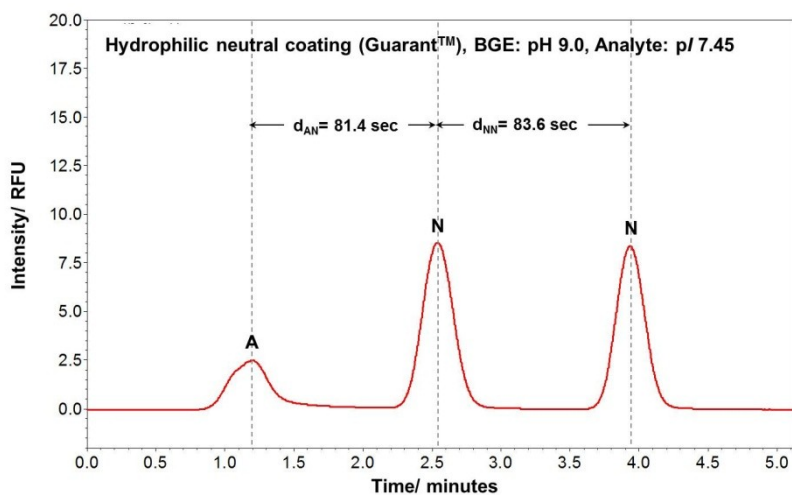


Figure 3.40 The LIF detector trace recorded in a PrMCE experiment with the *pI* marker having a calculated *pI* value of 7.45 and loaded as the first band in a background electrolyte of pH 9.0, in a Guarant™ capillary (ALCOR Biosystems).

Due to the fact that strong chromatographic retention was observed even on the best commercially available coated capillaries, we were not able to use the classical zone electrophoretic pI determination method for the APTS-based pI markers. Therefore, we designed and tested in proof-of-principle experiments a new pI value determination method that combines the advantages of the immobilized pH gradient technology used in the OFFGEL instrument and the carrier-ampholyte based IEF technology [87].

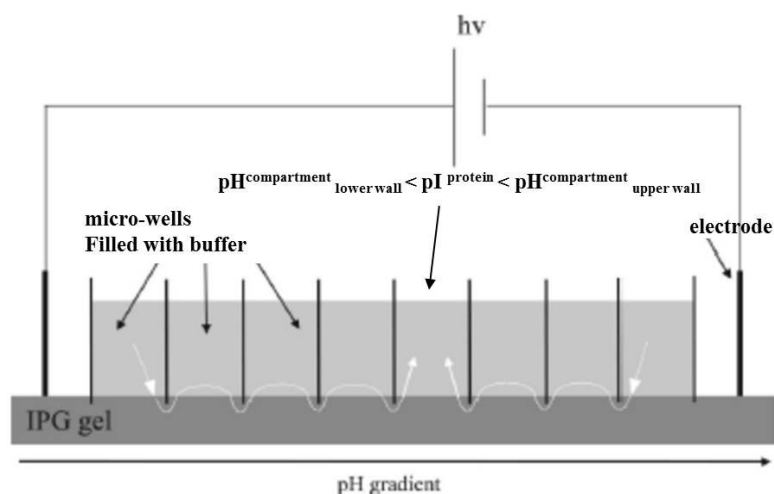


Figure 3.41 Schematic diagram of the OFFGEL electrophoretic process [87].

The OFFGEL instrument shown in Figure 3.41 consists of two parts: an immobilized pH gradient (IPG) gel strip and, on top of it, a frame that contains the collection compartments and is tightly sealed against the IPG gel strip. For the separation, the sample is typically prepared in a mixture of carrier ampholytes and is loaded into all wells. Since the compartments are isolated from each other by ion-impermeable walls, the sample components are forced to migrate through the IPG gel where the IEF process

takes place. The analytes become focused in the gel then move into solution in the corresponding compartments by diffusion.

The pyrene-based *pI* marker having a calculated *pI* value of 7.45 was selected to test whether the OFFGEL system could be used to determine the *pI* value of a *pI* marker. First, 100 μ L of a 4% w/w solution of 3-10 carrier ampholyte mixture (Beckman-Coulter, Fullerton, CA) was loaded into each of the 24 compartments of the well frame positioned over the pH 3-10 IPG strip and the carrier ampholytes were pre-focused to form the pH gradient. Once the pH gradient became stable (determined by repeated measurement of the pH of the solution in each compartment), the pyrene-based *pI* marker was loaded into one of the wells in the OFFGEL system. Specifically, the *pI* marker sample having a calculated *pI* value of 7.45 was loaded into the well numbered 18 as indicated by the light yellow color in the photograph taken of a section of the frame shown in Figure 3.42 (a). The colored spot eventually moved to the well numbered 17 (during 6.2 kV hours of focusing) and stayed in the same well during another 11.3 kV hours of focusing as shown in Figure 3.42 (b). The content of each well was transferred into an Eppendorf tube and illuminated by the 280 nm beam of a UV light. The migration of the *pI* marker can be seen clearly in the photographs shown in Figure 3.43. The pH values of all wells were measured and the pH profile is plotted in Figure 3.44. The solution in well numbered 17 in which the tested *pI* marker sample focused has a pH value of 7.45 which agrees very well with the calculated *pI* value of the marker.

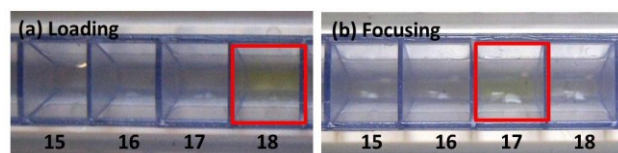


Figure 3.42 The OFFGEL experiment with the pI marker having a calculated pI value of 7.45 (a) loaded into the well numbered 18 and (b) focused into the well numbered 17.

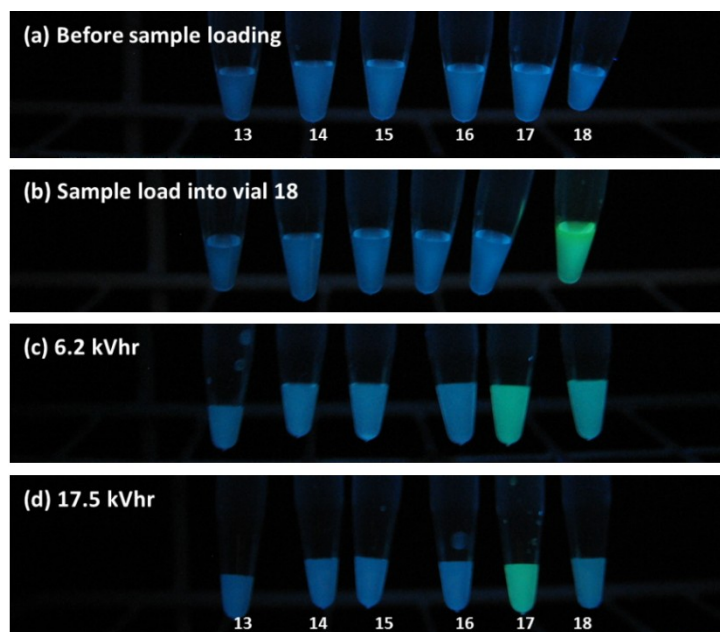


Figure 3.43 Photographs of the fractions collected from the OFFGEL experiment with the pI marker having a calculated pI value of 7.45. The vials were illuminated by the 280 nm beam of a UV light: (a) blank of the focused carrier ampholyte fractions in the absence of a pI marker (background fluorescence, blue); (b) pI marker sample loaded into the well numbered 18 (sample fluorescence green); (c) the collected fractions after 6.2kV hours of focusing and (d) the collected fractions after 17.5 kV hours of focusing.

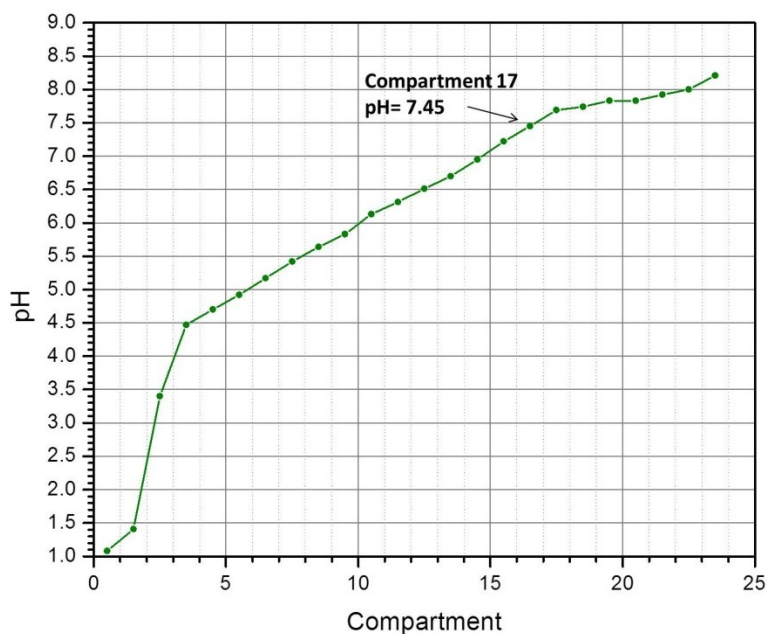


Figure 3.44 The pH gradient profile obtained in the OFFGEL experiment after 17.5 kV hours of focusing.

There are two problems that plague this pI determination method. The first is that after focusing, the pH of the solution in any well will correspond to the value expected from the position of the well over the IPG strip only when the concentration of the CAs trapped in the well is higher than the minimum concentration needed to achieve a concentration-independent pH value. This concentration varies from well to well and is much higher in the very low and very high pI regions than in the vicinity of $pI = 7$. These required high concentrations cause the second problem: to reach them, the concentration of the CA mixture initially loaded into the OFFGEL system must also be high. Therefore, any very acidic and very basic minor component or contaminant of the commercial CA mixture will accumulate in the first few wells on the anodic side and the

last few wells on the cathodic side. They will cause high conductivities – and corresponding low electric field strengths - in the first few wells and last few wells. Consequently, electrophoretic transport out of these wells will be very slow. Also, their high buffering capacity may overwhelm the buffering capacity of the IPG strip under the well and locally prevent the IPG strip from acting as an isoelectric trapping membrane.

To illustrate the severity of these problems, an OFFGEL experiment was set up using a 24 cm long 3 < *pI* < 10 IPG strip (Agilent) and a 24 compartment high resolution well frame. The wells were initially loaded with 150 μ L aliquots of a 4% w/w solution of a 3 < *pI* < 10 CA mixture (Agilent). The initial pH of the CA mixture was 6.85. Focusing was interrupted after 1.27 kVh, the solution from each well was transferred into an Eppendorf vial and their mass and pH were measured. Then the fractions were reloaded into the respective wells and focusing was continued until 2.2 kVh was reached. The mass and pH of the solution in the wells were again measured as before, then reloaded. The process was repeated at 4.8 kVh and 10 kVh. The results are plotted in Figure 3.45. The two teal-colored straight lines indicate the pH limits expected for the solutions in the wells based the positions of the respective wells. The 1.27 kVh curve indicates that focusing moves out the low and high *pI* CAs first from the 1st and the 24th wells, just as in cIEF, leaving the composition of the CA mixture in the middle mostly unchanged. By 4.8 kVh, the pH in the 1st well and the 24th well is more acidic and basic than expected from the position of the wells over the IPG strip and the nominal *pI* range of the CA mixture (3 to 10). By 10 kVh, the pH in the first four wells ranges from 1.4 to 1.8, well

below what can be expected from the nominal composition of the $3 < pI < 10$ CA mixture. The most basic components (that set the pH at 4.8 kVh to 10.6 in well 24) have mostly migrated out of the 24th well (into the cathodic electrode pad) by 10 kVh.

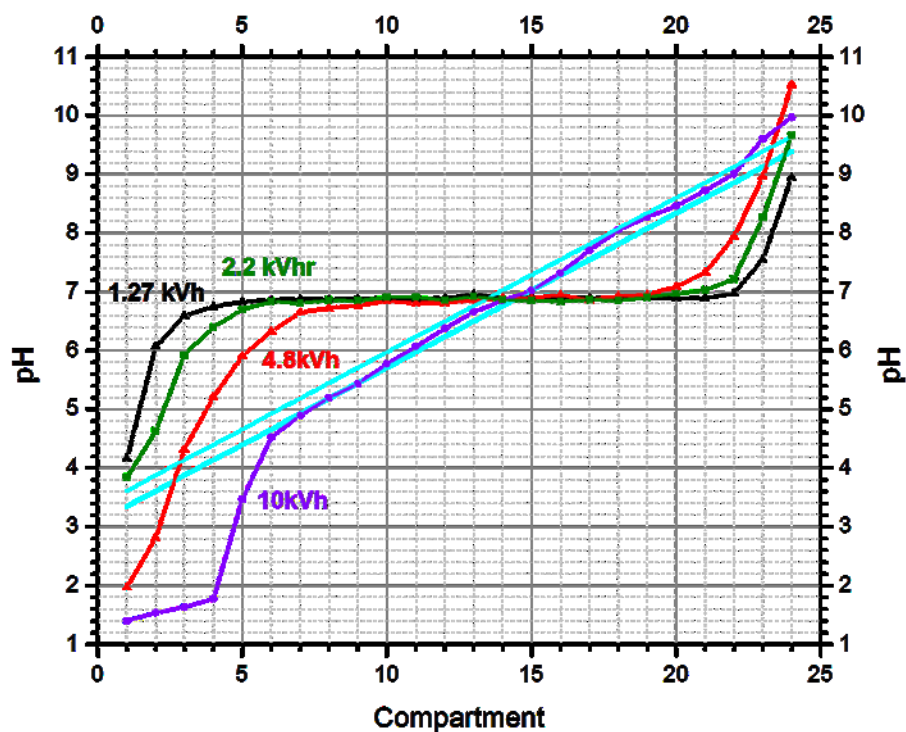


Figure 3.45 The relationship between the pH gradient profile and focusing volt hours obtained in the OFFGEL experiments with a 4% w/w solution of a $3 < pI < 10$ CA mixture (Agilent).

Therefore, in order to avoid the problems caused by the necessarily high initial CA concentration, another type of OFFGEL experiment was run with very low carrier ampholyte concentration and the pI range of the components trapped in a given well

were determined from the position of the well over the IPG strip [87]. 0.1% w/w pre-focused CA fractions were loaded into each of the 24 compartments of the well frame positioned over the pH 3-10 IPG strip and pyrene-based *pI* markers were loaded in a way that they would migrate toward pH 7 (opposite to the direction of any ITP transport, if present). The *pI* value of pyrene-based *pI* markers having calculated *pI* values of 4.16, 5.73, 7.45 were measured this way and the results are shown in Figures 4.46 to 4.48 and Table 3.8.

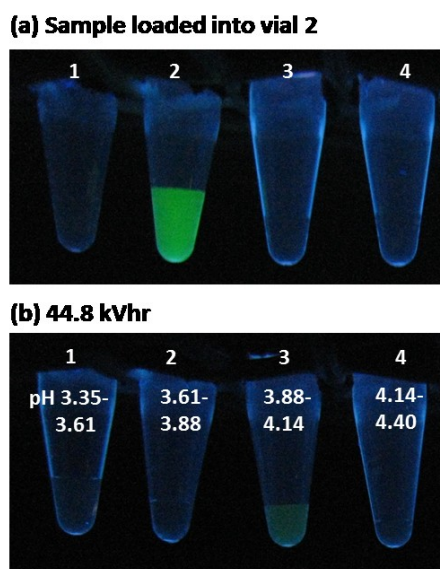


Figure 3.46 Photographs of the fractions collected from the OFFGEL experiment with the *pI* marker having a calculated *pI* value of 4.16. The vials were illuminated by the 280 nm beam of a UV light: (a) *pI* marker sample loaded into the well numbered 2; (c) the collected fractions after 44.8kVh of focusing.

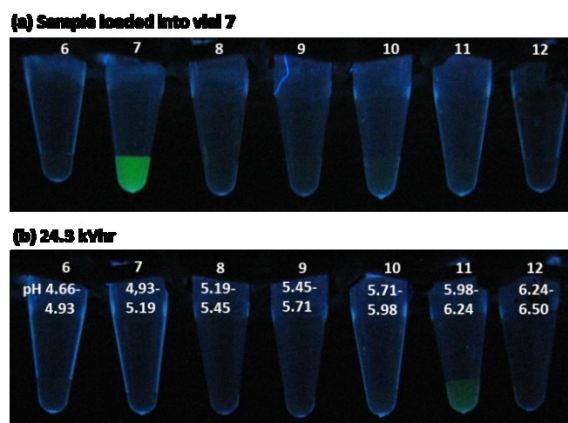


Figure 3.47 Photographs of the fractions collected from the OFFGEL experiment with the pI marker having a calculated pI value of 5.73. The vials were illuminated by the 280 nm beam of a UV light: (a) pI marker sample loaded into the well numbered 7; (c) the collected fractions after 24.3kVh of focusing.

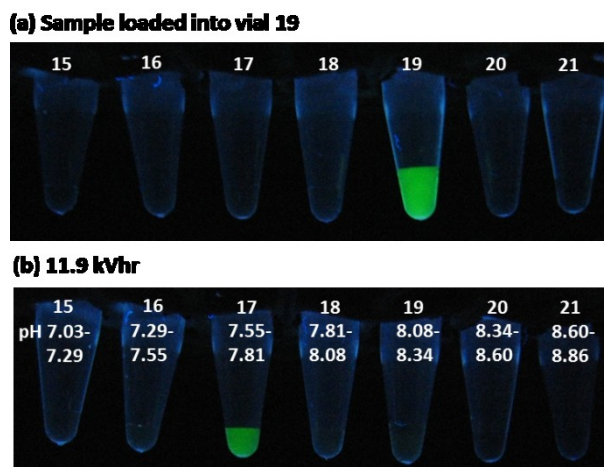


Figure 3.48 Photographs of the fractions collected from the OFFGEL experiment with the pI marker having a calculated pI value of 7.45. The vials were illuminated by the 280 nm beam of a UV light: (a) pI marker sample loaded into the well numbered 19; (c) the collected fractions after 11.9kVh of focusing.

Table 3.8 Comparison of calculated and measured pI values of the pyrene-based pI markers.

Calculated pI value	pI value measured in the OFFGEL experiment
4.16	3.88-4.14
5.73	5.98-6.24
7.45	7.75-7.81

Table 3.8 indicates that the calculated pI values are close to the possible pI range values found in the OFFGEL experiment with the help of the wide pH-range IPG strips.

Therefore, in order to narrow the range and get a better estimate for the pI values of the markers, the OFFGEL experiments will have to be repeated in the future once 24 cm long IPG strips are found with sufficiently narrow pH ranges.

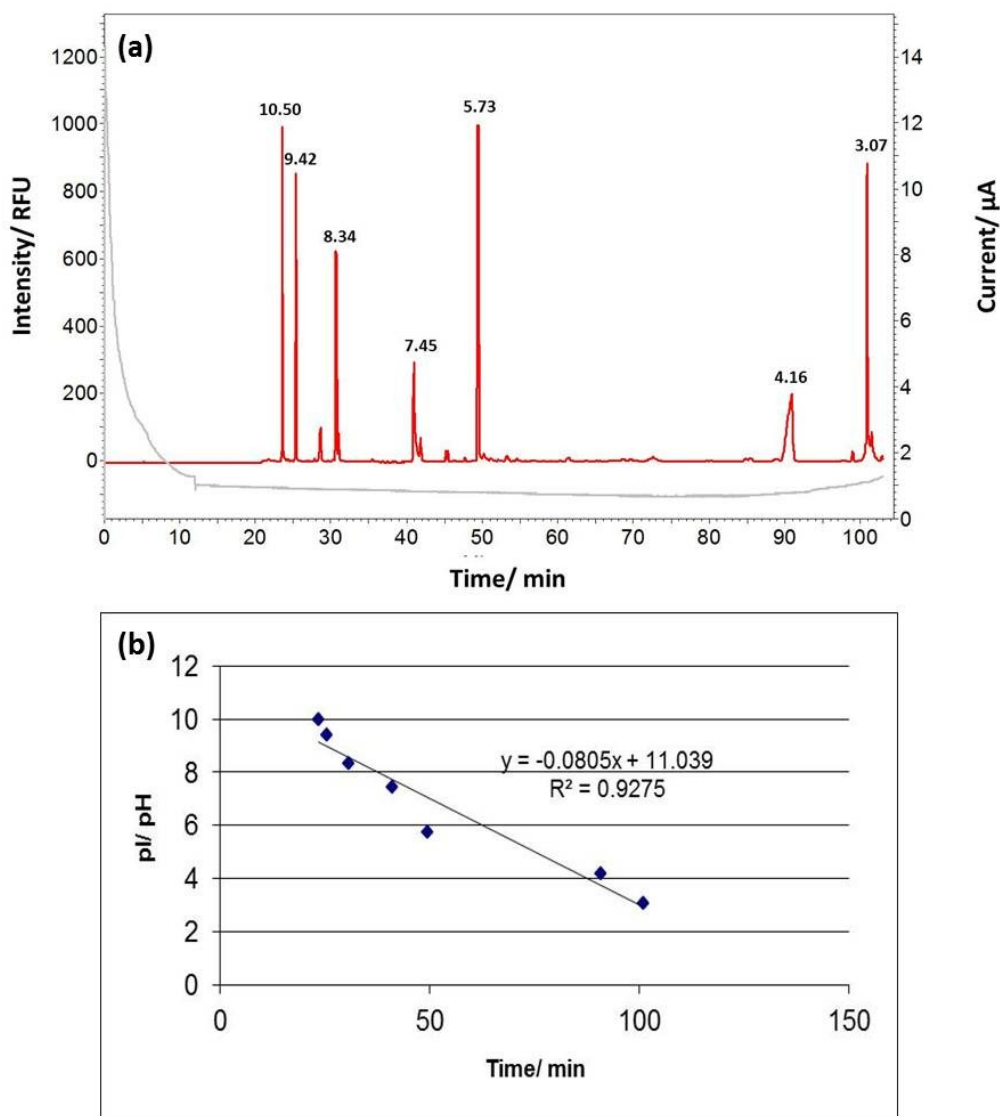
3.2.3.2 *pI* Values Measured by Capillary Isoelectric Focusing (cIEF)

Figure 3.49 (a) cIEF separation of 7 pyrene-based *pI* markers, the mobilization trace was obtained by simultaneously applying both pressure (0.5 psi) and potential (21 kV). The gray trace shown is the corresponding current. (b) The relationship between the calculated *pI* values of the markers and the mobilization times in the run shown in (a).

The carrier ampholytes have multiple anionic and cationic functional groups, just as the APTS-based *pI* markers. In a cIEF experiment, the carrier ampholytes are present in a 10^3 - 10^4 times higher concentration than the APTS-based *pI* markers. Therefore the carrier ampholytes efficiently compete with the *pI* markers for the surface binding sites and prevent – or at least greatly mitigate – the chromatographic retention of the *pI* markers. Therefore, in cIEF, the peak shapes of APTS-based *pI* markers are reasonable. Seven APTS-based *pI* markers were analyzed by cIEF under conventional cIEF settings by filling the capillary with a mixture of CAs and blockers. The *pI* marker samples were prepared in the same mixture of CAs and blockers and introduced into the capillary with pressure from the short end of the capillary. A focusing potential of 30 kV was applied for 9 minutes, then the mobilization trace was obtained using 0.5 psi pressure while potential was maintained at 21 kV. The calculated *pI* values were plotted as a function of mobilization time in Figure 3.49 and a linear fitting was applied which resulted in $R^2 = 0.9275$. The fitting result served as an indication of how much the calibration curve deviated from the expected linear relationship [88, 89].

In Figure 3.49, the basic end of the calibration curve is steeper than the acidic end. Though assumptions concerning the cause of the curvature were discussed in the literature [26, 27], a clear explanation is yet to be provided. A number of factors can alter the pH profile in cIEF. Righetti calls it a “chemical dogma” due to the fact that in all synthetic approaches of making CAs, the amount of acidic CAs made is larger than the amount of basic ones, resulting in a nonlinear pH profile [22]. The most significant

cause of the nonlinearity of the pH gradient might be the unequal rate of bi-directional isotachopheresis (ITP) in the capillary that both accompanies and follows IEF. ITP occurs in a discontinuous BGE system, *e.g.*, in a cIEF setting where the BGEs are nonhomogeneous. Since current is conserved along the capillary, the velocity of the analytes in ITP depends on the local field strength (E) and the effective mobility of the analyte (μ^{eff}). Species with the highest and lowest μ^{eff} are called the leading and terminating electrolytes, respectively, *i.e.*, $\mu_{\text{leading}}^{\text{eff}} > \mu_{\text{analyte}}^{\text{eff}} > \mu_{\text{terminating}}^{\text{eff}}$. Take anionic ITP for example: anions move toward anode with different velocities. The leading electrolyte accumulates at the anode and is present in a high concentration where the conductivity is the highest and the field strength is the lowest. The anion with the second fastest velocity follows the leading electrolyte anion and stacks to a certain concentration at the boundary due to the sudden drop of field strength in the leading electrolyte zone. With the same principle, all anion bands become arranged in order of their decreasing effective mobilities. The steady state velocity of any band in a developed ITP train is proportional to the effective mobility of the analyte in the band and the field strength at the position of the band. For monovalent strong electrolytes, the concentration of each adjacent band follows the Kohlrausch regulation function [90]:

$$\sum_i \frac{c_i z_i}{\mu_i} = \text{constant}$$

where c is the concentration, z is the charge and μ is the mobility of the analyte.

In cIEF, both anionic and cationic ITP take place simultaneously, going in opposite directions, leaving a segment of $pI \approx 7$ carrier ampholyte or water in the middle of the capillary [91]. This unavoidably distorts the shape of the pH gradient. In order to minimize the pH profile distortion caused by bi-directional ITP in the cIEF experiment, one should apply potential only as long as necessary to finish the focusing step. To prove this point, another cIEF experiment was performed using only pressure mobilization once the focusing was complete as shown in Figure 3.50. Compared to Figure 3.49, all peaks are much wider when mobilization is done by pressure only, because there is no electrophoretic process that mitigates Taylor dispersion caused by the laminar flow. The calibration curve obtained with pressure-only mobilization yields $R^2 = 0.9867$. The better linear fit obtained for the shorter application of the electric field, 12 minutes vs. 100 minutes in this case, implies that the distortion of the pH gradient caused by bidirectional ITP is less serious.

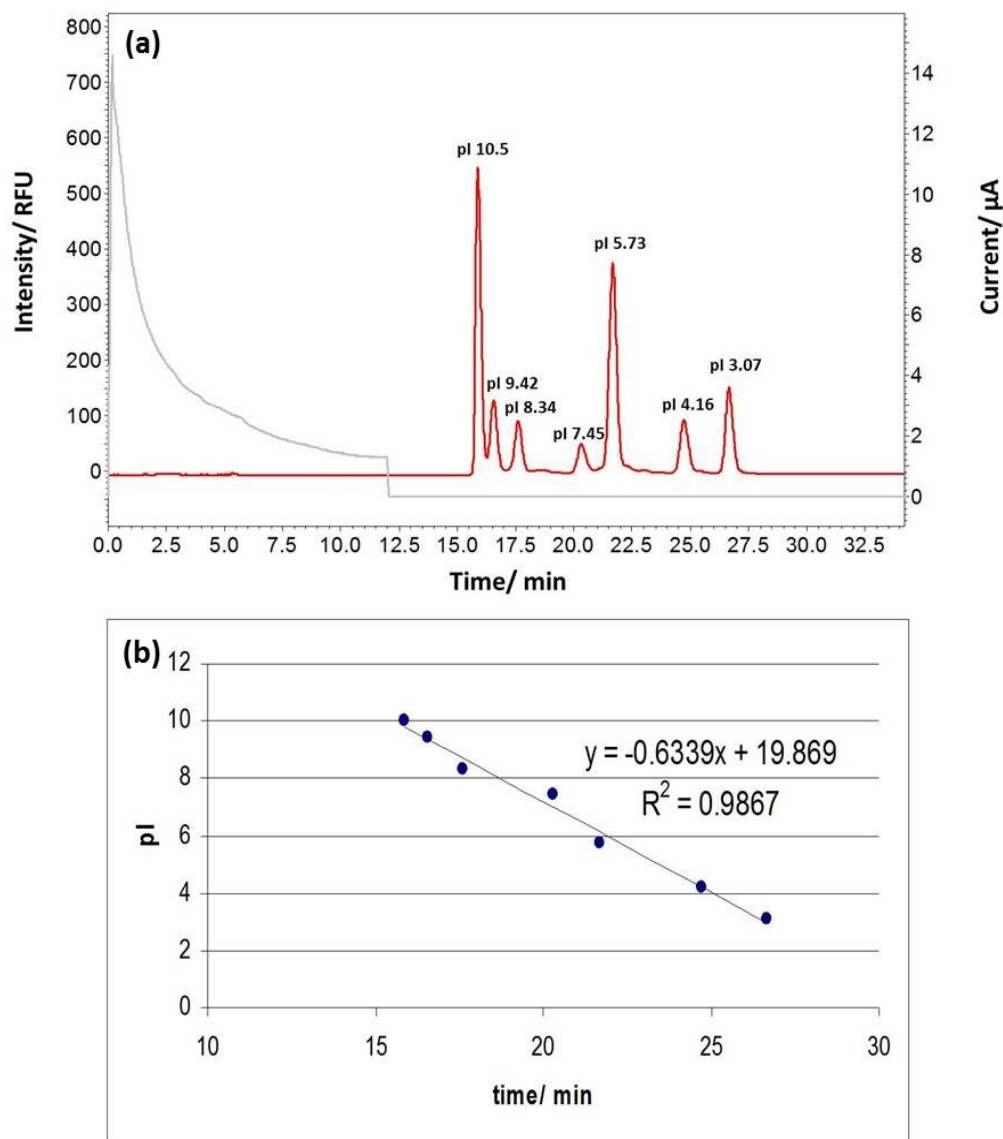


Figure 3.50 (a) cIEF separation of 7 pyrene-based pI markers, the trace was obtained using pressure-only mobilization (1 psi). The gray trace is the corresponding current. (b) The relationship between the calculated pI values of the markers and their mobilization time in the run shown in (a).

The cIEF experiments in the previous section were performed with a mixture of CAs, samples and blockers filled into the capillary. Arginine and IDA were used as blockers in the mixture and were mostly in their ionic forms [46, 47]. Therefore, in the beginning of the focusing step, most of the transported charges were carried by the blockers as they went through the capillary. The role of blocker in the cIEF process is to act as a sacrificial reagent to prevent the loss of CAs into the electrode vials. To shorten the focusing time needed, the blockers can be prepositioned by loading them segment-wise into the capillary. In these segments, most of the blocker molecules will already be in their zwitterionic form. The cIEF mobilization trace shown in Figure 3.51(b) was obtained by loading a 6 cm long plug of 200 mM arginine, a 6 cm long plug of 10% CA and sample mixture and an 8 cm long plug of 450 mM acetic acid as three sequential segments before the detection window of the capillary. A focusing potential of 30 kV was applied for 9 minutes, then the mobilization trace was obtained using 1 psi pressure. Three HPTS-based *pI* markers with *pI* values of 9.36, 7.83, 6.38 and an APTS-based *pI* marker with a *pI* value of 4.16 were used in this test to profile the pH gradient. APTS was injected before the pressure mobilization step to mark the position in the mobilization trace that corresponded to the end of the capillary. As it can be seen in the current trace, at about 7 minutes the current had decreased to a constant level suggesting that the focusing step was complete. The calculated *pI* values were plotted as a function of mobilization time in Figure 3.51(c) and a linear fitting was applied which resulted in $R^2 = 0.9906$. This is by far the best result we have observed in cIEF experiments.

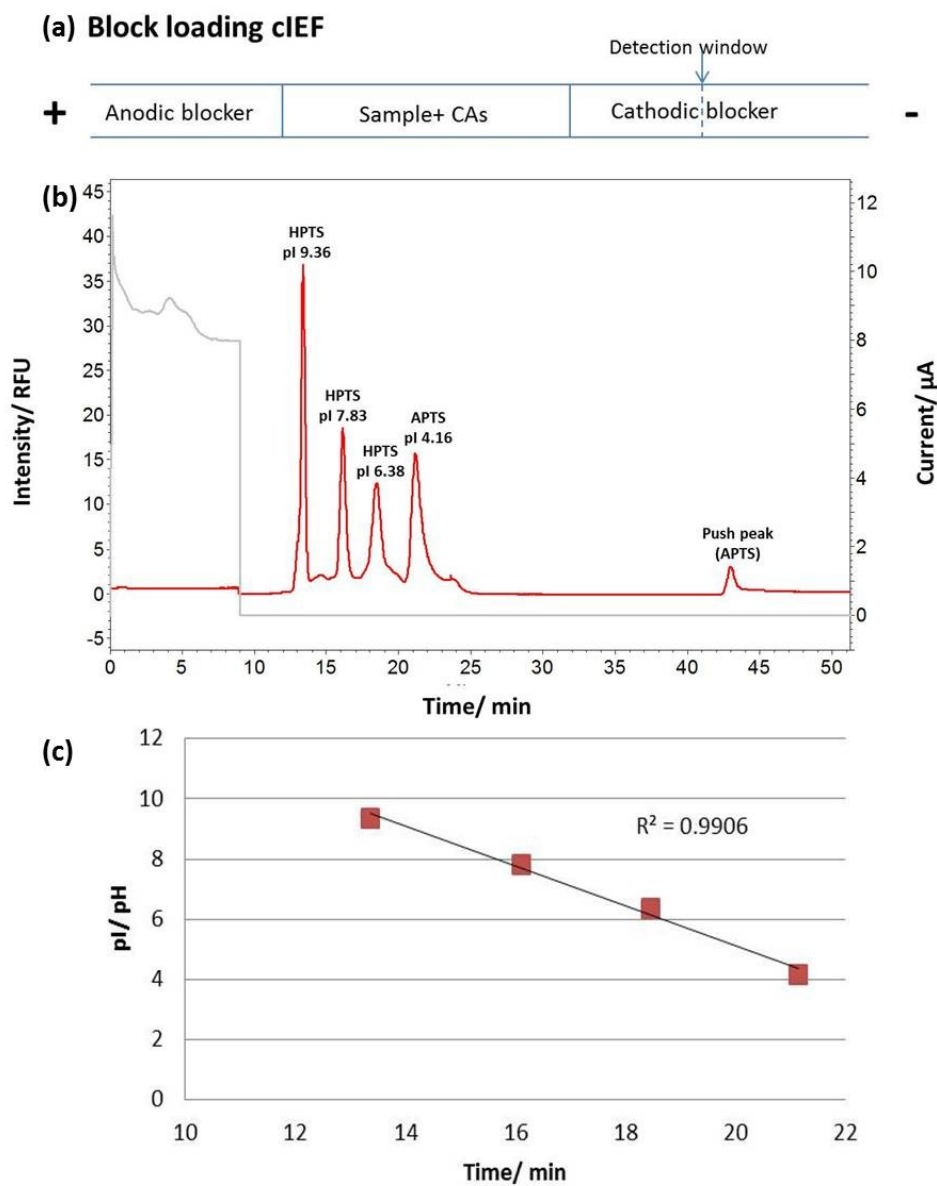


Figure 3.51 (a) In this cIEF test, the anodic blocker, analytes dissolved in the CAs and the cathodic blocker were loaded into the capillary as separate segments. (b) cIEF separation of 4 fluorescent *pI* markers. The gray trace is the corresponding current. (c) The relationship between the *pI* values of the markers and their mobilization time in the run shown in (b).

3.3 Ampholytic APTS-based Carbohydrate Tagging Reagent

3.3.1 Background and Objective

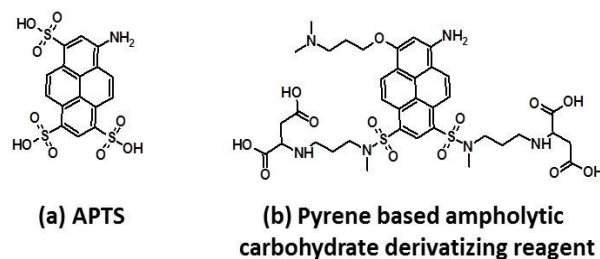


Figure 3.52 Structures of pyrene-based carbohydrate tagging reagents.

Carbohydrate analysis is challenging due to the structural diversity of carbohydrates and their lack of chromophores. Therefore, one common strategy is to derivatize carbohydrates with property-enhancing tags to facilitate their analysis and detection [92]. Nuclear magnetic resonance (NMR) spectroscopy is a powerful technique for the structural analysis of carbohydrates, but cannot be used when the amount (or concentration) of the available sample is too low. Capillary electrophoresis (CE) coupled with laser induced fluorescence (LIF) and/or mass spectrometric (MS) detection provides supreme detection sensitivity which makes it an excellent choice for carbohydrate analysis. Derivatizing reagents that facilitate carbohydrate analysis by CE coupled with LIF and/or MS detection need to be fluorescent and charged. 1-Aminopyrene-3,6,8-trisulfonic acid (APTS) (shown in Figure 3.52(a)) is a commercially available tagging agent and is widely used in CE-based carbohydrate analysis today. Jackson first used APTS [93] to derivatize oligosaccharide ladders by reductive

amination. His method then had been developed into a validated standard bioanalytical method by Evangelista [94]. With this method, APTS-derivatized sugars can be detected by LIF using the 488 nm argon-ion laser and by MS in negative ion mode.

Here, we propose to exploit a unique property of the newly developed fluorescent *pI* markers and use them as pyrene-based ampholytic carbohydrate derivatizing reagents. A proof-of-principle example is shown in Figure 3.52(b), which makes the carbohydrate derivatives have higher molar absorbance at 488 nm and make them detectable in positive ion mode of MS for better detection sensitivity compared to their APTS-based counterparts. Moreover, our proposed tag converts the derivatized carbohydrates into ampholytes allowing their manipulation by isoelectric focusing (IEF) and isoelectric trapping (IET). One common, major advantage of both IEF and IET is that they facilitate sample concentration, a major advantage in bioanalysis where samples are often very dilute.

3.3.2 Carbohydrate Derivatization

3.3.2.1 Chemicals and Equipment

The *pI* derivatizing agent was synthesized as described in 3.1. D-glucose, sodium cyanoborohydride and acetic acid were purchased from Sigma-Aldrich Co. (St. Louis, MO). HPLC analyses, CE analyses and LC-MS analyses were done with the instruments and column described in 2.1.2.1. The cIEF analysis kit was purchased from Beckman-Coulter Inc. (Fullerton, CA).

3.3.2.2 Derivatization of D-glucose with the p/4 Reagent

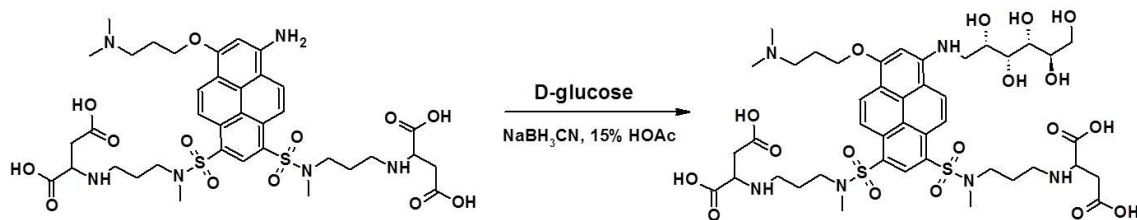


Figure 3.53 Reaction scheme of derivatizing D-glucose with the p/4 reagent.

3 mg of D-glucose was mixed with 50 μ g of the p/4 reagent in 42 μ L of 15% acetic acid followed by the addition of 17 μ L of 1 M sodium cyanoborohydride in tetrahydrofuran with stirring. Maltodextrin ladders were derivatized with the p/4 reagent under the same set of conditions.

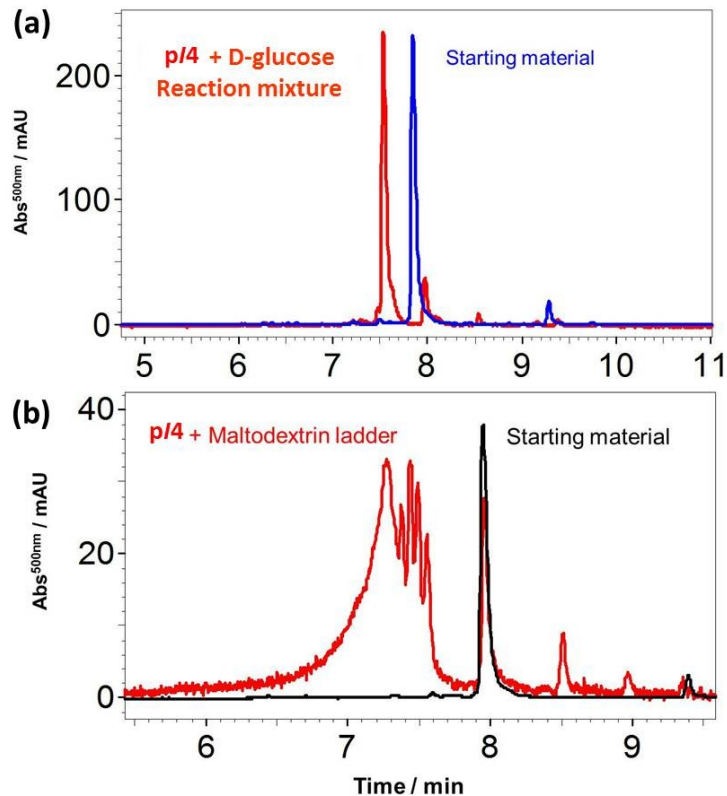


Figure 3.54 RP-HPLC analysis of samples of (a) D-glucose and (b) maltodextrin ladder derivatized with the *pI4* reagent.

The reaction mixtures were analyzed by RP-HPLC: the results are shown in Figure 3.54. Based on the integration of the peaks at 500 nm in the chromatogram, the derivatization of D-glucose was about 80% complete after 16 hours at 50°C. Under acidic conditions, the glucose derivative was retained in the C-18 column slightly less than the tag itself. The UV absorbance spectra of the *pI4* derivatizing agent and its glucose derivative are compared in Figure 3.55. The $\lambda_{\text{max}}^{\text{ex}}$ of the glucose derivative is red-shifted by about 20 nm due to the monoalkylation of the anilinic 8-amino group after reductive amination

with glucose. A group of peaks less retained than the p/4 derivatizing agent can be seen in the chromatogram of the derivatized maltodextrin ladder (Figure 3.54(b)) and they have the same red-shifted UV absorbance spectra as observed in the UV spectrum of glucose derivatized by the p/4 reagent.

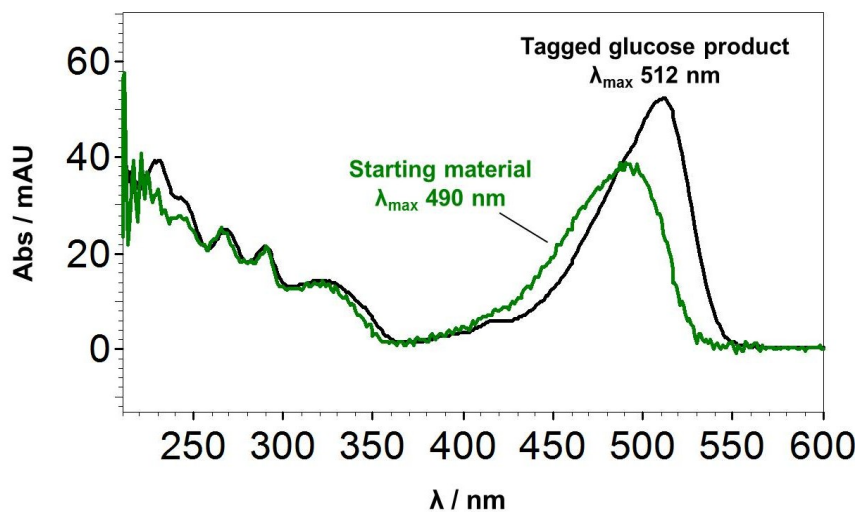


Figure 3.55 Overlaid UV absorbance spectra of the p/4 derivatizing agent and the derivatized D-glucose

Derivatization of D-glucose was confirmed with ESI mass spectrometry. The positive and negative ion mode spectra are shown in Figure 3.56: the signal obtained in the positive ion mode is about 200 times stronger than the signal obtained in the negative ion mode.

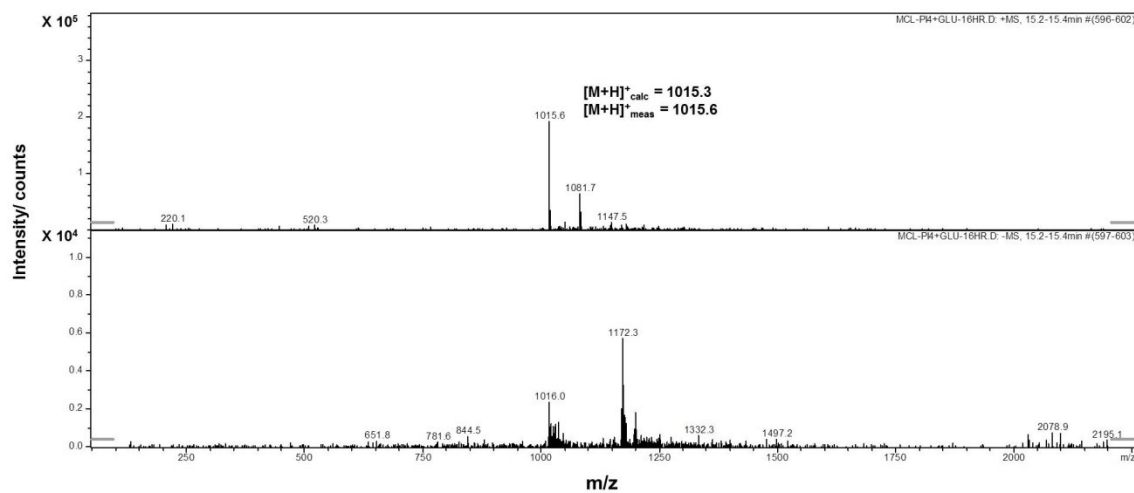


Figure 3.56 ESI mass spectra of D-glucose tagged with the pI4 derivatizing agent in positive ion mode (top) and negative ion mode (bottom).

The derivatized carbohydrate samples were also analyzed by CE in free zone mode using a pH 2.2, 20 mM sodium phosphate background electrolyte and a bare fused silica capillary. Electropherograms of the labeling reagent and the labeled D-glucose and maltodextrin ladder samples are shown in Figure 3.57: the pI4 derivatizing agent itself has a higher cationic mobility than its sugar derivatives.

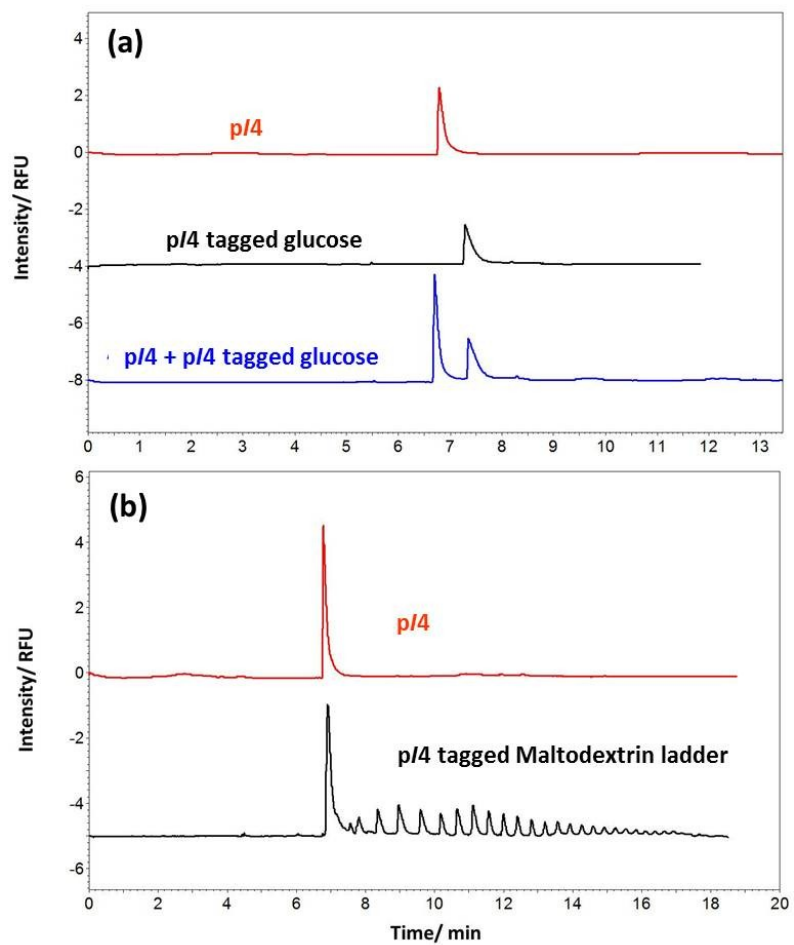


Figure 3.57 CE analyses of the p/4 derivatizing agent and its (a) D-glucose and (b) maltodextrin ladder derivatives.

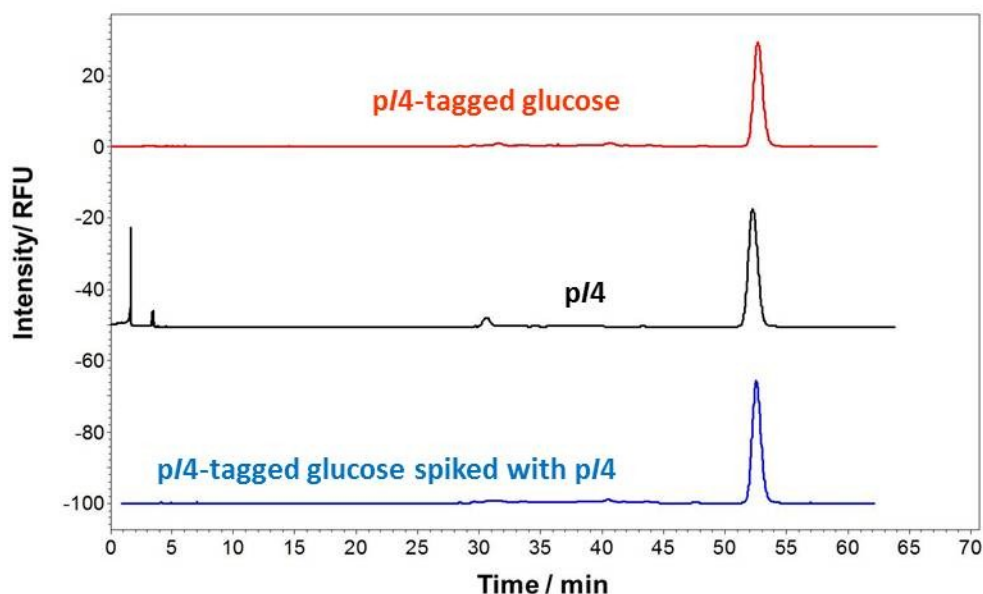


Figure 3.58 cIEF analyses of the pI4 derivatizing agent and its D-glucose derivative.

The pI4 reagent-tagged glucose sample was analyzed by capillary isoelectric focusing using the Beckman cIEF kit in the PA 800. As shown in Figure 3.58, the laser induced fluorescent signals of the pI4 derivatizing agent and its glucose derivative were observed at the same time in the electropherograms, which means that the addition of glucose does not alter the pI of the tag significantly. This was also confirmed by spiking the glucose derivative sample with pI4 derivatizing agent: only one peak could be observed during cIEF analysis.

3.4 Concluding Remarks

In this work, correlations between the structure of an ampholyte and its pI value were discovered and applied to design fluorescent pyrene-based pI markers in a methodical

and systematic way. The generic structure of the designed fluorescent pyrene-based *pI* markers contains two identical buffering groups as part of the sulfonamido substituents attached at the 1 and 3 positions and a charge-balancing (titrating) group attached as part of an alkoxy substituent at the 6 position of the pyrene core. We successfully made 7 pyrene-based *pI* markers that represent the highest structural complexity in the designed marker class: they were built using three amino acids (aspartic acid, histidine and lysine) as the buffering groups and amino, alcohol and sulfate functional groups as the charge balancing (titrating) groups proving that the proposed synthetic approach is feasible. Due to hydrophobic and electrostatic interactions between the pyrene-based *pI* markers and CE capillary walls, the widely used zone electrophoretic measurement-based *pI* determination method failed. An alternative electrophoretic *pI* determination method that combined the advantages of the IPG-based OFFGEL instrument and semipreparative-scale IEF method was designed and tested with the most hydrophobic pyrene-based *pI* marker (having histidines in the buffering groups and yielding a calculated *pI* of 7.45). The measured *pI* value was 7.45 which agrees with the calculated value.

The 7 pyrene-based *pI* markers were also used to profile the pH gradient in a conventional cIEF method. The calculated *pI* values were plotted as a function of the mobilization time and a linear fitting was applied which resulted in $R^2 = 0.9275$. The most significant cause of the nonlinearity of the pH gradient might be the unequal rate of bi-directional isotachopheresis (ITP) in the capillary that both accompanies and follows IEF. In order to minimize the pH profile distortions caused by bi-directional ITP in the

cIEF experiment, a cIEF experiment was modified using only pressure mobilization once the focusing was complete, this improved the R^2 value to 0.9867. An even better linear fit was obtained for the shorter application of the electric field, 12 minutes vs. 100 minutes in this case, implying that the distortion of the pH gradient caused by bidirectional ITP was rendered less serious. To shorten the focusing time, the blockers were prepositioned around the carrier ampholyte band by loading them segment-wise into the capillary. We optimized the cIEF method by loading a 6 cm long plug of 200 mM arginine, a 6 cm long plug of 10% CA and sample mixture and an 8 cm long plug of 450 mM acetic acid as three sequential segments before the detection window of the capillary. The calculated pI values of the pI markers were plotted as a function of mobilization time and a linear fitting was applied resulting in $R^2 = 0.9906$ which is by far the best result we have observed in cIEF experiments.

Moreover, we exploited a unique property of the newly developed fluorescent pI markers and used them as pyrene-based ampholytic carbohydrate derivatizing reagents. In a proof-of-principle experiment, D-glucose and maltodextrins were derivatized with the $pI4$ reagent using reductive amination. Derivatization of D-glucose was confirmed with ESI mass spectrometry and the signal obtained in the positive ion mode was found to be about 200 times stronger than the signal obtained in the negative ion mode with APTS as the derivatizing agent. In cIEF, the laser induced fluorescent signals of the $pI4$ derivatizing agent and its glucose derivative were observed at the same time in the electropherograms, indicating that the addition of the glucose moiety did not alter the pI

of the tag significantly. Compared to the commercially available carbohydrate derivatizing reagent, APTS, the pI4 reagent yielded carbohydrate conjugates with higher molar absorbance at 488 nm and rendered them detectable in positive ion mode MS affording better detection sensitivity.

4. CONCLUSIONS

Two types of fluorescent molecules had been designed and synthesized to improve the analytical infrastructure of capillary-electrophoretic separations.

4.1 Amine-Reactive Fluorescent Labeling Reagent

An ideal fluorescent labeling reagent for capillary electrophoresis should result in conjugates that are hydrophilic, stable and exhibit strong and pH-independent fluorescence emission. The acridine orange-based amine-reactive monocationic fluorescent labeling reagent synthesized in our laboratory two years ago possesses most of the ideal qualities mentioned above, but it is not sufficiently hydrophilic. A more water-soluble version of the permanently cationic acridine-based fluorophore, HEG₂Me₂-DAA, with a calculated log*P* of 0.18 was synthesized by connecting oligo(ethylene glycol) groups to the diamino acridine core structure. In the spectral studies of HEG₂Me₂-DAA, $\lambda^{\text{ex}}_{\text{max}}$ was found at 490 nm which remains compatible with the 488 nm line of the argon ion laser, while $\lambda^{\text{em}}_{\text{max}}$ was about 5 nm blue-shifted compared to acridine orange. The emission spectra of HEG₂Me₂-DAA are also pH-independent and the emission intensities are higher than in acridine orange due, presumably, to the presence of methyl-terminated oligo(ethoxy) chains. HEG₂Me₂-DAA was used in CE with pure aqueous background electrolyte and was found to be free of the majority of peak tailing that was caused by hydrophobic adsorption of the acridine orange-based fluorophore on the fused silica capillary. Bovine serum albumin was

labeled with excess of FL-CA-PFP and analyzed by SDS-CGE with LIF detection. The lowest tested concentration for tagged bovine serum albumin was 15 nM. Chicken ovalbumin was also labeled with FL-CA-PFP and analyzed by cIEF-LIF. The pI of the tagged proteins was shifted in the alkaline direction by about 0.02 compared to the non-tagged protein. A tri-functional probe potentially enabling selective enrichment and selective detection of a variety of molecules (*e.g.*, natural products, pharmaceuticals, inhibitors, *etc.*) that carry an alkyne anchoring group that minimally perturbs their biological function was also designed and synthesized by combining biotin, FL-CA and an azide group in a “proof-of-principle” level experiment.

4.2 Pyrene-based Fluorescent pI Markers

In cIEF, the profile of the pH gradient can only be determined with the help of pI markers. Up to now, the need for LIF-compatible pI markers remained unsatisfied which limits highly sensitive and accurate cIEF-LIF analysis. A large set of pyrene-based fluorescent pI markers was rationally designed to cover the pI range 3 to 10 and guarantee excellent focusing properties. To prove the feasibility of the proposed synthetic approach, the family with the greatest structural complexity among the designed pI markers was synthesized and characterized. The classical zone electrophoretic pI determination method that relies on the measurement of the effective mobilities of the markers in BGEs of different pH values failed, because hydrophobic and electrostatic interactions between the markers and the coated capillary wall caused strong chromatographic retention even on the best commercially available coated

capillaries. Exploratory work was done to design a new *pI* value determination method that combines the immobilized pH gradient technology of the OFFGEL instrument and carrier-ampholytes based IEF.

The method aspects of cIEF have also been improved in this work. After evaluating the currently known and used cIEF methods, two alternatives were developed to minimize the uneven stretch of the pH gradient caused by bi-directional ITP. The linearity of the pH gradient was first improved by replacing chemical mobilization of the focused bands by pressure-only mobilization. To shorten the time during which ITP acts on the pH gradient, the focusing time was significantly reduced by loading the anodic and cathodic blockers and the sample-containing carrier ampholytes as three sequential segments before the detection window. The new segmented loading method yielded a more linear pH gradient than the previously known methods.

To exploit a unique property of the newly developed fluorescent *pI* markers, we had used them as pyrene-based ampholytic carbohydrate derivatizing reagents. In proof-of-principle experiments, D-glucose and maltodextrins were derivatized by reductive amination. The *pI*4 carbohydrate derivatization reagent proved advantageous over APTS: the new derivatives have higher molar absorbance at 488 nm and become detectable in positive ion mode of MS affording better detection sensitivity.

cIEF-LIF can be a powerful analytical method for bio-analysis, however, three aspects need to be further improved. The first aspect is the need to synthesize a large set of closely-spaced ($\Delta pI = 0.5$) fluorescent *pI* markers with good focusing ability for properly profiling the pH gradient in cIEF. A list of 18 recommended pyrene-based *pI* markers covering the pH range from 2.7 to 11.3 with a ΔpI of 0.5 is shown in Table 4.1. The second aspect is to search for a more suitable capillary coating to minimize analyte adsorption onto the capillary wall facilitating the analysis of dilute samples in combination with highly sensitive detectors. The third aspect is the development of cIEF methods that minimize the distortion of the pH gradient and produce reproducible and reliable results.

Table 4.1 Calculated *pI* values of the eighteen selected pyrene-based *pI* markers having a ΔpI of approximately 0.5 and a pyrene-based neutral marker.

#	<i>pI</i>	dz/dpH		#	<i>pI</i>	dz/dpH
1	2.71	1.15		11	7.575	1.1
2	3.04	1.17		12	8.00	1.14
3	3.66	1.19		13	8.66	1.15
4	4.06	1.22		14	9.09	1.10
5	4.65	1.15		15	9.63	1.15
6	5.01	1.15		16	10.01	1.15
7	5.61	1.19		17	10.50	1.16
8	6.18	0.93		18	11.30	1.16
9	6.53	1.15		19	Neutral	marker
10	7.185	1.1				

REFERENCES

- [1] Jorgenson, J. W., Lukacs, K. D., *Anal. Chem.* 1981, 53, 1298-1302.
- [2] Shen, Y., Smith, R. D., *Electrophoresis* 2002, 23, 3106-3124.
- [3] Pinto, D. M., Arriaga, E. A., Craig, D., Angelova, J., Sharma, N., *et al.*, *Anal. Chem.* 1997, 69, 3015-3021.
- [4] Xue, Q., Yeung, E. S., *Nature* 1995, 373, 681-683.
- [5] Haugland, R. P., *Handbook of Molecular Probes*, Molecular Probes Inc., Eugene, OR, USA 2003.
- [6] Oswald, B., Gruber, M., Bohmer, M., Lehmann, F., Probst, M., *et al.*, *Photochem. Photobiol.* 2001, 74, 237-245.
- [7] Kuerner, J. M., Klimant, I., Krause, C., Preu, H., Kunz, W., *et al.*, *Bioconjugate Chem.* 2001, 12, 883-889.
- [8] Lamari, F. N., Kuhn, R., Karamanos, N. K., *J. Chromatogr. B: Anal. Technol. Biomed. Life Sci.* 2003, 793, 15-36.
- [9] Buschmann, V., Weston, K. D., Sauer, M., *Bioconjugate Chem.* 2003, 14, 195-204.
- [10] Szoeko, E., Tabi, T., *J. Pharm. Biomed. Anal.*, 53, 1180-1192.
- [11] Molina, M., Silva, M., *Electrophoresis* 2002, 23, 1096-1103.
- [12] Al-Dirbashi, O., Kuroda, N., Nakashima, K., *Anal. Chim. Acta* 1998, 365, 169-176.
- [13] Wu, J., Chen, Z., Dovichi, N. J., *J. Chromatogr. B: Biomed. Sci. Appl.* 2000, 741, 85-88.
- [14] Liu, J., Hsieh, Y. Z., Wiesler, D., Novotny, M., *Anal. Chem.* 1991, 63, 408-412.

- [15] Soper, S. A., Shera, E. B., Martin, J. C., Jett, J. H., Hahn, J. H., *et al.*, *Anal. Chem.* 1991, *63*, 432-437.
- [16] Unlu, M., Morgan, M. E., Minden, J. S., *Electrophoresis* 1997, *18*, 2071-2077.
- [17] Pham, W., Medarova, Z., Moore, A., *Bioconjugate Chemistry* 2005, *16*, 735-740.
- [18] Bouteiller, C., Clave, G., Bernardin, A., Chipon, B., Massonneau, M., *et al.*, *Bioconjugate Chem.* 2007, *18*, 1303-1317.
- [19] Wu, L., Burgess, K., *J. Org. Chem.* 2008, *73*, 8711-8718.
- [20] Schulze, P., Link, M., Schulze, M., Thuermann, S., Wolfbeis, O.S. and Belder, D., *Electrophoresis* 2010, *31*, 2739-2753.
- [21] Svensson, H., *Acta Chem. Scand.* 1962, *16*, 456-466.
- [22] Righetti, P. G., *J. Chromatogr. A* 2004, *1037*, 491-499.
- [23] Minarik, M., Groiss, F., Gas, B., Blaas, D., Kenndler, E., *J. Chromatogr. A* 1996, *738*, 123-128.
- [24] Huang, T.-L., Richards, M., *J. Chromatogr. A* 1997, *757*, 247-253.
- [25] Hjerten, S., Zhu, M. D., *J. Chromatogr.* 1985, *346*, 265-270.
- [26] Shimura, K., Zhi, W., Matsumoto, H., Kasai, K.-I., *Anal. Chem.* 2000, *72*, 4747-4757.
- [27] Shimura, K., Wang, Z., Matsumoto, H., Kasai, K.-I., *Electrophoresis* 2000, *21*, 603-610.
- [28] Hjerten, S., Liao, J., Yao, K., *J. Chromatogr.* 1987, *387*, 127-138.
- [29] Shimura, K., *Electrophoresis* 2009, *30*, 11-28.
- [30] Hiraoka, A., Tominaga, I., Hori, K., *J. Chromatogr. A* 2002, *961*, 147-153.

- [31] Horka, M., Ruazicka, F., Horky, J., Hola, V., Slais, K., *Anal. Chem.* 2006, 78, 8438-8444.
- [32] Hjerten, S., *J. Chromatogr.* 1985, 347, 191-198.
- [33] Zhou, F., Hanson, T. E., Johnston, M. V., *Anal. Chem. (Washington, DC, U. S.)* 2007, 79, 7145-7153.
- [34] Yang, C., Liu, H., Yang, Q., Zhang, L., Zhang, W., *et al.*, *Anal. Chem.* 2003, 75, 215-218.
- [35] Lopez-Soto-Yarritu, P., Diez-Masa, J. C., Cifuentes, A., de, F. M., *J. Chromatogr. A* 2002, 968, 221-228.
- [36] Gao, L., Liu, S., *Anal. Chem.* 2004, 76, 7179-7186.
- [37] Jager, A. V., Tavares, M. F. M., *J. Chromatogr. B: Anal. Technol. Biomed. Life Sci.* 2003, 785, 285-292.
- [38] Yang, C., Zhang, L., Liu, H., Zhang, W., Zhang, Y., *J. Chromatogr. A* 2003, 1018, 97-103.
- [39] Slais, K., Horka, M., Novackova, J., Friedl, Z., *Electrophoresis* 2002, 23, 1682-1688.
- [40] Shen, Y., Xiang, F., Veenstra, T. D., Fung, E. N., Smith, R. D., *Anal. Chem.* 1999, 71, 5348-5353.
- [41] Horka, M., Ruzicka, F., Horky, J., Hola, V., Slais, K., *J. Chromatogr. B: Anal. Technol. Biomed. Life Sci.* 2006, 841, 152-159.
- [42] Sandra, K., Stals, I., Sandra, P., Claeysens, M., Beeumen, J. V., *et al.*, *J. Chromatogr. A* 2004, 1058, 263-272.

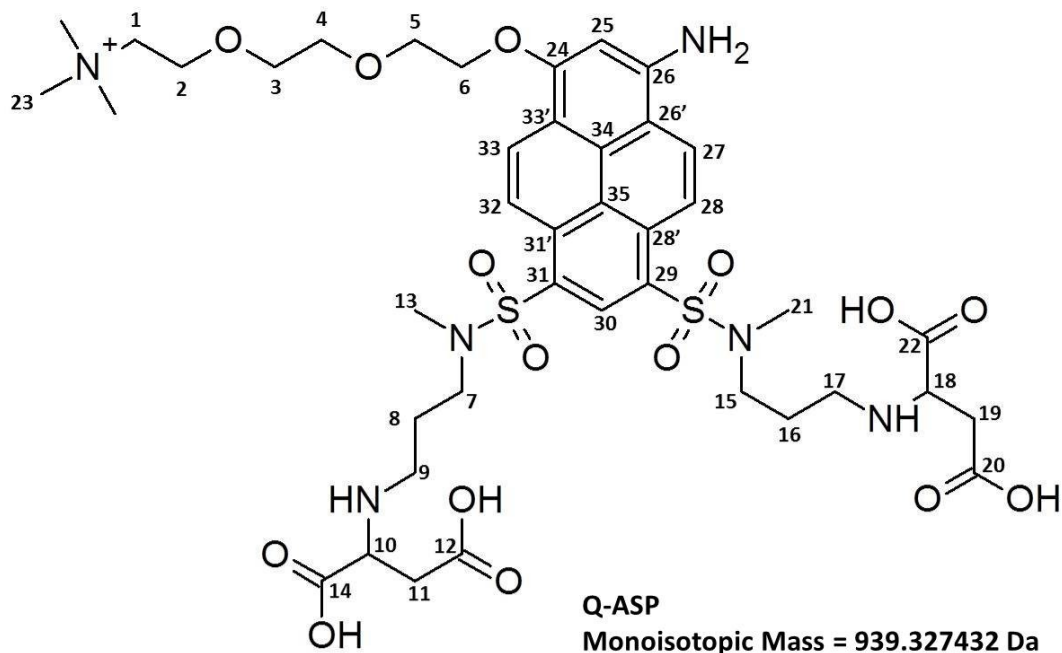
- [43] Liu, Z., Pawliszyn, J., *Anal. Chem.* 2003, 75, 4887-4894.
- [44] Busnel, J.-M., Varenne, A., Descroix, S., Peltre, G., Gohon, Y., *et al.*, *Electrophoresis* 2005, 26, 3369-3379.
- [45] Conti, M., Galassi, M., Bossi, A., Righetti, P. G., *J. Chromatogr. A* 1997, 757, 237-245.
- [46] North, R. Y., Vigh, G., *Electrophoresis* 2008, 29, 1077-1081.
- [47] Mack, S., Cruzado-Park, I., Chapman, J., Ratnayake, C., Vigh, G., *Electrophoresis* 2009, 30, 4049-4058.
- [48] Vesterberg, O., *Ann. N. Y. Acad. Sci.* 1973, 209, 23-33.
- [49] Vesterberg, O., *Acta Chem. Scand.* 1969, 23, 2653-2666.
- [50] Righetti, P. G., Simo, C., Sebastiano, R., Citterio, A., *Electrophoresis* 2007, 28, 3799-3810.
- [51] Bier, M., US Pat. 4 588 492, 1986.
- [52] Egen, N. B., Thormann, W., Twitty, G. E., Bier, M., de Gruyter 1984, pp. 547-550.
- [53] Rilbe, H., *Ann. N. Y. Acad. Sci.* 1973, 209, 11-22.
- [54] Slais, K., Friedl, Z., *J. Chromatogr. A* 1994, 661, 249-256.
- [55] Schulze, P., Link, M., Schulze, M., Thuermann, S., Wolfbeis, OS., *et al.*, *Electrophoresis* 2010, 31, 2749-2753.
- [56] Estrade, T. R., *Dissertation*, Texas A&M University, 2010.
- [57] Garmaise, D. L., Schwartz, R., McKay, A.F., *J. Am. Chem. Soc.* 1958, 80, 3332.
- [58] Kishimoto, K., Suzawa, T., Yokota, T., Mukai, T., Ohno, H., *et al.*, *J. Am. Chem. Soc.* 2005, 127, 15618-15623.

- [59] Bouzide, A. S., Gilles., *Organic Letters* 2002, 4, 2329-2332.
- [60] Ameijde, J. a. L. R. M. J., *Organic & Biomolecular Chemistry* 2003, 1, 2661-2669.
- [61] Xie, H. B., Orit; Gu, Li-Qun; Cheley, Stephen; Bayley, Hagan., *Chemistry & Biology* 2005, 12, 109-120.
- [62] Taber, D. F. A., J. C.; Jung, K. Y., *J. Org. Chem.* 1987, 52, 5621-5622.
- [63] Mancuso A. J., S. D., *Synthesis* 1981, 3, 165-185.
- [64] Adamczyk, M. C., Yon-Yih; Mattingly, Phillip G.; Pan, You; Rege, Sushil. , *J. Org. Chem.* 1998, 63, 5636-5639.
- [65] Hsieh, Y. Y., Y; Yeh, H; Lin, P; Chen, S., *Electrophoresis* 2009, 30, 644.
- [66] Rostovtsev, V. V., Green, L. G., Fokin, V. V., Sharpless, K. B., *Angew. Chem. Int. Ed.* 2001, 40, 2004.
- [67] Tetko, I. V. G., J.; Todeschini, R.; Mauri, A.; Livingstone, D.; Ertl, P.; Palyulin, V. A.; Radchenko, E. V.; Zefirov, N. S.; Makarenko, A. S.; Tanchuk, V. Y.; Prokopenko, V. V., *J. Comput. Aid. Mol. Des.* 2005, 19, 453.
- [68] Berry, A. F. H., Heal, W. P., Tarafder, A. K., Tolmachova, T., Baron, R. A., Seabra, M. C., Tate, E. W., *ChemBioChem* 2010, 11, 771.
- [69] Parikh, J. R., Doering, W. V. E., *J. Am. Chem. Soc.* 1967, 89, 5505-5507.
- [70] Abdel-Magid, A. F., Carson, K. G., Harris, B. D., Maryanoff, C. A., Shah, R. D., *J. Org. Chem.* 1996, 61, 3849-3862.
- [71] Harry, J. L., Wilkins, M. R., Herbert, B. R., Packer, N. H., Gooley, A. A., *et al.*, *Electrophoresis* 2000, 21, 1071-1081.

- [72] Mohan, D., Lee, C. S., *J. Chromatogr. A* 2002, 979, 271-276.
- [73] Conway-Jacobs, A., Lewin, L. M., *Anal. Biochem.* 1971, 43, 394-400.
- [74] Nakhleh, E. T., Abu, S. S., Awdeh, Z. L., *Anal. Biochem.* 1972, 49, 218-224.
- [75] Shimura, K., Kasai, K.-I., *Electrophoresis* 1995, 16, 1479-1484.
- [76] Zhao, J.-Y., Chen, D.-Y., Dovichi, N. J., *J. Chromatogr.* 1992, 608, 117-120.
- [77] Shimura, K., Kamiya, K.-I., Matsumoto, H., Kasai, K.-I., *Anal. Chem.* 2002, 74, 1046-1053.
- [78] Stastna, M., Travnicek, M., Slais, K., *Electrophoresis* 2005, 26, 53-59.
- [79] Righetti, P. G., Gianazza, E., Brenna, O., Galante, E., *J. Chromatogr. A* 1977, 137, 171-181.
- [80] Glukhovskiy, P. V., Vigh, G., *Electrophoresis* 1998, 19, 3166-3170.
- [81] Survey, M. A., Goodall, D. M., Wren, S. A. C., Rowe, R. C., *J. Chromatogr. A* 1996, 741, 99-113.
- [82] Koval, D., Kasicka, V., Jiracek, J., Collinsova, M., Garrow, T. A., *Electrophoresis* 2002, 23, 215-222.
- [83] Vcelakova, K., Zuskova, I., Kenndler, E., Gas, B., *Electrophoresis* 2004, 25, 309-317.
- [84] Williams, B. A., Vigh, G., *Anal. Chem.* 1996, 68, 1174-1180.
- [85] Katayama, H., Ishihama, Y., Asakawa, N., *Anal. Chem.* 1998, 70, 5272-5277.
- [86] Tiselius, A., *Nova Acta Regiae Soc. Sci. Ups.* 1930, 7, 107 pp.
- [87] Hoerth, P., Miller, C. A., Preckel, T., Wenz, C., *Mol. Cell. Proteomics* 2006, 5, 1968-1974.

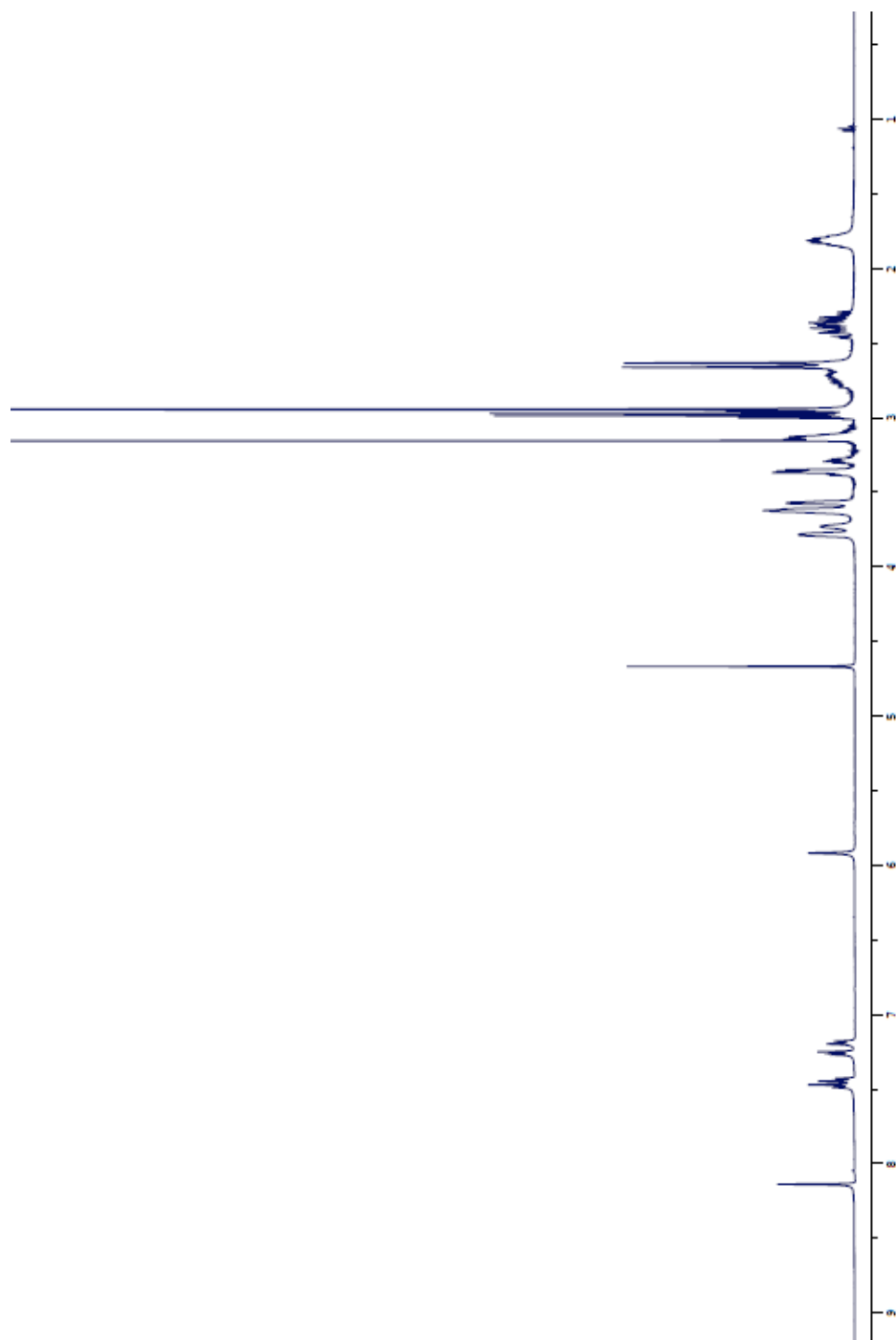
- [88] Kobayashi, H., Aoki, M., Suzuki, M., Yanagisawa, A., Arai, E., *J. Chromatogr. A* 1997, 772, 137-144.
- [89] Santora, L. C., Krull, I. S., Grant, K., *Anal. Biochem.* 1999, 275, 98-108.
- [90] Kohlrausch, F., *Ann. Phys. Chem.* 1897, 62, 209-239.
- [91] Chrambach, A., Doerr, P., Finlayson, G. R., Miles, L. E. M., Serins, R., *et al.*, *Ann. N. Y. Acad. Sci.* 1973, 209, 44-64.
- [92] Harvey, D. J., *J. Chromatogr. B: Anal. Technol. Biomed. Life Sci.* 2011, 879, 1196-1225.
- [93] Jackson, P., *Biochem. J.* 1990, 270, 705-713.
- [94] Evangelista, R. A., Liu, M.-S., Chen, F.-T. A., *Anal. Chem.* 1995, 67, 2239-2245.

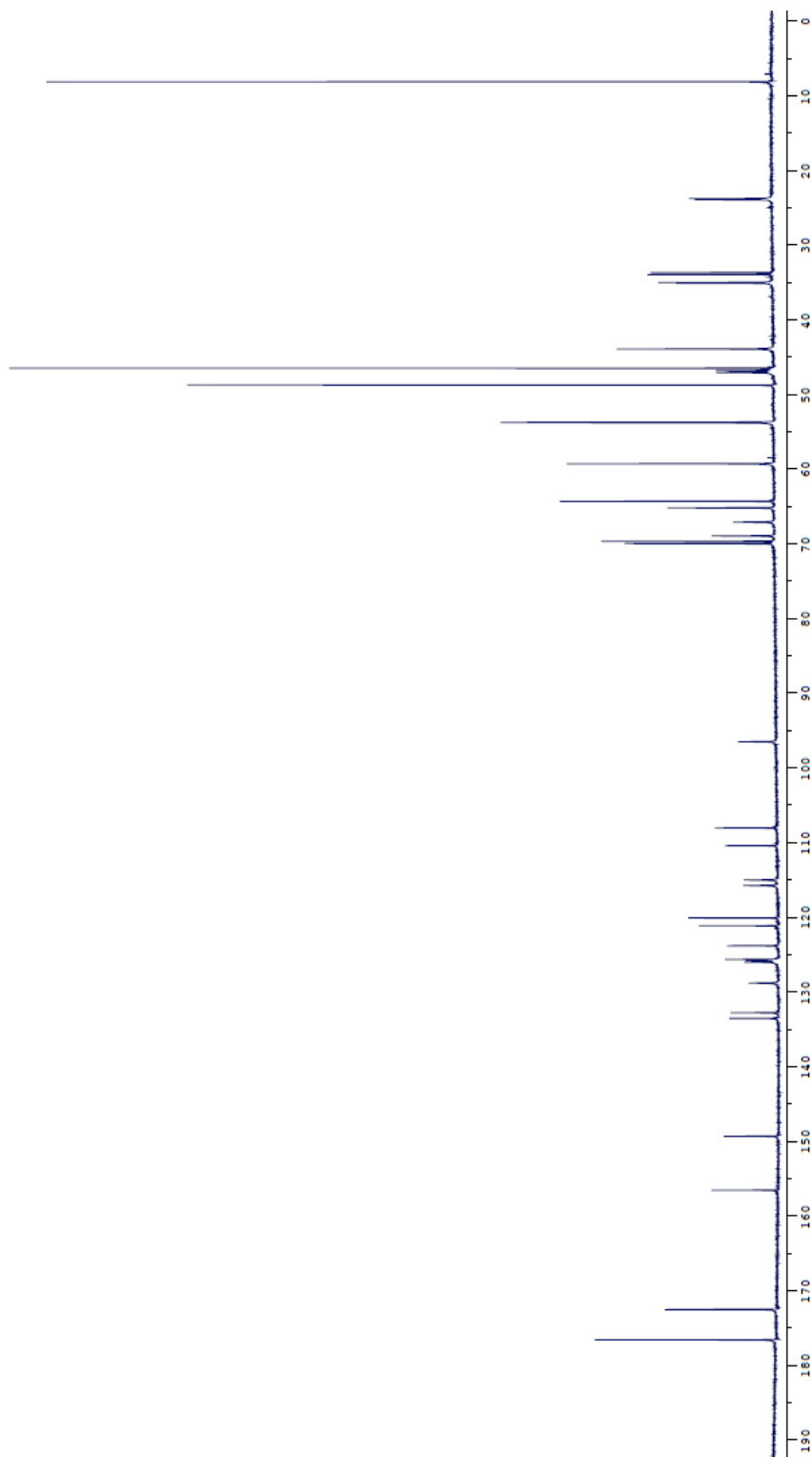
APPENDIX A



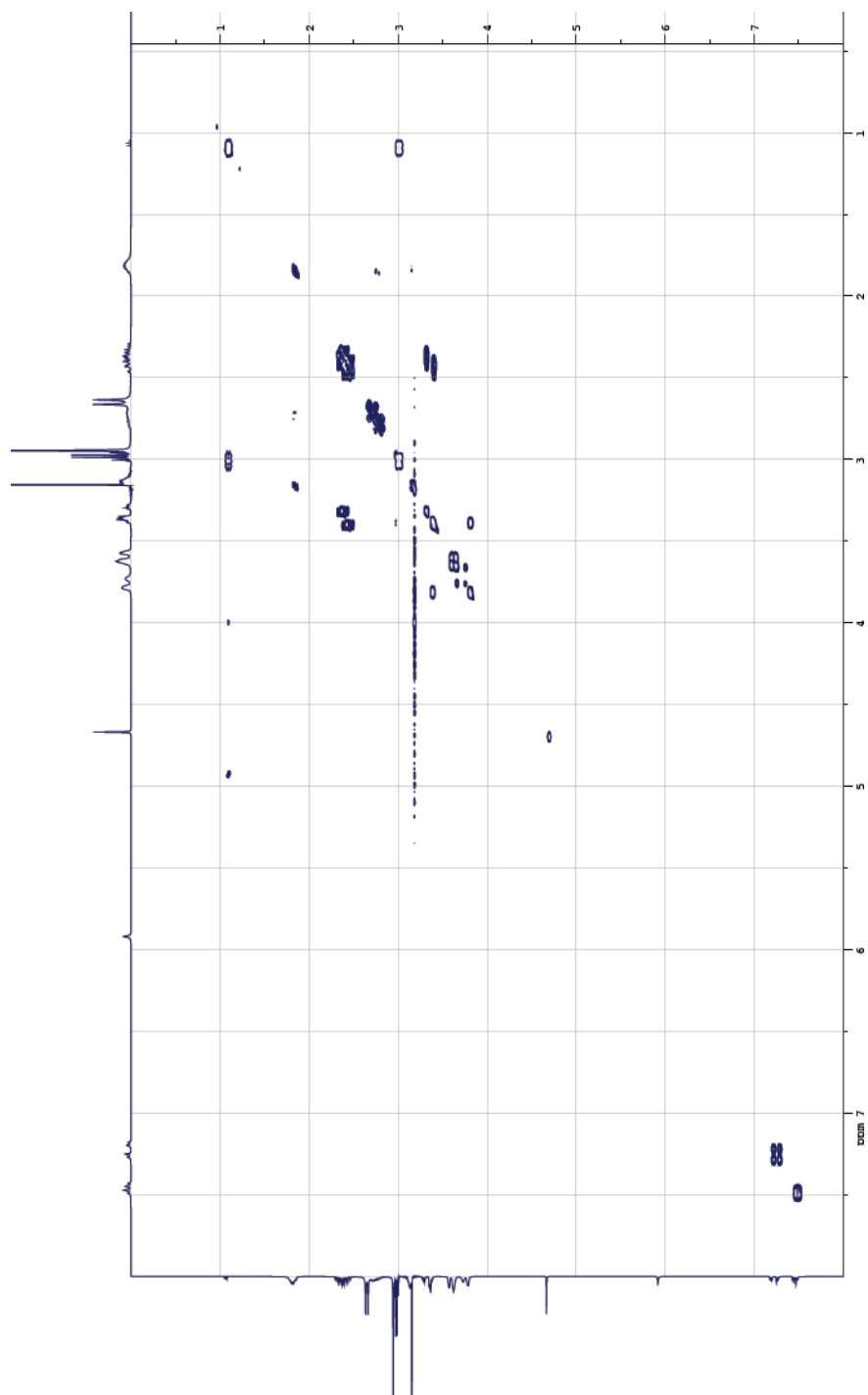
$^1\text{H-NMR}$ (500 MHz, D_2O) δ 8.26 (s, 1H), 7.61-7.55 (m, 2H), 7.38 (d, 1H, $J=9.0$ Hz), 7.31 (d, 1H, $J=9.0$ Hz), 6.04 (s, 1H), 3.91 (broad, 2H), 3.852 (broad, 2H), 3.75-3.73 (m, 4H), 3.70-3.68 (m, 2H), 3.51-3.47 (m, 3H), 3.43-3.40 (m, 1H), 3.26-3.25 (m, 4H), 3.06 (s, 9H), 2.91-2.81 (m, 4H), 2.79 (s, 3H), 2.76 (s, 3H), 2.59-2.41 (m, 4H), 1.98-1.89 (m, 4H); $^{13}\text{C-NMR}$ (500 MHz, D_2O) δ 176.6, 172.5, 156.6, 149.3, 133.5, 132.8, 128.8, 126.0, 125.8, 125.7, 123.8, 121.1, 120.1, 115.8, 115.0, 110.4, 108.0, 96.5, 70.0, 69.7, 68.9, 67.1, 65.2, 64.3, 59.3, 53.7, 48.7, 47.1, 46.8, 46.5, 43.9, 35.1, 35.0, 33.9, 33.7, 23.9, 23.8, 8.14.

position	δ , ^{13}C (ppm)	δ , ^1H (ppm)	position	δ , ^{13}C (ppm)	δ , ^1H (ppm)
1	64.3	3.51-3.40	21	33.7	2.79
2	70.0-65.2	3.91-3.68	22	176.6	
3	70.0-65.2	3.91-3.68	23	53.7	3.06
4	70.0-65.2	3.91-3.68	24	156.6	
5	70.0-65.2	3.91-3.68	25	96.5	6.04
6	70.0-65.2	3.91-3.68	26	149.3	
7	47.1	3.26-3.25	26'	108.0	
8	23.9	1.98-1.89	27	115.8	7.61-7.55
9	43.9	2.91-2.81	28	125.8	7.61-7.55
10	59.3	3.51-3.40	28'	120.1	
11	35.1	2.59-2.41	29	123.8	
12	172.5		30	128.8	8.26
13	33.9	2.76	31	125.7	
14	176.6		31'	121.1	
15	46.8	3.26-3.25	32	126.0	7.38
16	23.8	1.98-1.89	33	115.0	7.38
17	43.9	2.91-2.81	33'	110.4	
18	59.3	3.51-3.40	34	133.5	
19	35.0	2.59-2.41	35	132.8	
20	172.5				

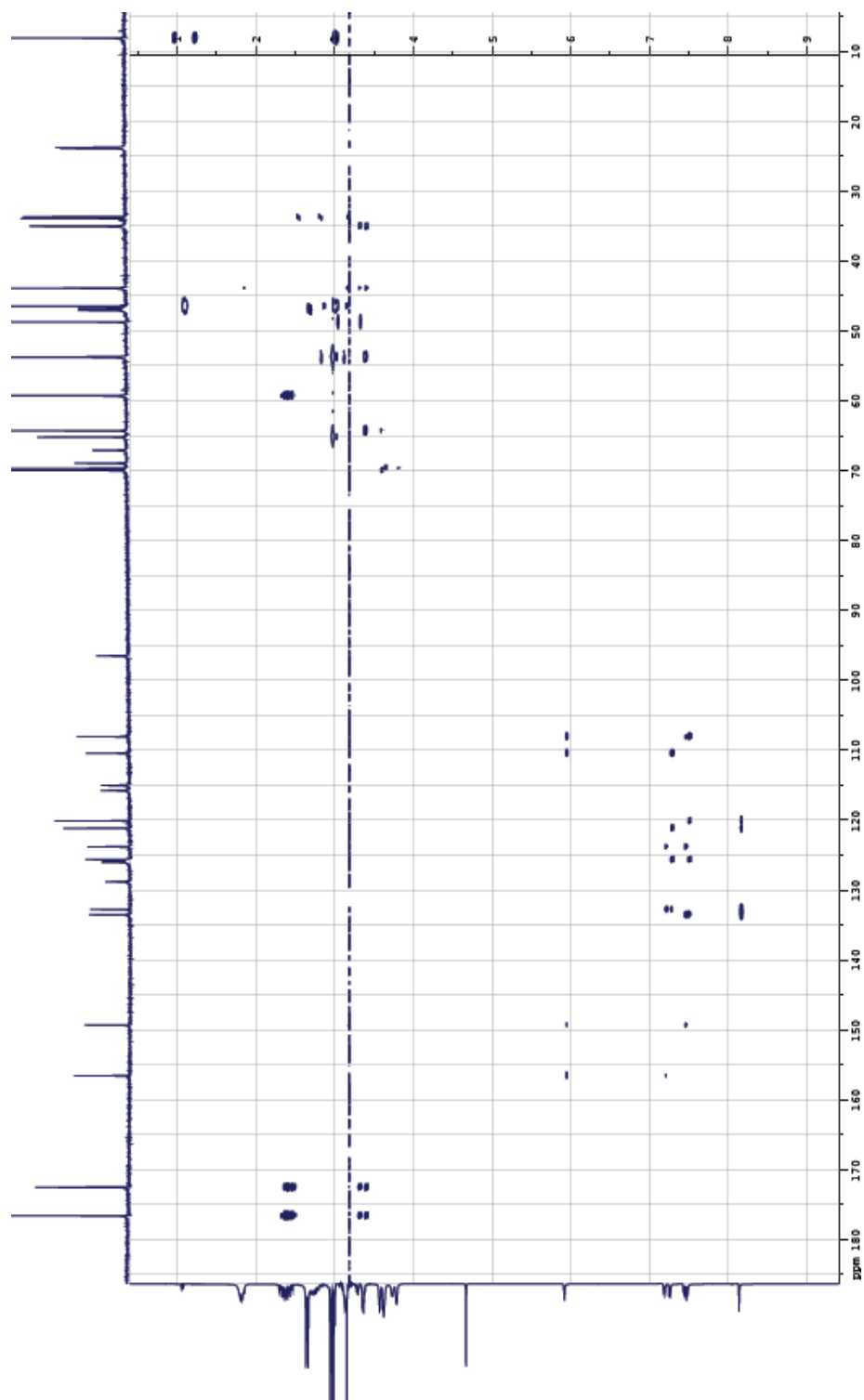
$^1\text{H-NMR}$ (D_2O)

^{13}C -NMR (D_2O)

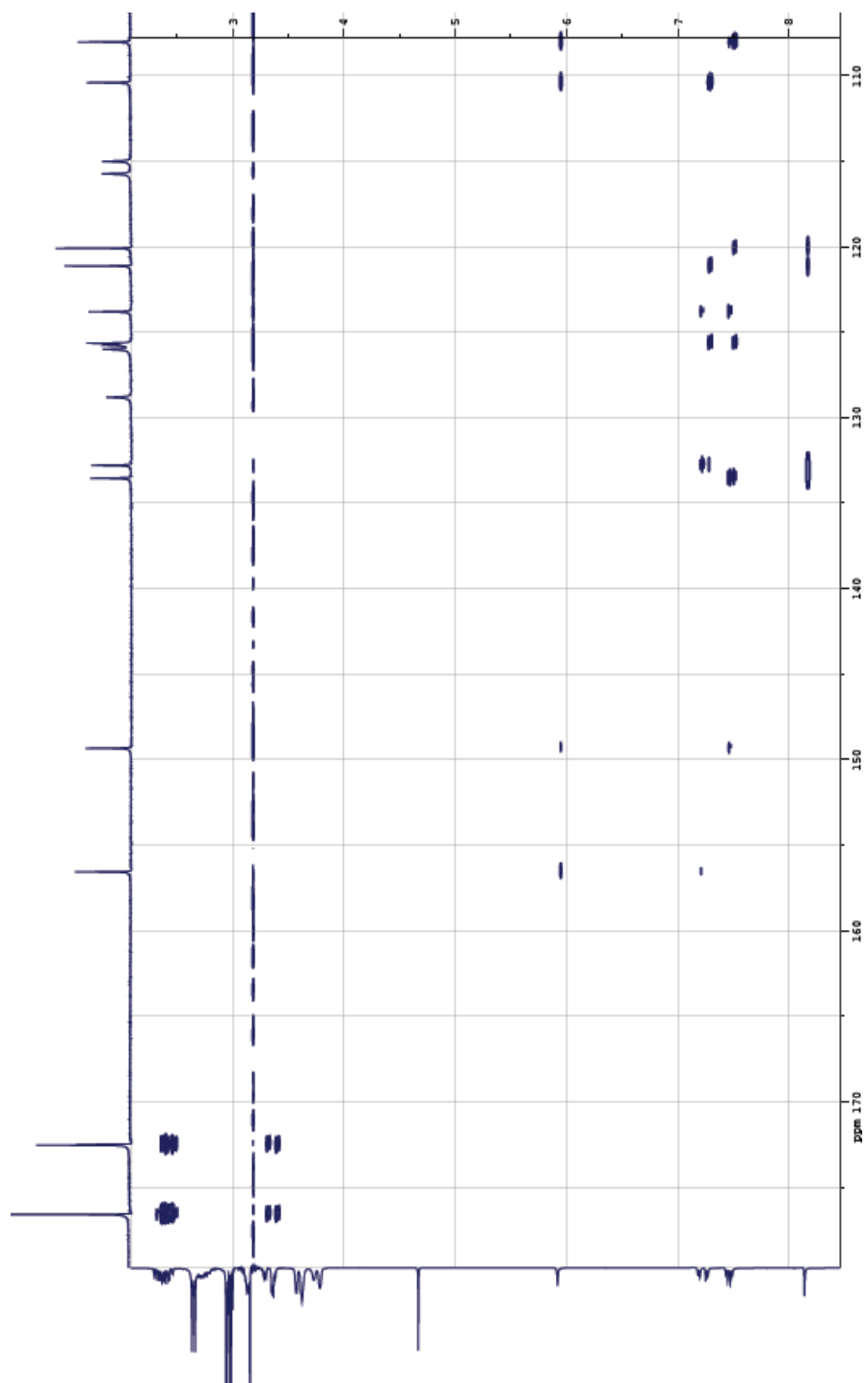
COSY



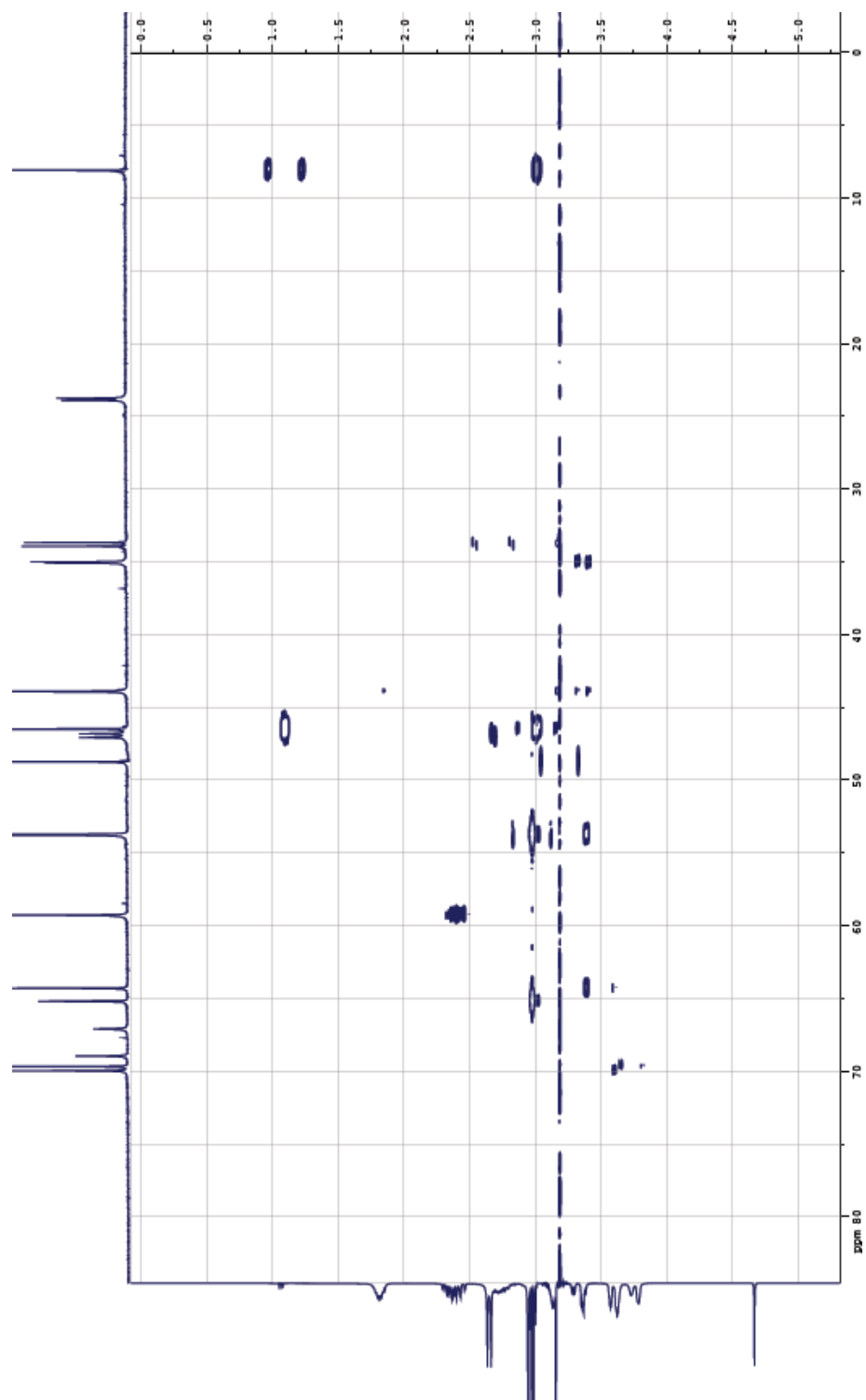
HMBC-1



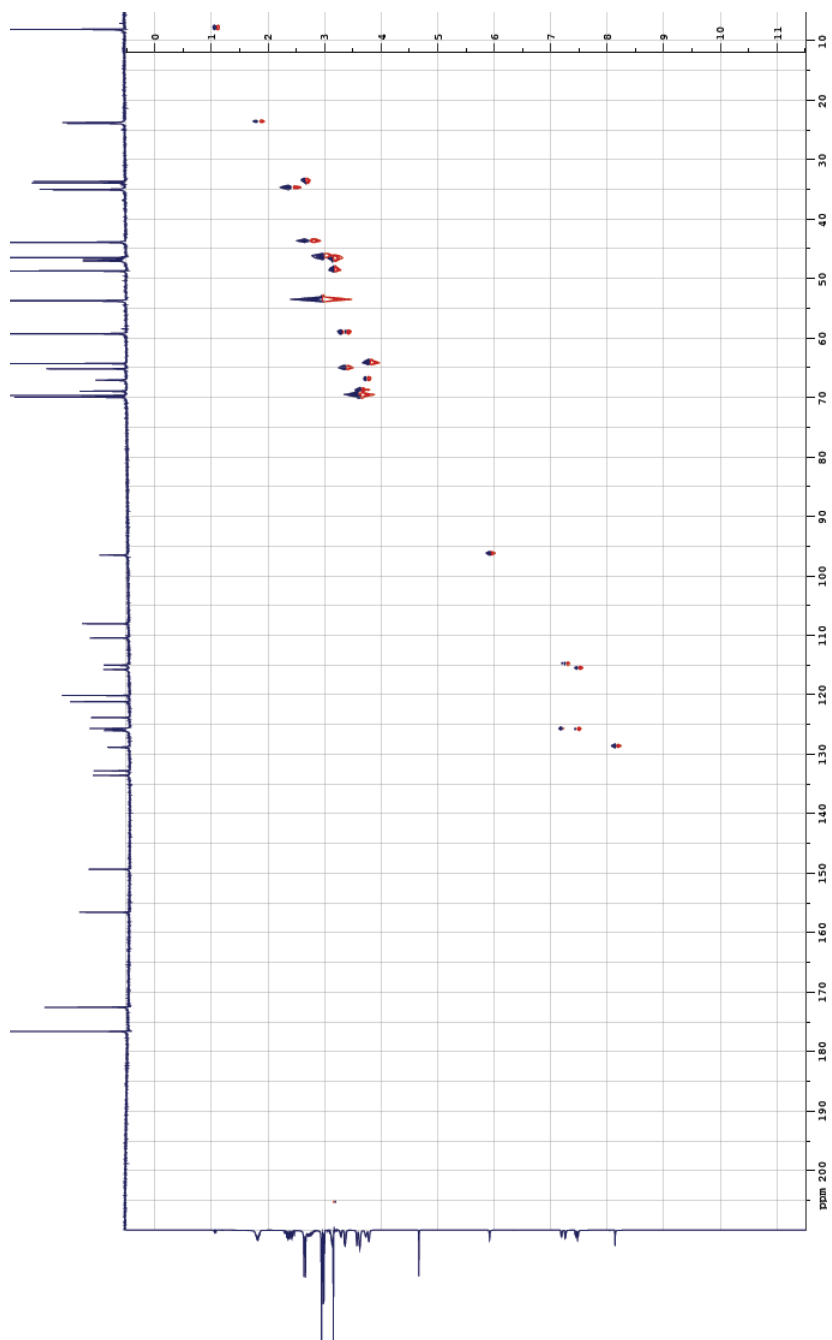
HMBC-2



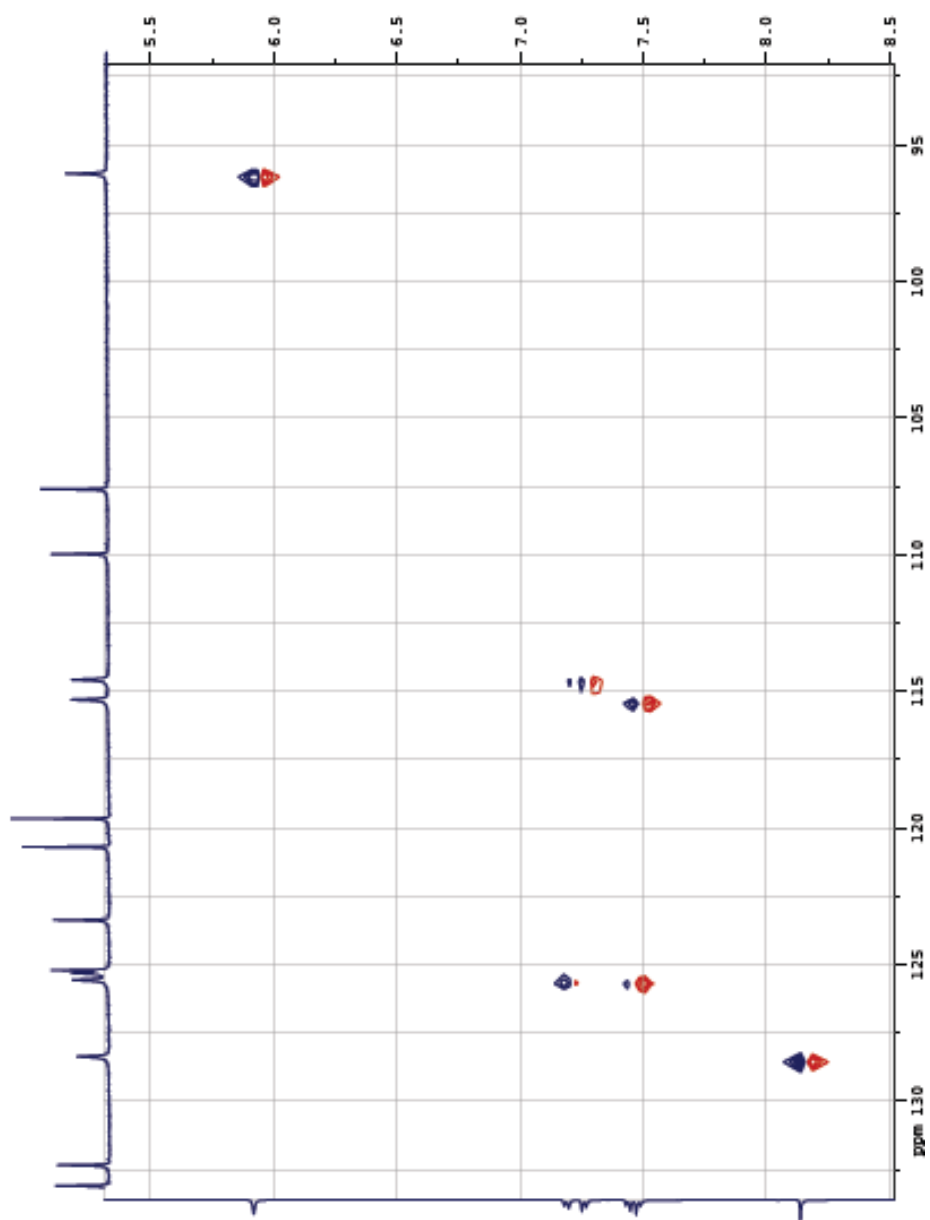
HMBC-3



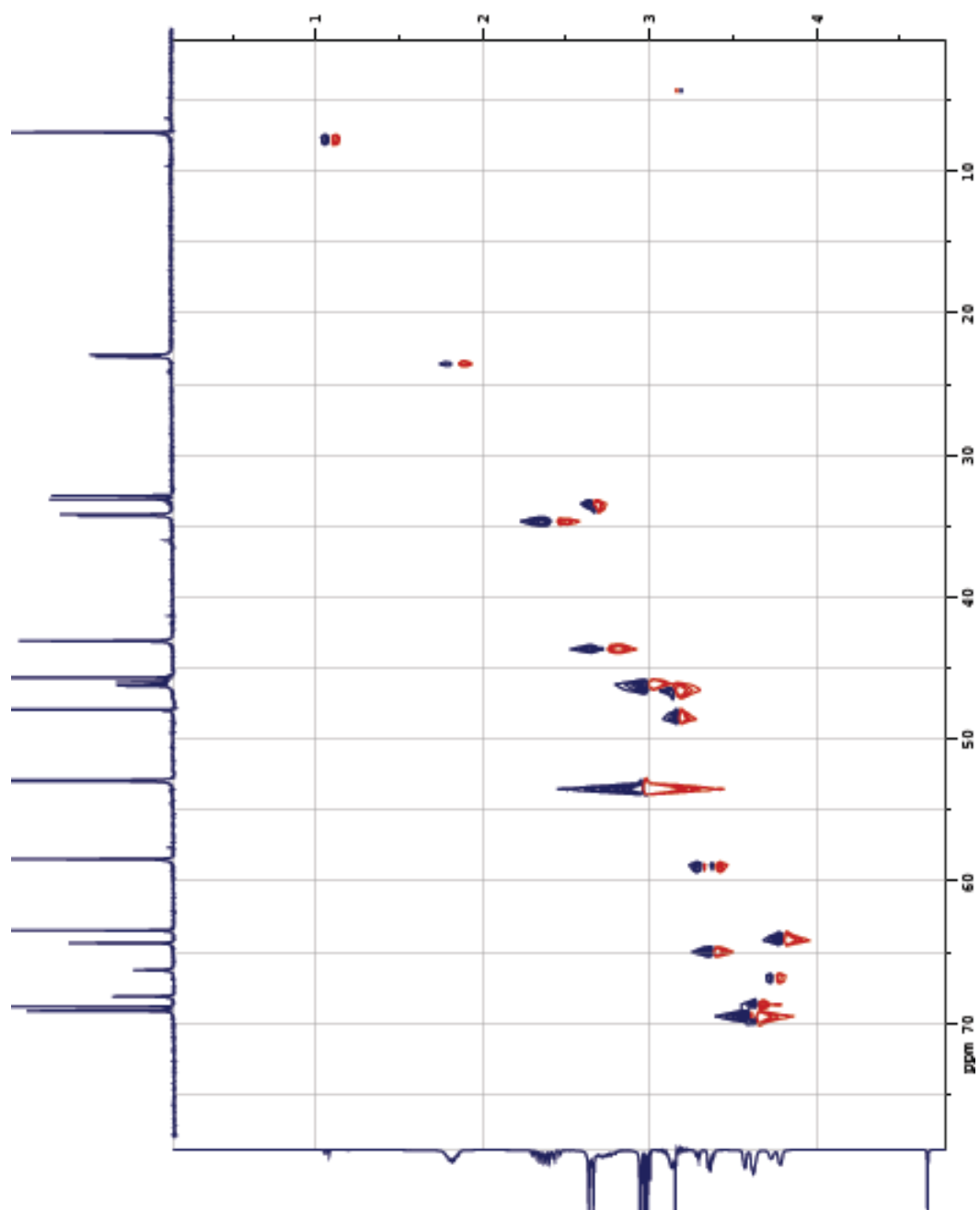
HMQC-1



HMQC-2



HMQC-3



VITA

Name: Ming-Chien Li

Address: 154 Ren-Ai Road,
Yuli, Hualien County
Taiwan

Email Address: mli@mail.chem.tamu.edu

Education: B.S., Tankang University, Taipei, Taiwan, 2002

M.S., National Tsing Hua University, Hsinchu, Taiwan, 2004

Ph.D., Texas A&M University, College Station, Texas, USA, 2012